



## DENDRITIC SOLIDIFICATION OF AQUEOUS SOLUTIONS

by

Pradeep K. Rohatgi

SUBMITTED TO THE DEPARTMENT OF METALLURGY

ON MAY 15, 1964, IN PARTIAL FULFILLMENT OF THE  
REQUIREMENTS FOR THE DEGREE OF DOCTOR OF SCIENCE

---

ABSTRACT

Dendritic structures produced on fairly rapid solidification of aqueous solutions have been studied. Both single and mixed solute systems have been examined; the principal variables investigated are changing freezing rates, the nature of the solute and its concentration, combinations of solutes, and external magnetic and electrical fields. A theoretical analysis of dendritic growth is presented which predicts the square root of dendrite spacing to be directly proportional to the diffusion coefficient of the solute and the constitutional supercooling, and inversely proportional to the solute concentration, the freezing rate, and the slope of the liquidus curve. The fact that the dendrite spacing increases with solute concentration has been attributed to the simultaneous increase in the capacity of the liquid to withstand constitutional supercooling. The development of side branches depends

on the solute concentration, the primary dendrite spacing and the freezing rate; further breakdown of primary ice plates occurs when the concentration gradients in the interdendritic liquid exceed the maximum value which it can sustain. Under identical freezing conditions, the dendrite spacing is higher, the higher is the solute diffusivity.

Thermal analysis of the unidirectional freezing from a constant temperature chill shows that the solution at each plane is subjected to a spectrum of freezing rates. Dendrite spacing at each level has been found to be inversely proportional to the square root of the maximum freezing rate. During progressive solidification, the dendrite spacing changes with the changing freezing conditions by actual divergence or convergence of neighboring plates.

Application of external magnetic fields has been found to increase the dendrite spacing; however, the effect is measurable only in systems in which the entire liquid is supercooled before the initiation of freezing. Possible interactions between external fields and aqueous freezing systems have been examined; the effect of a magnetic field has been attributed to its capacity of promoting the nucleation of ice.

Thesis Supervisor: Professor C. M. Adams, Jr.  
Professor of Metallurgy

## TABLE OF CONTENTS

|  | <u>Page<br/>Number</u> |
|--|------------------------|
| TITLE PAGE . . . . .   | i                      |
| ABSTRACT . . . . .   | ii                     |
| TABLE OF CONTENTS . . . . .  | iv                     |
| LIST OF TABLES . . . . .   | vi                     |
| LIST OF ILLUSTRATIONS . . . . .  | vii                    |
| ACKNOWLEDGEMENTS . . . . .   | xv                     |
| I. INTRODUCTION . . . . .  | 1                      |
| II. THEORY . . . . .   | 10                     |
| 1. MASS TRANSPORT . . . . .  | 10                     |
| 2. UNIDIRECTIONAL FREEZING OF A SOLUTION FROM A<br>CONSTANT TEMPERATURE CHILL . . . . .                | 16                     |
| 3. DIFFUSION IN SINGLE AND MIXED ELECTROLYTE<br>SYSTEMS . . . . .                                      | 21                     |
| 4. THE EFFECT OF FIELDS ON THE FREEZING OF<br>AQUEOUS SOLUTIONS . . . . .                              | 23                     |
| III. EXPERIMENTAL PROCEDURES . . . . .   | 27                     |
| 1. FREEZING SYSTEMS . . . . .  | 27                     |
| 2. SPECIMEN PREPARATION AND MICROGRAPHY . . . . .  | 29                     |
| 3. APPLICATION OF EXTERNAL FIELDS . . . . .  | 30                     |
| IV. RESULTS AND DISCUSSION . . . . .   | 33                     |
| 1. GENERAL CHARACTER OF THE ICE-BRINE AGGREGATE<br>OBTAINED ON FREEZING OF AQUEOUS SOLUTIONS . . . . . | 33                     |
| 2. STRUCTURES OBTAINED WITH VARYING FREEZING<br>RATES . . . . .  | 35                     |

|  | <u>Page<br/>Number</u> |
|--|------------------------|
| 3. THE EFFECT OF CONCENTRATION ON DENDRITIC<br>STRUCTURE . . . . .   | 40                     |
| 4. SECONDARY BREAKDOWN OF PRIMARY ICE DENDRITES .  | 43                     |
| 5. THE EFFECT OF SOLUTE DIFFUSIVITY OF DENDRITE<br>SPACING . . . . .   | 45                     |
| 6. SOLIDIFICATION STRUCTURES FROM MIXED SOLUTIONS  | 45                     |
| 7. THE EFFECT OF EXTERNAL FIELD ON THE DENDRITIC<br>PATTERN . . . . .  | 47                     |
| V. CONCLUSIONS . . . . .   | 51                     |
| VI. SUGGESTIONS FOR FURTHER WORK . . . . .   | 53                     |
| VII. APPENDIX I: DEFINITIONS OF SYMBOLS USED IN THE TEXT . .   | 54                     |
| VIII. APPENDIX II: SOLIDIFICATION PATTERN OF 1 N POTASSIUM<br>CHLORIDE SOLUTION IN CONTACT WITH A CHILL AT $-70^{\circ}\text{C}$ . . | 57                     |
| IX. APPENDIX III: ANALYSIS OF CHILL SURFACE TEMPERATURE . .  | 64                     |
| X. APPENDIX IV: CALCULATION OF CONSTITUTIONAL SUPERCOOLING<br>IN THE INTERDENDRITIC LIQUID . . . . .                                 | 66                     |
| XI. TABLES . . . . .   | 67                     |
| XII. ILLUSTRATIONS . . . . .   | 73                     |
| XIII. BIBLIOGRAPHY . . . . .   | 108                    |
| XIV. BIOGRAPHICAL NOTE . . . . .   | 113                    |

## LIST OF TABLES

| <u>Table<br/>Number</u> | <u>Title</u>  | <u>Page<br/>Number</u> |
|-------------------------|---|------------------------|
| I                       | Observations on Phase Boundary Movements During<br>Unidirectional Freezing of 1 N Potassium Chloride<br>Solution Against a $-70^{\circ}$ C Chill . . . . .  | 67                     |
| II                      | Calculated Temperature and Freezing Rate Distributions<br>at 2 Centimeters from a $-70^{\circ}$ C Chilled Surface During<br>Unidirectional Freezing of 1 N Potassium Chloride<br>Solution . . . . . | 68                     |
| III                     | Measured Dendrite Spacings and Calculated Maximum<br>Freezing Rates at Different Distances from a $-70^{\circ}$ C<br>Chill for Freezing of 1 N potassium Chloride Solution. . . . .                 | 69                     |
| IV                      | Dendrite Spacing Measurements on Droplets of Sodium<br>Chloride Solutions at Different Concentrations, in<br>the Absence and in the Presence of an External<br>Magnetic Field . . . . .             | 70                     |
| V                       | Dendrite Spacing Measurements on Ingots at Different<br>Distances from a $-70^{\circ}$ C Chilled Surface for Different<br>Solutions . . . . .   | 71                     |
| VI                      | Diffusion Coefficients for Single and Binary<br>Electrolyte Systems . . . . .   | 72                     |

## LIST OF ILLUSTRATIONS

| <u>Figure<br/>Number</u> | <u>TITLE</u>   | <u>Page<br/>Number</u> |
|--------------------------|--|------------------------|
| 1                        | Concentration Profile Ahead of a Moving<br>Solid-Liquid Interface . . . . .  | 73                     |
| 2                        | Actual Temperature and Liquidus Temperature Profiles<br>Ahead of the Interface. Finite Temperature Gradient<br>In the Liquid. . . . .  | 73                     |
| 3                        | Same as Figure 2 Except with Negligible Temperature<br>Gradient in Liquid . . . . .  | 73                     |
| 4                        | Schematic Representation of Concentration Distribution<br>in the Interdendritic Liquid. . . . .  | 74                     |
| 5                        | Actual Temperature and Liquidus Temperature<br>Distributions in the Interdendritic Liquid . . . . .  | 74                     |
| 6                        | Concentration Profiles in the Interdendritic Liquid<br>at Different Stages of Growth. . . . .  | 75                     |
| 7                        | a. Phase Diagram of potassium chloride-water System<br>b. Phase Distribution Under a Temperature Gradient,<br>Equilibrium Conditions. . . . .<br>c. Phase Distribution Under a Temperature Gradient,<br>Dendritic Growth . . . . . | 76<br>76<br>76         |

| <u>Figure<br/>Number</u> | <u>Title</u>  | <u>Page<br/>Number</u> |
|--------------------------|---|------------------------|
| 8                        | Schematic Representation of Variation in Heat<br>Content of Aqueous Solutions During Solidification<br>Cycle . . . . .  | 77                     |
| 9                        | Schematic Representation of Temperature Profiles<br>When an Aqueous Solution is Brought into Contact<br>with a Cold Chill . . . . .   | 78                     |
| 10                       | Calculated Cooling Curves for 1.0 N potassium chloride<br>Solution at Different Distances from a Surface at<br>-70° C, in contact with the Solution . . . . .   | 79                     |
| 11                       | Fraction Solidified from 1.0 N potassium chloride<br>Solution Versus Time at Different Distances from a<br>Surface at -70°C in Contact with the Solution . . . .  | 80                     |
| 12                       | Freezing Rates of 1.0 N potassium chloride Solution<br>Versus Fraction Solid at Different Distances from<br>a Surface at -70°C in Contact with the Solution . .   | 81                     |
| 13                       | Distance of Eutectic Temperature $T = T_E$ Isotherm<br>From The Chill Surface at -70° C as a Function of<br>Time, for 1.0 N potassium chloride Solution.<br>Movement of isotherm observed as the limit of all<br>solid zone in the ingot. . . . . | 82                     |



| <u>Figure<br/>Number</u> | <u>Title</u>  | <u>Page<br/>Number</u> |
|--------------------------|---|------------------------|
| 14                       | Schematic Representation of the Set Up for<br>Freezing Droplets of Aqueous Solutions in Low<br>Magnetic Fields . . . . .  | 83                     |
| 15                       | Diagram Showing the Arrangement for Freezing<br>Droplets of Aqueous Solutions in High Magnetic<br>Fields . . . . .  | 83                     |
| 16                       | Diagram Showing the Assembly for Growing<br>Unidirectional Ingots from Aqueous Solutions with<br>High Magnetic Fields Parallel to the Growth<br>Direction . . . . . | 84                     |
| 17                       | Same as Figure 16 Except for Field being<br>Perpendicular to the Growth Direction . . . . .   | 84                     |
| 18                       | Unidirectional Freezing of Two Ingots One of Which<br>is Under the Influence of an Oscillating Magnetic<br>Field . . . . .  | 85                     |
| 19                       | Liquid Solid Interface During Unidirectional<br>Freezing, Perpendicular to the Growth Direction .   | 85                     |
| 20                       | Typical Dendritic Aggregate of Ice and Brine<br>Obtained on Fairly Rapid Freezing of Aqueous<br>Solutions (Under Polarized Light) . . . . .                         | 86                     |

| <u>Figure<br/>Number</u> | <u>Title</u>   | <u>Page.<br/>Number</u> |
|--------------------------|--|-------------------------|
| 21                       | Characteristic Parameters of a Ice-Brine Aggregate<br>After Dendritic Solidification . . . . .   | 87                      |
| 22                       | Randomly Arranged Ice Crystals Produced Under Very<br>Slow Growth Rates. Ingot from 1.0 N potassium chloride<br>Solution 1.0 cm from the Chill Surface at $-20^{\circ}$ C. . . | 88                      |
| 23                       | A Large Segregate of Salt Between Neighboring Groups<br>of Dendrites . . . . .   | 88                      |
| 24                       | Transverse Section of Unidirectional Ingot from 1.0 N<br>potassium chloride Solution 0.90 cm from the Chill<br>Surface at $-70^{\circ}$ C, X26 . . . . .                       | 89                      |
| 25                       | Same Ingot as in Figure 24, 1.3 cm from the Chilled<br>Surface, X26 . . . . .  | 89                      |
| 26                       | Same Ingot as in Figure 24, 3.0 cm from the Chilled<br>Surface, X26 . . . . .  | 90                      |
| 27                       | Same Ingot as in Figure 24, 3.2 cm from the Chilled<br>Surface, X26 . . . . .  | 90                      |
| 28                       | Transverse Section of an Ingot from 1.0 N potassium<br>chloride Solution 0.80 cm from the chill Surface, at<br>$-20^{\circ}$ C, X26 . . . . .                                  | 91                      |

| <u>Figure<br/>Number</u> | <u>Title</u>  | <u>Page<br/>Number</u> |
|--------------------------|---|------------------------|
| 29                       | Same Ingot as in Figure 28, 1.1 cm from the Chill,<br>but with Chill Temperature Reduced to $-70^{\circ}$ C during<br>Growth, Causing Faster Freezing . . . . .   | 91                     |
| 30                       | Variation of Dendrite Spacing with Distance from the<br>Chill and the Effect of Concentration on Dendrite<br>Spacing in Ingots from potassium chloride Solutions .  | 92                     |
| 31                       | Plot of Dendrite Spacings in 1.0 N potassium chloride<br>Ingot Versus the Reciprocal of the Square Root of the<br>Maximum Freezing Rates at Different Distances from the<br>Chill Surface at $-70^{\circ}$ C . . . . .              | 93                     |
| 32                       | Dendrite Spacing and Thickness of Salt Pockets Versus<br>Concentration in Sodium Chloride Solution. Droplets,<br>Freezing Rate $0.36 \text{ minutes}^{-1}$ . Also the Effect of<br>Superimposed Magnetic Field on Spacing . . . . . | 94                     |
| 33                       | Effect of Concentration on Dendrite Spacing in Ingots<br>from Sodium Chloride Solutions . . . . .   | 95                     |
| 34                       | Effect of Concentration on Dendrite Spacing in Ingots<br>from Lithium Chloride Solutions . . . . .  | 96                     |

| <u>Figure<br/>Number</u> | <u>Title</u>  | <u>Page<br/>Number</u> |
|--------------------------|---|------------------------|
| 35                       | 0.2 N sodium chloride Solution Droplet, Freezing<br>Rate $0.36 \text{ minutes}^{-1}$ , X26 . . . . .  | 97                     |
| 36                       | 1.5 N sodium chloride Solution Droplet, Freezing<br>Rate $0.36 \text{ minutes}^{-1}$ , X26 . . . . .  | 97                     |
| 37                       | 3.0 N sodium chloride Solution Droplet, Freezing<br>Rate $0.36 \text{ minutes}^{-1}$ , X26 . . . . .  | 98                     |
| 38                       | 3.0 N sodium chloride Solution Droplet, Freezing<br>Rate $0.72 \text{ minutes}^{-1}$ , X26 . . . . .  | 98                     |
| 39                       | Liquidus Curves of Water with Sodium Chloride,<br>potassium chloride, Hydrogen chloride and Lithium<br>chloride as Solutes. . . . .             | 99                     |
| 40                       | Effect of Solute Diffusivity on Dendrite Spacing .  | 100                    |
| 41                       | Effects of Small Solute Additions on Dendrite<br>Spacings Obtained with 0.2 N sodium chloride<br>Solution . . . . .                             | 101                    |
| 42                       | Effects of Large Solute Additions on Dendrite<br>Spacings Obtained with 0.1 N sodium chloride<br>and 0.1 N Lithium Chloride Solutions . . . . . | 102                    |

| <u>Figure<br/>Number</u> | <u>Title</u>   | <u>Page<br/>Number</u> |
|--------------------------|--|------------------------|
| 43                       | Effect of Large Solute Additions on Dendrite<br>Spacings Obtained with 0.1 N Lithium Chloride<br>and 0.1 N potassium chloride Solutions . . . . .                      | 103                    |
| 44                       | Ingot from 0.1 N Sodium Chloride Solution, 2.5 cm<br>from the chill surface at $-70^{\circ}$ C, X25 . . . . .  | 104                    |
| 45                       | Ingot from 0.1 N Sodium Chloride + 0.10 N Lithium<br>Chloride Solution, 2.5 cm from the Chill Surface<br>at $-70^{\circ}$ C, X25 . . . . .                             | 104                    |
| 46                       | Ingot from 0.1 N Lithium Chloride Solution, 2.5 cm<br>from the chill Surface at $-70^{\circ}$ C, X25 . . . . .   | 104                    |
| 47                       | Effect of Total Solute Concentration on Dendrite<br>Spacings with Solutions Containing Equal<br>Proportions of Sodium Chloride and Potassium<br>Chloride . . . . .     | 105                    |
| 48                       | 0.5 N Sodium Chloride Solution Droplet, Freezing<br>Rate $0.36 \text{ min}^{-1}$ , X75. No Field . . . . .   | 106                    |
| 49                       | 0.5 N Sodium Chloride Solution Droplet, Freezing<br>Rate $0.36 \text{ min}^{-1}$ , X75. Frozen Under the Influence<br>of a 2 Kilogauss Static Magnetic Field . . . . . | 106                    |

| <u>Figure<br/>Number</u> | <u>Title</u>  | <u>Page<br/>Number</u> |
|--------------------------|---|------------------------|
| 50                       | 1.0 N Sodium Chloride Solution Droplet, Freezing<br>Rate $0.36 \text{ min}^{-1}$ , X25. No Field . . . . .  | 107                    |
| 51                       | 1.0 N Sodium Chloride Solution Droplet, Freezing<br>Rate $0.36 \text{ min}^{-1}$ , X25. Frozen Under the Influence<br>of a 4.0 Kilogauss Static Magnetic Field. . . . . | 107                    |

## ACKNOWLEDGEMENTS

The author is extremely grateful to Professor C. M. Adams, Jr. for his technical guidance and encouragement during the course of this work. He is also indebted to the other staff members of the Ice Research Laboratory and the Welding Laboratory of M. I. T. for their assistance during the experimental phases of the program, especially to K. Pulkonik, G. Eldis, B. Jain and E. Brush, Jr.

The author also wishes to express his sincere thanks to Drs. W. A. Tiller, W. G. Pfann, C. Wagner, E. R. Gilliland, D. Turnbull, B. Chalmers and others with whom he discussed the solidification of aqueous solutions. The financial supports of the Office of Saline Water and the Air Force Cambridge Laboratories, and the loan of the facilities by the National Magnet Laboratories Cambridge are deeply appreciated by the author. He is also thankful to Mrs. Katrina Avery and Mrs. Natalie White for their help with the typing of this work.

## I. INTRODUCTION

The principal objective of this work is to promote the fundamental understanding of the mechanism of solidification of aqueous solutions, especially with regard to the phase distribution in the frozen mass. Aqueous solutions offer the advantage of being transparent; in addition their study is of special significance, since the freezing process is receiving increasing attention among the methods of separating fresh water from saline water. In general during the freezing of solutions, the phase change is accompanied by an impurity redistribution due to the different capacities of the solid and the liquid to accommodate the solute. In aqueous solutions the impurity is more or less completely rejected into the liquid phase, since with very few exceptions there is virtually no solid solubility of ionic salts in the crystallizing ice. For this reason the resulting solid consists of an aggregate of salt and pure ice. The phase morphology governs the efficiency of the freezing process of desalination as well as the strength of the aggregate. The latter is of importance in the polar operations where frozen sea water is used as a construction material.

Water molecules possess a dipole moment, and are almost tetrahedrally arranged in the case of pure water. There is no definite agreement, however, on the details as to whether the structure is quartz - <sup>1,2,3</sup> like, tidymite-like or closer to methane hydrate <sup>4</sup>. Nevertheless it is agreed that water has considerable structural



regularity and that the formation of ice may be considered merely as a process of increase in order. This statement can be extended to aqueous solutions, although it is known that ionic impurities increase order<sup>5</sup> in their immediate vicinity but decrease the long-range order of water molecules.

Cooling the solution down to its freezing point is accompanied by a change in its structure. This is manifested in the case of pure water by a maximum in the density at  $+4^{\circ}\text{C}$ . At this point there is a balance between the decrease of intermolecular distances with decreasing temperature and the simultaneous tendency for the structure to open up and get closer to that of ice. This temperature of maximum density depends upon the composition of liquid, and at higher concentrations it can be suppressed below the liquidus temperature. This further indicates that aqueous solutions have structural regularity which is of considerable importance in the formation of ice.

On further cooling below the liquidus temperature ice crystals start to precipitate from the solution. Usually the liquid undergoes a certain amount of supercooling before the first crystal of ice nucleates. This supercooling is referred to as the bulk supercooling and its magnitude depends upon the freezing variables. There is not enough quantitative information available on the molecular mechanics of the nucleation process to make possible a theoretical **computation**

of supercooling as a function of the composition and the structure of liquid. The experimental measurements are difficult to reproduce because of their extreme sensitivity to the presence of heterogeneous impurities. Pure water has been found to sustain a maximum supercooling<sup>6</sup> of 70°F.

Once the nucleus of ice has formed it grows further by the addition of individual water molecules from the liquid, since it is rather unlikely that the water molecules are added to the solid in preoriented groups. In spite of the short range order in the liquid and the complex structure of ice, a molecule in water needs very little activation energy to join the solid phase. Under normal freezing conditions, interface kinetics are not the rate-controlling step and the deviation of only a few microdegrees<sup>7</sup> from equilibrium provides enough activation energy for growth. Usually the removal of the latent heat of fusion is the rate controlling step. In a system where the heat of fusion is to be removed through the solid the rate of ice formation is proportional to the rate of heat extraction. However when the growing solid is surrounded by supercooled liquid the rate of formation of solid depends upon the bulk supercooling<sup>8</sup>. This is because of the tendency of the system to immediately form equilibrium amounts of two phases corresponding to the temperature.

The growth of ice is accompanied by simultaneous rejection of solute in the liquid next to the solid-liquid interface. The resulting concentration gradient in the liquid causes simultaneous diffusion of the solute away from the interface into the bulk liquid. Except at extremely slow growth rates the rate of diffusion of solute is **slow** compared to the rate of rejection, and a solute rich layer is produced next to the interface with a concentration profile as shown in Figure 1. Figure 2 shows the corresponding profile of equilibrium liquidus temperature ahead of the interface; the same figure also shows the actual temperature prevalent in the liquid. Equilibrium has been assumed at the interface in view of the fast interface kinetics<sup>7,9</sup>. Mass transport events take place on such a local scale that the temperature gradients over these distances can be neglected. Figure 3 is therefore more representative of the actual conditions in the liquid. This is an immediate consequence of the fact that the thermal diffusivities are much higher compared to the mass diffusivities.

It can be seen from Figures 2 and 3 that the liquid next to the interface is supercooled since it is below its equilibrium liquidus temperature. This liquid can achieve equilibrium either by the formation and growth of fresh nuclei or by the formation of solid protrusions on the already existing surface extending into the unstable liquid. The latter is more favorable in terms of surface area; however, there is a definite activation barrier to be scaled before the

protrusion mechanism can operate. It is on account of this barrier that the liquid ahead of an equilibrium interface can be supercooled to a finite extent. This supercooling, usually referred to as constitutional supercooling is distinctly different from bulk supercooling, which represents the barrier to the formation of new solid nuclei from the liquid.

A theoretical computation of constitutional supercooling presents difficulties in connection with the surface energy and the critical protrusion size, as in the case of homogeneous nucleation. Its evaluation is further complicated by the fact that the volume free energy driving force differs from point to point in the system. There have been few direct measurements<sup>10,11</sup> of constitutional supercooling with almost pure metal systems. The magnitude of supercooling has been reported to be very small, which makes the direct experimental measurements very difficult and unreliable. Brown<sup>12</sup>, French<sup>13</sup> and Rohatgi<sup>14</sup> have indirectly calculated the supercooling from the final structures and have found it to be less than a tenth of a degree centigrade for several metallic and aqueous systems.

The fact that liquid can sustain only very small amounts of constitutional supercooling implies that only certain maxima of concentration gradients are permissible in the liquid ahead of an interface (Figure 3). The gradients depend upon the rate of rejection of solute at the interface and its removal from the interface by diffusional means. Since the rate of diffusion is more or less

constant<sup>5</sup> for a particular liquid, a plane interface can continue to be stable only if it moves below a certain maximum rate.

The rate of heat extraction governs the overall rate of formation of the solid from the liquid. For a given interface area, the faster the rate of heat extraction, the faster the interface would move. Above a certain rate of heat extraction, the concentration gradients in the liquid will exceed the maximum permissible value, and the plane interface will break down. After the breakdown the interface assumes a new morphology with increased surface area. The increase in surface area is sufficient to prevent the supercooling in the liquid from exceeding the maximum it can sustain. This comes about because with increased surface area, for the same amount of total solid formed, a smaller amount of solute will have to be rejected per unit area of the interface. The character of the protrusions of the interface will therefore depend upon the extent of solute build up. A considerable amount of work has been done analyzing the interface breakdown problem in metallic systems<sup>11,15</sup>. Most of the work has been directed towards analyzing the development of the instability before the breakdown and trying to correlate it with the final dendritic structure. Here an attempt will be made to analyze the conditions after the breakdown of interface and correlate them to the final structure.

The protrusions ahead of a planar front are generally referred to as dendrites. Their shape is found to be different in different freezing systems. In aqueous solutions these protrusions are plate-

shaped and arranged parallel to each other in distinct groups. Once these platelets are formed ahead of a plane interface their subsequent growth takes place by their extension into the bulk liquid and their simultaneous increase in thickness to consume the interdendritic liquid. Diffusion at the sides of the platelets is much more difficult than at their tips, since the sides have to reject the solute in very small closed interdendritic puddles; on the other hand, the tips have large volume of liquid ahead of them. Once again, the criterion of constitutional supercooling governs the stability of the surfaces of plates growing into the interdendritic liquid. The theory presented here is based on the assumption that the dendritic breakdown of the interface is such that the interdendritic liquid is not subjected to more supercooling than it can sustain.

Brown<sup>12</sup> and French<sup>13</sup> have developed relationships for dendrite spacing using a similar approach and have experimentally tested them for metallic systems and for aqueous solutions respectively. According to them, the dendrite spacing increases with the diffusivity of the solute, the capacity of the liquid to sustain supercooling and the freezing time; it decreases with the solute concentration and the slope of the liquidus curve. Their theories analyze a case where the freezing rate remains constant throughout the entire solidification process, and they assume that the interdendritic puddle is subjected to maximum under-cooling in the very initial stage of dendritic growth. In the current work a more general case is discussed where the freezing rate changes during solidification.

Most of the experimental work done on the freezing of aqueous systems has been either with pure water or with very dilute solutions. Also a considerable portion of the effort has been directed towards the study of nucleation of ice<sup>16</sup>. Harrison and Tiller<sup>17,18</sup> have studied the crystallographic aspects of cell formation during growth of ice from water and dilute aqueous solutions. Knight<sup>19</sup> has discussed the curvature of growing ice crystals and the effects of the addition of small amounts of impurities. Himes<sup>20</sup> et al. describe a process for zone refining of sea water to freeze out pure ice under slow growth conditions. French<sup>13</sup> has measured dendrite spacings in dilute aqueous solutions as a function of freezing rates and the diffusivity of solutes.

The present study has been conducted on aqueous solutions embracing a very wide range of concentrations. The system variables examined include the nature of solute, its concentration and the presence of several solutes. Two different types of freezing systems were used: in one of them the entire liquid becomes supercooled before freezing starts, in the other, progressive solidification takes place from a chill. The effects of changing freezing rates have been examined in the latter system.

In addition, the effects of external magnetic and electric fields on the dendritic pattern of ice have been studied. Magnetic<sup>21-23</sup> and electric fields<sup>24-27</sup> have been reported to affect the solidification phenomena in a variety of freezing mediums. The approach so far has been mainly experimental without many theoretical correlations. The majority of these observations have been on supersaturated solutions

with slow growth rates. In the present study, fairly high growth rates have been used and various possible types of field have been explored. The possible interactions of external fields with dendritic growth are analyzed in the next section in connection with the specific properties of aqueous solutions and ice.



## II. THEORY

(1) Mass Transport:

In the freezing of aqueous solutions, the plane interface breaks down into parallel plates of ice to maintain the solute concentration gradient at the interface below a certain maximum. Further growth takes place by the extension of these plates and their simultaneous increase in thickness to consume the interdendritic liquid. An analysis of mass transport events in the interdendritic liquid between two growing plates is presented here. The understanding of solute distribution in this zone is important, since it governs the stability of the plate surfaces. Most analyses on the redistribution<sup>28-32</sup> of a solute have been for a case when the solute is being rejected into a large volume of liquid ahead of a plane interface. In the present situation the solute is being manufactured on both sides of a finite channel of liquid; in addition, the sides are simultaneously moving to the center of the channel.

Figure 4 represents two adjacent plates of ice growing into the interdendritic liquid. The solute rejected at the two interfaces ( $|x| = l$ ) moves toward the center of the puddle ( $x = 0$ ) giving rise to a concentration gradient in the liquid. The concentration difference ( $\Delta C$ ), between the center ( $C = C_0$ ) and the extremes ( $C = C_l$ ) of the puddle gives rise to the constitutional supercooling ( $\Delta T$ ) of the

liquid (Figure 5). Temperature gradients in the liquid have been assumed to be negligible since the distances considered are of the order of few microns. The concentration profiles, and therefore the constitutional supercooling in the interdendritic liquid, changes as solidification progresses (Figure 6). With a fixed coordinate system (Figure 4), the change in solute concentration on the liquid will be governed by the Ficks Second Law:

$$\frac{\partial C}{\partial \theta} = D \frac{\partial^2 C}{\partial x^2} \quad (1)$$

It is extremely difficult to obtain a rigorous solution of this partial differential equation for the present case because of the lack of knowledge of the transient boundary conditions. However, the absence of side branches, except at very high concentrations, suggests that all through the growth cycle the supercooling in the interdendritic liquid never exceeds the maximum permissible value. This implies that the concentration gradients in the liquid remain very small, because all the evidence up to now indicates that the permissible constitutional supercooling is of the order of one tenth<sup>12,13,14</sup> of a degree centigrade. The concentration differential ( $\Delta C$ ) therefore appears always to remain under a very small fraction of a mole per cubic centimeter. Since this is very small compared to the increase in the average concentration\*

---

\* 1.  $C_a$  represents the average solute concentration in the puddle, since  $\Delta C$  is very small  $C_a \approx C \approx C_0$

2.  $C_a$  is almost equal to the initial liquid concentration  $\bar{C}$  at the start of freezing; it rises to the eutectic composition or higher during growth.

of the liquid (Figure 6), the increase in concentration at different points in the liquid can be considered independent of its location.

This boundary condition can be expressed as:

$$\frac{\partial C}{\partial \theta} \neq \psi(x) \quad (2)$$

According to this condition, Equation (1) can be simplified to the following form:

$$\frac{dC}{d\theta} = D \cdot \frac{d^2 C}{dx^2} \quad (3)$$

Integrating (3) with respect to  $x$  gives:

$$\int D \cdot d \left( \frac{dC}{dx} \right) = \int \frac{dC}{d\theta} (dx)$$

or

$$D \left( \frac{dC}{dx} \right) = \frac{dC}{d\theta} \cdot x + C_1 \quad (4)$$

The integration constant,  $C_1$  is equal to zero, since the concentration gradient  $\left( \frac{dC}{dx} \right)$  is always zero at the center of the puddle. Therefore the relationship between the concentration gradient and the rate of change of concentration with time may be expressed as:

$$D \left( \frac{dC}{dx} \right) = \frac{dC}{d\theta} \cdot x \quad (5)$$

Equation (5) can be integrated to evaluate the difference in concentration between the center and the edges of the puddle as follows:

$$\frac{dc}{d\theta} \int_0^l x dx = D \int_{C_0}^{C_l} dc$$

$$\text{or, } \frac{dc}{d\theta} \cdot \frac{l^2}{2} = D (C_l - C_0) = D \cdot \Delta C \quad (6)$$

The average solute concentration in the interdendritic liquid  $C_a$  will increase as the amount of liquid in the puddle decreases in accordance with the relationship:

$$\left( \frac{\bar{C}}{C_a} \right)^{\frac{1}{1-K}} = f_l \quad (7)$$

where

$\bar{C}$  = starting composition of liquid

$K$  = distribution coefficient

$f_l$  = fraction liquid

Differentiation of Equation (7) gives the rate of change of concentration in terms of freezing rates:

$$\frac{dC_a}{d\theta} = \bar{C} \cdot (K-1) \cdot (f_l)^{K-2} \cdot \left( \frac{df_l}{d\theta} \right) \quad (8)$$

The width of the interdendritic puddle,  $2\ell$ , is related to the fraction solidified,  $f_s$ , in the following way:

$$f_\ell = \frac{2\ell}{L} = 1 - f_s \quad (9)$$

Substituting the values of  $\frac{dC}{d\theta}$  and  $\ell$ , from Equations (8) and (9) into Equation (6) and further rearranging of the terms gives the concentration difference  $\Delta C$  as:

$$\Delta C = \frac{L^2}{8D} \cdot (f_\ell)^K \cdot \bar{c} \cdot (K-1) \cdot \left(\frac{df_\ell}{d\theta}\right) \quad (10)$$

Making use of the relation  $m = \frac{\Delta T}{\Delta C}$ , the dendrite spacing can be written in terms of constitutional supercooling:

$$L^2 = \frac{8 \cdot \Delta T \cdot D}{m \bar{c} \cdot (1-K) \cdot (f_\ell)^K \cdot \left(\frac{df_s}{d\theta}\right)} \quad (11)$$

In aqueous solutions where  $K \approx 0$  and also  $\bar{c} = \frac{T_M - T_L}{m}$ , this relationship may be simplified to the following form:

$$L^2 = \frac{8 \cdot \Delta T \cdot D}{(T_M - T_L) \cdot \left(\frac{df_s}{d\theta}\right)} \quad (12)$$

This equation implies that for a fixed value of supercooling the square root of the dendrite spacing is directly proportional to the solute diffusivity and inversely proportional to the initial concentration of the liquid and the freezing rate. However, this equation can be interpreted in a different way, that is for a fixed value of dendrite spacing, the supercooling increases directly with the initial solute concentration and the freezing rate, and inversely with the solute diffusivity.

A relation between the cooling rate and the freezing rate is obtained from the equilibrium relationship.

$$1 - f_s = \frac{T_M - T_L}{T_M - T} \quad (13)$$

Equation (13) on differentiation gives:

$$\frac{df_s}{d\theta} = - \frac{(T_M - T_L)}{(T_M - T)^2} \cdot \left( \frac{dT}{d\theta} \right) \quad (14)$$

The dendrite spacing can be written in terms of the cooling rate as follows:

$$L^2 = - \frac{8 \cdot \Delta T \cdot D \cdot (T_M - T)^2}{\left( \frac{dT}{d\theta} \right) \cdot (T_M - T_L)^2} \quad (15)$$

(2) Unidirectional freezing of a solution from a constant temperature chill:

Unidirectional growth from a constant temperature chill has been used as a means to obtain varying freezing rates, and also to detect the effects of other solidification variables. The solution at its liquidus temperature is brought in contact with a flat bounding surface of a relatively large mass of copper\* which is kept cool by freezing mixtures. This immediately sets up temperature gradients in the liquid (Figure 9), accompanied by the formation of a layer of solid next to the chill; the layer of solid grows larger with time in accordance with the temperature pattern. Growth patterns in pure metals under such conditions have been analyzed by several workers<sup>33</sup>. In solutions the situation is complicated by the fact that the latent heat of fusion is evolved over a range of temperatures, which gives rise to a solid plus liquid region under temperature gradients (Figure 7). In order to understand the solidification events in detail, a complete knowledge of thermal conditions of the system is necessary.

The temperature distribution in the system will be according to Fourier's Law of heat conduction:

$$\frac{\partial T}{\partial \theta} = \alpha \frac{\partial^2 T}{\partial y^2} \quad (16)$$

---

\* Calculations in Appendix III show that under such conditions the chill surface remains practically at the same temperature.

The particular solution to this equation for freezing of a pure component is generally of the error function type. In the present case, where freezing takes place over a range of temperatures, an attempt will be made to describe the temperature distribution by a combination of several error function equations. In view of the growth conditions, (Figures 8 and 9) it appears that the actual temperature distribution can be reasonably well approximated by a combination of two error function equations describing the conditions in different temperature regions. This in effect implies that for heat transfer analysis the entire material ahead of the chill is approximated by a combination of two zones of constant specific heats. Since the freezing events at the start of solidification are most important, the specific heat of one of the zones will be taken as equal to the effective specific heat of the solution just below the liquidus temperature. Figure 8 shows the exact form of the approximation; the material above the temperature  $T_s$  is referred to as Zone II and that below  $T_s$  is Zone I. The error function equations describing the temperature profiles in each zone (Figure 9) are of the following form:

$$T - T_i = A \operatorname{erf} \frac{y}{2 \sqrt{\alpha_{I\theta}}} \quad \dots \dots \text{Zone I} \dots \dots \quad (17)$$

$$T - T_L = B \operatorname{erfc} \frac{y}{2 \sqrt{\alpha_{II\theta}}} \quad \dots \dots \text{Zone II} \dots \dots \quad (18)$$



where  $\alpha_I$  and  $\alpha_{II}$  are the thermal diffusivities in the two zones. The evaluation of the constants  $T_s$ ,  $C_p^{II}$ ,  $A$ ,  $B$ ,  $\alpha_I$  and  $\alpha_{II}$  is illustrated in Appendix II for the particular case of 1 N potassium chloride solution. The results from both zones are combined to give the complete cooling curves at different distances from the chill surface (Figure 10). These temperature distributions can be transformed into a description of freezing events by making use of the equilibrium relationship (Equation 13). The results are following:

$$\frac{T_L}{1-fs} = T_i + A \operatorname{erf} \frac{y}{2\sqrt{\alpha_I\theta}} \quad \dots \dots \text{Zone I} \dots \dots \quad (19)$$

$$\frac{T_L}{1-fs} = T_L + B \operatorname{erfc} \frac{y}{2\sqrt{\alpha_{II}\theta}} \quad \dots \dots \text{Zone II} \dots \dots \quad (20)$$

Figure 11 shows the progress of freezing at different distances from the chill for 1.0 N potassium chloride solution. Freezing rates at different distances from the chill, obtained by differentiation of Equations (19) and (20) are of the following form:

$$\left(\frac{dfs}{d\theta}\right)_y^I = \frac{A y}{2 T_L \sqrt{\alpha_I}} \cdot \frac{(1-fs)^2}{\theta^{3/2}} \cdot \frac{2}{\sqrt{\pi}} \cdot e^{-\left(\frac{y}{2\sqrt{\alpha_I\theta}}\right)^2} \quad (21)$$

$$\left(\frac{df_s}{d\theta}\right)_y^{II} = - \frac{B y}{2 T_L \sqrt{\alpha_{II}}} \cdot \frac{(1 - f_s)}{\theta^{3/2}} \cdot \frac{2}{\sqrt{\pi}} \cdot e^{-\left(\frac{y}{2 \sqrt{\alpha_{II} \theta}}\right)^2} \quad (22)$$

These freezing rates are complex functions of  $\theta$  and  $f_s$ . A numerical computation for 1.0 N potassium chloride solution (Figure 12) shows that the freezing rate at a fixed distance from the chill starts out at a low value, goes through a maximum and then falls off during the freezing cycle. Equating the second derivative of  $f_s$  to zero shows that at all distances from the chill, the freezing rate goes through a maximum at a fixed stage of solidification when  $f_s = f_s^M$ . This also implies (Equation 20), that the time  $\theta^M$  at which a particular level experiences the maximum freezing rate is proportional to the square of its distance from the chill:

$$\frac{y}{\sqrt{\theta^M}} = C_2 \quad (23)$$

where  $C_2$  is constant.

By substituting  $f_s = f_s^M$  and  $\theta = \theta^M$  on the right hand side of Equation (22), one obtains the value of the maximum freezing rate at any level as:

$$\left(\frac{df_s}{d\theta}\right)_y^M = - \frac{B}{2 T_L \sqrt{\alpha_{II}}} \cdot \frac{1}{\theta^M} \cdot \left(\frac{y}{\sqrt{\theta^M}}\right) \cdot (1 - f_s^M) \cdot \frac{2}{\sqrt{\pi}} \cdot e^{-\left(\frac{y}{2 \sqrt{\alpha_{II} \theta^M}}\right)^2} \quad (24)$$

Collecting all the constants in the Equation (24) into a single constant,  $C_3$ , one gets:

$$\left(\frac{dfs}{d\theta}\right)_y^M = \frac{C_3}{e^M} \quad (25)$$

A combination of Equations (23) and (25) gives the maximum freezing rate as a function of distance from the chill:

$$\left(\frac{dfs}{d\theta}\right)_y^M = \frac{C_3 C_2^2}{y^2} \quad (26)$$

The results of this analysis can be summarized in the following sentences:

- (1) When an aqueous solution at its liquidus temperature is presented to a constant-temperature chill surface, the liquid at each level is subjected to a spectrum of freezing rates.
- (2) The freezing rate at each level starts out at low values, goes through a maximum and then falls off, during the freezing cycle.
- (3) The spectrum of freezing rates is different at different levels, and the maximum freezing rate at each level is inversely proportional to the square of its distance from the chill.
- (4) The total freezing time at any particular level increases with its distance from the chill.

### (3) Diffusion in Single and Mixed Electrolyte Solutions:

In the diffusion of single electrolytes<sup>5</sup> the two component ions move in the same direction, down the chemical potential gradient. In addition, the anions and cations are obliged to move in pairs to conserve overall electrical neutrality. The resultant electrolytic mobility is therefore a compromise between the mobilities of the component ions. However on a microscopic scale these different mobilities create short-range electric fields in the electrolyte which supplement the chemical potential gradient and therefore affect the diffusion. Table VI presents diffusion data on some electrolyte solutions.

Diffusion in mixed electrolytes<sup>5</sup> is complicated because there are several ways of satisfying the requirement of electrical neutrality. In addition, there is a mutual interaction between different electrolytes affecting both the chemical and electrical potential gradients of any individual electrolyte. The interactions depend upon the nature and the concentrations of the constituent electrolytes. Gosting<sup>34,35</sup> and his associates have measured the direct and cross diffusion coefficients for several ternary combinations from the family NaCl-KCl-LiCl-H<sub>2</sub>O. The fluxes of individual electrolytes are given in terms of the concentration gradients of both electrolytes:

$$J_1 = -D_{11} \left( \frac{\partial c_1}{\partial x} \right) - D_{12} \left( \frac{\partial c_2}{\partial x} \right) \quad (27)$$

$$J_2 = -D_{21} \left( \frac{\partial c_1}{\partial x} \right) - D_{22} \left( \frac{\partial c_2}{\partial x} \right) \quad (28)$$

where  $J_1$ ,  $J_2$  are the fluxes of two electrolytes and  $\left( \frac{\partial c_1}{\partial x} \right)$ ,  $\left( \frac{\partial c_2}{\partial x} \right)$  are their concentration gradients,  $D_{11}$  and  $D_{22}$  are the main diffusion coefficients,  $D_{12}$  and  $D_{21}$  are the cross diffusion coefficients. Table VI presents the measured values of these coefficients for some electrolyte solutions.

Fluxes of individual electrolytes can be calculated by substituting the values of measured diffusion coefficients and picking suitable values for the gradients. It turns out that during simultaneous diffusion the fluxes of different electrolytes remain different because their mutual interactions are relatively small. This is reflected by the low values of the cross diffusion coefficients. For most combinations in question the flux of a fast-moving electrolyte is further increased or remains constant on addition of a slowly moving electrolyte. Similarly a slowly moving electrolyte is usually further decelerated or remains unaffected on addition of a fast moving electrolyte. A solute like potassium chloride does not affect the movement of other electrolytes appreciably, because its anions and cations move at almost the same speed.

The diffusion in electrolyte mixtures can be treated in terms of the movements of individual ions. Previous studies<sup>36,37</sup> show that a fast-moving ion like  $H^+$  is further accelerated in the presence of other slowly moving cations. Gosting<sup>34</sup> has presented relationships for the diffusivities of individual ions in a binary electrolyte mixture with

common anion. He points out that in a ternary mixture of type NaCl-KCl-H<sub>2</sub>O the same diffusivity values describe the motion of individual cations (K<sup>+</sup> and Na<sup>+</sup>) as well as that of entire electrolyte molecules (KCl and NaCl).

(4) The Effect of Fields on the Freezing of Aqueous Solutions:

An external electric or magnetic field can interact with the freezing aqueous solution in the following ways:

(a) The Effect of Fields on the Motion of Species in the Liquid:

The force exerted on a moving charged particle by magnetic and electric fields is given by Lenz's Law:

$$\vec{F} = q (\vec{E} + \vec{V} \times \vec{B})$$

where

$\vec{F}$  = Force on a charge of  $q$  coulombs moving with a velocity  $V$ .

$\vec{E}$  = Electric Field, intensity vector

$\vec{B}$  = Magnetic Induction

$\vec{V}$  = Velocity of a particle relative to the magnetic field.

This force can affect short-range movement of ions as well as their mass flow. Directional magnetic and electric fields change the course of Brownian jumps of ions and, at the same time, restrict the random jumps to certain preferred planes. Another mechanism by which the mobility of ions can be influenced is through the interaction of external fields with the electric fields generated

in the freezing system. In any diffusional process involving an ionic aqueous solution, low-order electric fields are developed in the liquid<sup>5</sup>. Moreover, surprisingly high potential differences are reported<sup>38</sup> to exist at the ice-liquid interface during freezing. This indicates that external fields may change the character of the ice-liquid interface.

Considering the magnetic fields in particular, it appears that a stationary field can exert appreciable Lenzs force if the relative velocity of the ion in question is sufficiently high. Gilliland<sup>39</sup> has demonstrated this principle by bringing about partial separation of solutes from sea water streams flowing between the magnet poles. For the same reasons an oscillating magnetic field appears to be more promising than stationary fields. However, a non-uniform stationary magnetic field can create potential gradients in the liquid and cause ion migration perpendicular to the planes of constant field intensity. It therefore appears that a suitably applied magnetic field can affect the motion of ions in a solution. Kibardin<sup>40</sup> confirms that in general particles in a electrolytic solution move perpendicular to the electrophoretic motion under the influence of a magnetic field.

Electric fields have been used to cause directional movement of impurity ions and thereby change the solute distribution pattern during the solidification of metals<sup>41</sup> and semiconductors<sup>42</sup>. This particular technique of field freezing,<sup>41,43</sup> is not directly applicable to individual ions in an aqueous electrolyte, since it will lead to charge separation.

However, one can affect the diffusional characteristics of the electrolyte molecule as a whole. Ole Lamm<sup>44</sup> has dealt with the theoretical aspects of this problem and has shown that electrodiffusion phenomena can change the diffusivities of electrolytes by as much as 100%, depending upon the characteristics of the field.

A combination of electric and magnetic fields appears most potent for moving ions in an aqueous solution. Rao<sup>45</sup> has demonstrated the motion of particles by spraying powder on an electrolyte under the influence of oscillating electric and magnetic fields.

#### (b) Effect of Field on the Structure of the Liquid

External electric and magnetic fields can influence the structure and short-range order in the liquid solution because of the dipole characteristic of the water molecule. Piccardo<sup>46</sup> attributes a change in the surface tension of water, in the presence of an external magnetic field, to a change in its structure. Mineko<sup>47</sup> et al. show that a magnetic field changes the structure and physicochemical properties of water.

#### (c) Effects Due to Differences in Susceptibilities and Permeabilities of Ice and Aqueous Solutions:

Since the susceptibility of water is higher<sup>48,49</sup> than that of ice, application of an external magnetic field would change



the volume free energy<sup>50</sup> of the liquid-solid transformation. This would change both the nucleation and the growth characteristics of the ice. Even though the susceptibility differences involved are small, a computation shows that the formation of ice will be favored in the presence of a magnetic field. In addition, the fact that ice is magnetically anisotropic<sup>51</sup> would cause a preference for certain crystalline orientations<sup>22</sup>.

Similar effects would be produced upon application of an electric field since the dielectric constant<sup>49,52</sup> of ice is about 20% higher than that of water. When electrolytic solutes are present, this difference is further increased since they lower the permeability of water<sup>5</sup>.

#### (d) Conclusions:

It appears from the above discussion that both magnetic and electrical fields have the potential to alter the solidification pattern of aqueous solutions by changing both nucleation and growth conditions. However, it is not possible to calculate quantitatively the magnitude of these individual effects and their interactions. The question of how these factors manifest themselves in the final structure, therefore, remains to be answered by actual experimentation.

### III. EXPERIMENTAL PROCEDURES

#### 1. Freezing Systems:

(a) Freezing of Droplets:- This technique consists of immersing small droplets of aqueous solution into a large quantity of a cold organic liquid (20% kerosene, 80% mineral oil). The organic medium is kept cool by either placing the entire setup in a cold chamber or by means of cooling mixtures. The relative density and the viscosity of the organic liquid are such that the aqueous solution droplet sinks slowly through it. The droplet is therefore cooled by a constant temperature medium throughout its descent through a tube full of organic liquid. The droplet remains perfectly spherical due to surface tension forces.

The size of the droplet and the ratio of its thermal diffusivity to that of medium are such that the temperature gradients within the droplet during freezing are negligible, and the rate of solidification is substantially uniform throughout the specimen. Droplet diameters are typically of the order of 0.2 - 0.3 inches. The principal advantage of maintaining uniformity of freezing conditions is that the resulting dendrite spacings are uniform from the surface to the center of the droplet. The chief disadvantage of the droplet system, especially when field effects are being studied, is that no satisfactory method could be evolved for indexing or maintaining the orientation of the droplet during freezing.

The freezing time of the droplet<sup>13</sup> is proportional to the square root of its diameter at any given initial temperature of the organic coolant. Moreover the freezing rate remains practically the same from the beginning to the end of solidification. The frozen droplet at the end of its descent is scooped out and its diameter measured. It is then sectioned to a thin slice for microscopic examination.

(b) Unidirectional Ingot Freezing System:

The setup consists of a calibrated tygon tube mounted on a cylindrical copper chill. The chill is kept cool by means of freezing mixtures (dry-ice + acetone or ice + brine). Aqueous solutions, pre-cooled to their liquidus temperature are poured into the tygon tube. A layer of solid immediately forms next to the chill and then grows into the solution. Ahead of the solid zone there is a two-phase (solid + liquid) zone; the movement of the boundary between the two zones is easily observed through the tubing (Figure 13). After the specimen freezes to a desired height, it is removed from copper chill and the tygon mold is stripped out. Longitudinal and transverse sections are cut out at suitable places for micrographic examination.

It has been shown in a previous chapter that for such a system, the freezing rate varies from point to point in the specimen. Unless if otherwise stated most of the micrographs in the text represent transverse sections perpendicular to the growth direction. The chill temperature and the distance from the chill are the indexes of the freezing rates. The unidirectional dendritic pattern facilitates spacing

measurements as well as the indexing of orientation effects on the application of external fields.

## 2. Specimen Preparation and Micrography:

Specimens in the form of a thin slice are mounted on a transparent glass slide by freezing small amounts of water around its periphery. They are then polished on a series of emery papers; the final finishing is done on a soft tissue paper. Exposure of polished surface to cold dry air for several hours etches the ice-brine boundaries and improves the contrast. A Leitz Biological microscope was used for structural observations; photography was done by mounting a 35 mm Exacta camera on the eyepiece tube. Light transmission microscopy was found to be the most satisfactory technique for observing the dendritic structure, its only limitation being the need for thin specimens. Some of the early work was also done using back reflection technique which was simpler to implement but brought out much less structural detail.

The photomicrographs are enlarged to a convenient size, and dendrite spacing measurements are taken directly from the prints. Final magnifications were determined by photographing millimeter grids. Specimen preparation and photography was done in cold chambers at  $-40^{\circ}\text{C}$ . Some attempts have been made to photograph the dendritic interface directly during growth, but the optics of this system could not be perfected. An example of such a photograph taken during the freezing of a unidirectional specimen is shown in Figure 19.

### 3. Application of External Fields:

#### (a) Magnetic Fields:

(1) Low Static Fields:- Relatively weak magnetic fields were applied, using permanent magnets. Field strengths from 1 to 4.5 kilogauss were obtained; the field strength was changed by varying the pole gaps by the use of soft iron tabs. In the droplet freezing system, fields were applied by containing the liquid organic coolant in a cylindrical glass tube and moving the permanent magnet outside the tube in such a way that the droplet was always kept between the magnet poles (Figure 14). In the unidirectional system, the magnet was placed above the freezing bath so that the entire tygon mold was between the pole pieces.

(2) High Static Fields:- High magnetic fields ranging up to 50 kilogauss were generated in the core of a Bitter Solenoid at the National Magnet Laboratories in Cambridge. To make droplets under the influence of such a field, organic medium was cooled by an ice-brine mixture and the entire freezing assembly was placed in the core of the magnet (Figure 15). Similarly with the unidirectional system the entire freezing assembly had to be placed in the core. Styrofoam insulations were used to avoid any heat transfer from the magnet. Figures 16 and 17 show the arrangements used to apply fields parallel and perpendicular respectively to the growth direction.

(3) Non-uniform Fields:- With small permanent magnets the field gradients are produced by sharply pointed pole pieces, but the region of

steep field gradients thus obtained is very small. Even with larger magnets, it is extremely difficult to expose larger sections of the freezing specimen to gradients. In the Bitter Solenoid this field drops off from the center of the core to its ends, giving rise to gradients up to 3 kilogauss per centimeter. A unidirectional freezing system is subjected to these gradients merely by shifting the assembly away from the center of the core.

(4) Oscillating Fields:- Periodic relative movement of the specimen and the magnetic field was produced by mechanical and electrical techniques. Low-frequency oscillations were produced by mechanical vibration of a permanent magnet, and a field oscillation of 60 cycles per second was obtained with an electromagnet producing fields up to 6 kilogauss. Oscillating fields were applied to the droplet freezing system by placing the electromagnet around the tube containing the organic medium and always maintaining the drop in the field. Figure 18 shows an arrangement for applying oscillating fields perpendicular to the growth direction in the unidirectional scheme. Oscillating fields were applied parallel to the growth direction by placing the electromagnet coil horizontally around the tygon mold.

(b) Electrical Fields:

Initial attempts to apply electrical fields involved placing electrodes in the freezing solution. This method was not very successful, because aqueous solutions undergo electrolysis at very low voltages. Later on, fields were applied by placing the electrodes outside the

freezing system, the field permeating through the air gaps and other dielectrics. Even with such an arrangement only high frequency fields can be applied; otherwise, charge separation will generate an electric potential in the solution which will annihilate the applied field. The frequency should be higher than the critical value above which the solution behaves as a dielectric. Fields were applied to droplet freezing system, by placing long copper electrodes in the organic medium and allowing the drop to descend between the electrodes. For the ingot system, shorter electrodes are placed just outside the tygon tubing. The electrodes in both cases are connected to a low - power, high frequency oscillator.

## IV. RESULTS AND DISCUSSION

1. General Character of the Ice-Brine Aggregate Obtained on Freezing  
Of Aqueous Solutions:

Under the freezing conditions used in the present work, the solute rejection accompanying the solidification of aqueous solutions causes the breakdown of the plane interface into plate-shaped projections. Further solidification is accomplished by the length wise growth of these plates and their simultaneous increase in thickness. Due to this increase in thickness the liquid entrapped between the plates continues to be enriched in the solute until it precipitates as a salt-rich phase, marking the end of the solidification process.

The final structure, therefore, consists of groups of parallel plates of ice with salt entrapped between these plates. The crystallographic orientation of the plates within a group is the same, but the individual groups are randomly oriented with respect to each other. In Figure 20, a photograph of a section taken with polarized light, the parallel dendrites within a group show the same polarization color, but different groups show different colors. The dark region between the neighboring ice plates is the salt-rich phase. It appears that eutectic divorcement takes place under these growth conditions; that is, after the interdendritic liquid reached the eutectic composition, instead of the simultaneous appearance of two phases, only ice continued to separate on the already-present ice plates. This resulted in the



precipitation of pure salt in the interdendritic regions, rather than the salt hydrate eutectic. This hypothesis is substantiated by the relatively small volume of the interdendritic phase.

The parameters characterizing a group of ice-brine layers are schematically represented in Figure 21. In transverse sections as in Figure 20, two dimensions of the plates namely their width,  $W$ , and thickness,  $F$ , can be observed. The dimension most uniform, and most characteristic of the freezing conditions is the dendrite spacing,  $L$ , the distance between the centerlines of neighboring plates. The dendrite spacing is also an approximate measure of plate thickness,  $F$ , since the thickness of salt pockets,  $P$ , is usually quite small. The area occupied by a particular group of dendrites in the entire aggregate, generally referred to as grain size, depends upon the plate width,  $W$ , the group width,  $B$ , and the height of the group,  $H$ . However with very slow growth rates the crystals of ice are no longer arranged in distinct groups, and the neighboring plates are randomly arranged with respect to each other (Figure 22).

The brine, in addition to being present in parallel interdendritic regions, is sometimes found in the form of large irregular segregates existing between neighboring groups of dendrites (Figure 23). Tiller<sup>56</sup> has suggested that grain boundaries can act as sites for solute segregation. However, in aqueous solutions, this macrosegregation is related to the fact that ice expands on freezing; the growing plates physically displace the brine from the interdendritic puddles into the grain boundary grooves. These segregates are more often found under slow

growth rates, probably because more time is available for the process to operate and due to the larger volumes of liquid to be frozen in the interdendritic regions.

## 2. Structures Obtained with Varying Freezing Rates:

In unidirectional ingots frozen from a constant temperature chill the dendrite spacing increases with distance from the chill surface. Figures 24 through 27 show transverse sections of a particular zone of an ingot at increasing distances from the chill; the ingot was made from 1.0 N potassium chloride solution against a chill at  $-70^{\circ}\text{C}$ . Examination of successive sections enables one to follow a particular group of dendrites through the entire height of the ingot. Careful scrutinizing of sections such as these, as well as of some longitudinal sections, has indicated quite conclusively that the mechanism for dendrite spacing change is by the divergent growth of neighboring plates. In other words, the plates instead of lying perfectly parallel to one another diverge slightly with increasing distance from the chill. The divergence of plates is spatially accommodated by the simultaneous decrease in the number of groups per unit area with increasing distance from the chill.

Out of the large number of groups that are produced next to the chill by very rapid, initial freezing only a few survive at larger distances from the chill. Certain favorably oriented groups continue to become larger with progressive growth while others become eclipsed. A preferred group gets larger principally by the divergent growth of its

dendrites; in addition, fragments gradually grow to the normal width of the group by consumption of dendrites from a neighboring group which is unfavorably oriented. The fragments of newly added plates at the extremes of the central group in Figure 26 have grown to the normal width of the group in Figure 27 and newer fragments have been added.

In general, during unidirectional freezing; from a constant-temperature chill, in addition to the dendrite spacing, the dendrite width and the group size also increases with the distance from the chill. Theoretical analysis has shown that in this freezing system the freezing rate varies from point to point in the ingot, and also with passage of time at a given location. The average freezing rate decreases with increasing distance from the chill. Qualitatively, this implies that during progressive solidification the dendritic structure adjusts itself; specifically the dendrite spacing increases, along the length of the ingot, under the influence of decreasing freezing rates. In terms of surface area this means that even after the initial breakdown of a plate interface, if the solute rejection rate decreases, the interface reduces its area. In other words the interface maintains the minimum surface area necessary to solve the problem of solute diffusion.

The capacity of the interface to change its contours in accordance with changing freezing conditions has also been verified for the reverse conditions, where the freezing rate increases. With the unidirectional freezing set up, the increase in freezing rate was achieved by starting with a low chill temperature of  $-20^{\circ}\text{C}$ , and, after some solidification

had taken place, lowering the chill temperature to  $-70^{\circ}\text{C}$ . Figures 28 and 29 show transverse sections of an ingot frozen in this manner at distances 0.8 cm and 1.1 cm from the chill. It may be seen that coarse irregular dendrites (Figure 28) arrange themselves in regular groups with finer spacing (Figure 29) thereby decreasing the surface area, when the freezing rate is increased.

Of all the structural parameters of an ingot which change with increasing distance from a constant-temperature chill, only the dendrite spacing lends itself to quantitative measurements. In both single and mixed solute systems studied so far, the dendrite spacing has been found to increase linearly with the distance from the chill (Figures 30, 33, 34, 40, 41, 42). It has been shown in the previous section that each level in the ingot is subjected to a spectrum of freezing rates (Figure 12); the maximum freezing rate at any level is inversely proportional to the square root of its distance from the chill. The dendrite spacing at any level in the ingot is therefore inversely proportional to the square root of the maximum freezing rate at that level (Figure 31). For 1.0 N potassium chloride ingot frozen from  $-70^{\circ}\text{C}$  chill, the exact relationship is following:

$$L = \frac{37}{\sqrt{\left(\frac{dfs}{d\theta}\right)_y^M}} + 48 \quad (29)$$

where the spacing  $L$  is in microns and the maximum freezing rate  $\left(\frac{dfs}{d\theta}\right)_y^M$  is in minutes<sup>-1</sup>.

The inconsistency of a finite dendrite spacing at an infinite freezing rate in the above equation is caused by the abnormal dendrite spacings observed in the immediate vicinity of the chill (Figure 30). The growth conditions right next to the chill are not clearly understood; they are probably different from those in the rest of the ingot because the solution in immediate contact with the chill gets highly supercooled before growth starts and also the chill temperature fluctuates in the beginning (Appendix III).

An examination of this result (Equation 29) in the light of the theory presented before (Equation 12) suggests that in a system subjected to a spectrum of freezing rates, the ultimate dendrite spacing is governed by the maximum freezing rate. In the ingot system this implies that freezing conditions at a critical instant of the freezing cycle are responsible for the final structure. A comparison of dendrite spacings in the ingot freezing systems and the droplet freezing system was made; the freezing rate in the former changes but the freezing rate in the latter remains practically constant during the entire freezing cycle. The dendrite spacings in the two systems were equal when the maximum freezing rate in the ingot system was equal to the constant freezing rate of the droplet system. This further confirms the decisive role of maximum freezing rate; it is equivalent to the freezing rate of constant rate systems with regard to the establishment of the final dendrite structure.

The physical mechanism by which the ultimate dendrite spacing is established at a critical stage in the freezing cycle however remains a mystery, especially in cases such as that of potassium chloride in which the maximum freezing rate occurs when 0.395 fraction of liquid had already solidified. There seem to be two possible ways in which this can be brought about. First the dendrite spacing changes during the freezing cycle, until the maximum in freezing rate occurs, and then remains constant at that value; or, second, the dendrite spacing corresponding to the maximum freezing rate is established at the very beginning of the cycle. The former seems to be physically impossible especially in the ingot freezing system; because of the different freezing rates at successive levels at the same time, this mechanism would necessitate very sharp bends in the plates, and also a change in the character of the bends with time. The possibility that the final spacing is established at the start of the freezing cycle implies an anticipation of the maximum freezing rate much before it takes place. Sections from those regions of the ingot where the freezing was interrupted show a gradual increase in the spacing just as in the regions where the freezing was complete; this gives some support to the anticipation mechanism.

The role of the maximum freezing rate can also be interpreted in terms of constitutional supercooling. Equation (12) shows that the interdendritic liquid is subjected to the maximum constitutional supercooling when the freezing rate is maximum. The present observations imply that the dendritic pattern is established in such a manner as to prevent the

interdendritic supercooling from exceeding a certain fixed value; this value seems to be independent of freezing rate. The mechanism by which this is brought about is not clear.

### 3. The Effect of Concentration on Dendritic Structures:

Dendrite spacing obtained on freezing aqueous solutions increases with an increase in the solute concentration. Figure 32 shows an increase in the dendrite spacing in the droplets with an increase in sodium chloride concentration. Sections of droplets from 0.2, 1.0 and 3.0 Normal sodium chloride solutions frozen under identical thermal conditions are shown respectively in Figures 35, 36, and 37. Similar effects of concentration have been observed in the unidirectional ingots frozen from potassium chloride (Figure 30), sodium chloride (Figure 33) and lithium chloride (Figure 34) solutions.

Solute concentration has been found to have a similar effect on dendrite spacings obtained on freezing of metallic solutions. Alexander and Rhines<sup>53</sup>, and Rohatgi<sup>14</sup> have reported an increase in dendrite spacing with copper content in aluminum-copper alloys. The only experiments in which dendrite spacing is reported to decrease with the solute concentration are those of Mondolfo<sup>54</sup> et.al. and Engler<sup>55</sup> et.al. Their results could be different either because of the crudness of their setup for evaluating freezing rates or because of their freezing system which involved the freezing of a crucible full of metal.

The results of the present study positively confirm that dendrite spacing increases with an increase in solute concentration.

In addition to increasing the dendrite spacing, increasing solute concentration also influences the surface character of the individual plates of ice. In freezing of very dilute solutions, the plate surfaces are extremely smooth, but as the concentration increases they become serrated, and with a still greater increase in concentration, distinct side branching of the primary plate elements occur. The dendritic morphology can be roughly classified in three categories corresponding to three concentration ranges, as shown in Figure 32 for sodium chloride solutions. Upto about 1.2 N sodium chloride solution, plates are perfectly smooth (Figure 35), from 1.2 N to 2.4 N the plates develop serrated sides (Figure 36), at normalities above 2.4 the serrations develop into distinct side branches on the original dendrite plates (Figure 37). The critical concentrations between the zones shown in Figure 32 correspond to a freezing rate of  $0.36 \text{ minutes}^{-1}$ . The extent of side branching in concentrated solutions decreases with increasing freezing rates as shown by Figure 38 which is a section from a droplet frozen from 3 N sodium chloride solution at a rate of  $0.72 \text{ minutes}^{-1}$ .

An increase in solute concentration would be accompanied by a rejection of increasing amounts of solute (Figure 7a). To maintain the solute build-up at the interface below a certain limit, a larger



surface area would be needed; and this corresponds to a smaller dendrite spacing. Equation (11) predicts that the spacing will be inversely proportional to the square root of the solute concentration provided that the other parameters remain the same. The fact that it varies in the opposite manner indicates conclusively that interdendritic supercooling increases with increasing salt concentration. Qualitatively, the increase in the supercooling is apparently large enough to override the increased solute buildup (Equation 12) and produce a net increase in the dendrite spacing. These observations imply that the activation barrier for the breakdown of liquid-solid interfaces by the growth of protrusions increases with increasing concentration.

Our present understanding of constitutional supercooling is not sufficient to arrive at this conclusion on theoretical grounds. Qualitatively, however, it appears reasonable to expect that the formation of an ice protrusion should be more difficult the larger the number of solute atoms to be pushed away. There have been very few actual measurements of constitutional supercooling to demonstrate this phenomenon by direct experimental means. However, Wienberg<sup>10</sup> and Chalmers report an increase of dendrite spacing with measured supercooling in case of very dilute metallic solutions.

All the direct and indirect evidence therefore suggests that the increase in spacing with concentration is due to an increase in permissible constitutional supercooling.

#### 4. Secondary Breakdown of the Primary Ice Dendrites:

Side branching and serrations are the result of a breakdown of primary ice plates due to excessive solute buildup ahead of them. It may be seen from Figure 6, that during growth, the overall concentration of the interdendritic liquid increases. This implies that the amount of solute to be rejected by the liquid and its capacity to withstand supercooling, increase simultaneously in the puddle as its volume decreases.

Instability will set in if at any instant the concentration gradients in the liquid exceed the maximum it can sustain; otherwise the plates will continue to grow with smooth surfaces until the end of solidification.

The effect of concentration on side branching (Figure 32) can be interpreted in the following way. It appears that in dilute solutions the capacity of the interdendritic liquid to withstand supercooling increases rapidly enough to take care of the increasing concentration gradients. This state of affairs prevails until the end of solidification, and therefore the final structure consists of smooth plates. At higher concentrations the situation appears to be different: at same stage of growth the high rates of solute rejection create sharper gradients than the puddle can sustain and thereby causing a further breakdown of plates. The cause of this reversal, in addition to the higher solute rejection rates, appears to be the larger primary dendrite spacings at higher concentrations. Higher dendrite spacings give rise to larger interdendritic puddles, necessitating the rejection of a larger amounts of solute in each puddle.

The results in Figure 32 can therefore be interpreted in terms of critical dendrite spacings; the instability in the interdendritic liquid sets in when the primary dendrite spacing exceeds a critical value. In the presence of a magnetic field, even though the critical concentration limits for side branching are shifted to lower values, the critical dendrite spacings remain practically the same. It seems that the magnetic field does not interact directly with the interdendritic liquid; the appearance of side branching at lower concentrations in the presence of a field is an indirect outcome of the increase in the primary spacing.

The decrease in the extent of side branching with faster freezing rates (Figures 37 and 38) is probably a consequence of the decrease in the primary dendrite spacing and the concomittant decrease in the amount of solute to be rejected in each interdendritic puddle.

The combined effects of solute concentration, dendrite spacing and freezing rate on side branching is further illustrated in unidirectional ingots. Neither very rapidly frozen sections (Figure 24) nor very slowly frozen sections (Figure 27) of the ingot show any side branching; only the sections frozen at intermediate rates (Figure 25) exhibit distinct side branches. At extremely slow growth rates there seems to be enough time for the concentration gradient in the interdendritic liquid to maintain itself below the instability limit; at very rapid rates, even though the concentration gradients have hardly any time to level out, the onset of instability is prevented because the primary spacings are so small.

### 5. The Effect of Solute Diffusivity on Dendrite Spacing:

Dendrite spacings have been measured for similar solutions of potassium chloride, sodium chloride and lithium chloride under identical freezing conditions (Figure 40). These three solutes have almost identical liquidus curves (Figure 39) but their diffusivities are different (Table VI). Figure 40 shows that for the same concentration of each solute, the dendrite spacing is larger the larger the diffusivity of the solute. This is in direct agreement with the theory since the faster the solute can move the smaller is the surface areas needed to solve its diffusion difficulty. However, the increase in spacing with diffusivity is not exactly linear as predicted by equation (12) probably because other parameters are slightly different for different solutes. Nevertheless, the qualitative increase in dendrite spacing with solute diffusivity is demonstrated by these results.

### 6. Solidification Structures from Mixed Solutions:

Solutions containing more than one solute freeze dendritically in the same manner as single salt solutions. The freezing of multicomponent solutions involves the simultaneous rejection of more than one solute species at the solid liquid interface. The following generalizations can be made about the dendritic structures in multicomponent systems on the basis of studies with some ternary solutions from the family  $\text{NaCl-KCl-LiCl-H}_2\text{O}$ . The structures obtained on freezing unidirectional ingots under the same conditions have been used as the basis of comparison

(Table V).

(1) If one solute is present in a larger concentration, than the other, it tends to govern the dendrite spacing. The presence of small quantities other solutes changes the spacing very little. If the secondary solute has a higher diffusivity than the principal solute, the dendrite spacing is increased, and vice versa (Figure 41).

(2) If two solutes are present in equal amounts, the resultant dendrite spacing lies in between the values obtained with individual solutions in which each solute is present alone at its same concentration (Figures 42 and 43). Microphotographs (Figures 44,45, 46) show that the dendrite spacing obtained from 0.1 N NaCl + 0.1 N LiCl solution is in between these obtained individually from 0.1 N NaCl and 0.1 N LiCl solutions.

(3) In solutions containing the same proportion of the two solutes, the spacing is larger the greater is the overall concentration (Figure 47).

The fact that the addition of a fast-moving solute to a solution increases the resultant dendrite spacing implies that the diffusion of the more slower moving solute is not the rate-controlling factor. The concentration and the diffusivities of each of the constituent solutes seem to affect the dendritic structure. It is interesting to note that the addition of a slowly-moving solute to a solution decreases the spacing, irrespective of the fact that the total solute concentration in the liquid

increases. However the effect of the total concentration in mixed solutions is demonstrated by the spacings obtained from equiproportion mixtures of sodium chloride and potassium chloride (Figure 47).

The dendritic structures in mixed solute systems do not seem to be related in a simple way (as in the case of single solute systems) to the diffusion coefficients measured in simple diffusion experiments. The results of such experiments show (Page 22) that two solutes move at different rates during simultaneous diffusion. In addition a slowly moving solute further accelerates the fast moving solute instead of **slowing** it down. These results fail to explain the present observations on dendrite spacing, where a mixture of two solutes effectively behaves as a single solute of intermediate diffusivity present in the same concentration as the principal solute.

The lack of correlation between the simple diffusion data and the dendritic structures obtained with mixed solutes is probably due to the fact that during solidification the conditions are changed; both the solutes have to diffuse away from a moving solid-liquid interface.

## 7. The Effect of External Fields on the Dendritic Pattern:

(i) Magnetic Fields: Since the effects of magnetic fields were found to differ in the droplet and the ingot freezing systems, they will be discussed separately.

(a) Effect on Structure in Droplets:

External magnetic fields increase the dendrite spacing for a given freezing rate in as much the same ways as does increasing the salt concentration. The effect of a magnetic field at different solute concentrations is demonstrated by curves A and B in Figure 32. Curve A presents the dendrite spacings observed in droplets of sodium chloride solutions frozen under the influence of a 4 kilogauss static magnetic field. The appearance of side branches at lower solute concentrations in the presence of a magnetic field is probably due to the higher primary dendrite spacings obtained with fields (page 44 ). A comparison of Figures 48 and 49 and Figures 50 and 51 shows the effects of a stationary magnetic field (4 kilogauss) on dendritic structure at different solute concentrations.

Similar effects were observed at different field intensities. However over the range 2 kilogauss to 40 kilogauss the structure does not seem to depend appreciably upon the intensity of the field.

(b) The Effects on Structure in Ingots:

External magnetic fields seem to have no measurable effect on the dendritic structures obtained on unidirectional growth from a chill. Experiments were conducted with stationary fields ranging from 2 kilogauss to 50 kilogauss, with oscillating fields (60 cycles per second) and with field gradients of the order of 3 kilogauss per centimeter. In all cases, the fields were applied both perpendicular and parallel to the growth directions (Figures 16, 17, and 18).

(c) Discussion:

It has been shown in Chapter II that there are several mechanisms by which an external magnetic field can affect the freezing of aqueous solutions.

The experimental observations indicate that magnetic fields increase the dendrite spacing in the droplet system but have no effect on the ingot freezing systems. The difference between the two systems is that in the former the entire liquid is supercooled before solidification starts, whereas in the latter, except near the chill, growth occurs by gradual cooling of the liquid ahead of the solid-liquid interface. In both systems, however, the liquid right next to the moving interface is constitutionally supercooled.

These facts suggest that a magnetic field affects dendritic structure in the droplet system because it affects the bulk supercooling of the liquid. Under the present growth conditions magnetic fields do not seem to affect measurably the constitutional supercooling or the movement of solute in the liquid. For this reason, magnetic fields do not affect the structure obtained with ingots. This hypothesis is further substantiated by the fact that both the droplet and the ingot freezing systems react identically to other variables, such as the freezing rates, the nature and concentration of the solute, which affect the constitutional supercooling and the diffusion conditions in the liquid.

Magnetic fields cause an increase in the dendrite spacing in the droplets probably because they facilitate the nucleation of ice.



The entire liquid is to be supercooled to a lesser degree in the presence of the field, to form a nucleus of ice. The less is the bulk supercooling the lower is the freezing rate<sup>8</sup> under similar thermal surroundings. Therefore, the reduction in the effective freezing rate in the presence of a magnetic field causes the observed increase in dendrite spacing under identical thermal conditions.

It seems worthwhile to mention at this point that most of the effects of magnetic field on solidification reported in the literature<sup>21,22</sup> have been observed in systems in which the entire liquid was supercooled. In addition, there are direct observations<sup>23</sup> on the promotion of nucleation in the presence of a magnetic field. The inference from the present study, that magnetic fields promote the nucleation of ice from aqueous solutions, can be caused by two mechanisms. First, due to the susceptibility differences the magnetic field will promote the formation of the ice phase. Second, the field probably facilitates the nucleation of ice by changing the structure of the liquid solution.

#### (ii) Electric Fields:

Preliminary experiments have been conducted on the effect of electric fields on the dendritic pattern with the droplet system. The fields used so far were of low voltage (3 volts/cm) and high frequency. The results obtained so far are inconclusive except for slight indications of a preferred orientation of the crystals along the direction of the field. Further investigations are needed, using higher voltages and covering a wider frequency range, for confirmation of these results.

## V. CONCLUSIONS

- (1) Binary and ternary aqueous solutions over a wide range of concentrations upon relatively fast freezing (above  $0.36 \text{ minutes}^{-1}$ ), produce groups of parallel plate-shaped dendrites of pure ice with salt entrapped between them. Within each group the plates have a common crystallographic orientation.
- (2) Under unidirectional growth conditions from a constant-temperature chill the solution at each level is subjected to a spectrum of freezing rates. The spectrum is different at each level and the final dendrite spacing at every level is inversely proportional to the square root of the maximum freezing rate.
- (3) Under progressive solidification, the dendrite spacing adjusts itself by the actual convergence or divergence of platelets, according to the changing growth conditions.
- (4) An increase in solute concentration causes an increase in dendrite spacing, and at relatively high concentrations further branching of primary dendrites takes place. The increase in spacing is due to the increase in the capacity of the liquid to sustain constitutional supercooling with an increase in solute concentration.
- (5) Side branching of primary ice platelets depends upon the concentration of solute, dendrite spacing, and the freezing rate; it occurs when the concentration gradients in the interdendritic liquid rise more rapidly than the capacity of liquid to sustain them.

(6) Under similar freezing conditions, the dendrite spacing is higher the more is the solute diffusivity.

(7) When more than one solute is present in the solution, the resultant dendrite spacing is governed by the concentration and the diffusivity of each of the solutes. In general the spacing is principally governed by the solute present in larger quantity. Addition of a slowly moving solute decreases the dendrite spacing, and vice versa.

(8) Externally applied static and oscillating magnetic fields cause an increase in the dendrite spacing, but only in freezing systems in which the entire liquid is supercooled before the initiation of growth. This effect of field is attributed to its capacity to promote nucleation of ice from a supercooled liquid.

## VI. SUGGESTIONS FOR FURTHER WORK

- (1) Theoretical work should be done to evaluate directly the magnitude of constitutional supercooling and to check its dependence on freezing variables which has been indirectly derived from the experimental results.
- (2) Closer observations of the dendritic pattern should be made during the actual solidification itself. Special emphasis, should be laid on observing the establishment of dendrite spacing when the freezing rate fluctuates during the process.
- (3) The significance of maximum freezing rate in establishing the final structure should be tested by subjecting the system to different freezing spectrums maintaining the same maximum.
- (4) Diffusivity values in mixed solutions should be calculated for diffusion ahead of a moving interface and a correlation be sought with the solidification structures.
- (5) Direct observations should be made on the effect of magnetic fields on the nucleation of ice. The effects of field on solidification structures should be examined at slower freezing rates than used in this study, especially when looking for any orientation effects.
- (6) The effect of electrical and combined electrical and magnetic fields, should be further investigated. Higher intensities and wider frequency ranges should be applied than those used in the present work.
- (7) Theoretical calculations should be made in order to evaluate the magnitudes of the various possible effects of fields on freezing systems.

## VII. APPENDIX I

Definitions of Symbols Used in the Text

|                    |   |  |
|--------------------|---|--|
| $T$                | = | temperature in degrees centigrade  |
| $T_M$              | = | melting temperature of ice = $0^{\circ}\text{C}$   |
| $T_L$              | = | liquidus temperature of the solution   |
| $T_E$              | = | eutectic temperature   |
| $T_a$              | = | actual temperature of interdendritic liquid  |
| $T_c$              | = | initial temperature of copper chill  |
| $T_i$              | = | temperature at the surface of the chill  |
| $T_s$              | = | temperature between Zone I and Zone II   |
| $T_o$              | = | a reference temperature = $-16^{\circ}\text{C}$  |
| $\Delta T$         | = | constitutional supercooling  |
| $C$                | = | solute concentration moles per litre   |
| $\bar{C}$          | = | initial concentration of the solution  |
| $C_l$              | = | concentration at the liquid solid interface  |
| $C_o$              | = | concentration at the center of interdendritic puddle                                     |
| $^{\circ}\text{C}$ | = | degrees centigrade   |
| $C_a$              | = | average concentration in the interdendritic puddle                                       |
| $\Delta C$         | = | concentration difference between the center and the extreme of the interdendritic puddle |
| $C_p$              | = | specific heat, calories per degrees centigrade per mole                                  |
| $C_p^L$            | = | specific heat of the solution  |
| $C_p^I$            | = | specific heat of Zone I next to the chill  |
| $C_p^{II}$         | = | specific heat of Zone II   |

- $C_p^{Cu}$  = specific heat of copper  
 $\alpha$  = thermal diffusivity in  $cm^2$  per minute  
 $\alpha_I$  = thermal diffusivity of Zone I  
 $\alpha_{II}$  = thermal diffusivity of Zone II  
 $\alpha_{Cu}$  = thermal diffusivity of copper  
 $K$  = thermal conductivity calories per degrees centigrade per centimeter per minute  
 $K_I$  = thermal conductivity of Zone I  
 $K_{II}$  = thermal conductivity of Zone II  
 $K_{Cu}$  = thermal conductivity of copper  
 $\rho$  = density  
 $\rho_I$  = density of Zone I  
 $\rho_{II}$  = density of Zone II  
 $\rho_{Cu}$  = density of copper  
 $L$  = dendrite spacing in microns  
 $W$  = dendrite width  
 $F$  = thickness of ice plate  
 $P$  = thickness of salt pocket  
 $l$  = distance of solid-liquid interface from the center of the puddle  
 $x$  = distance from the center of the interdendritic puddle  
 $y$  = distance from the chill surface, centimeters  
 $H_T$  = heat content at temperature  $T$  in calories per mole  
 $H_0$  = heat content at the reference temperature  $T_0$   
 $\Delta H_f$  = heat of fusion of ice calories per mole  
 $m$  = slope of the liquidus curve, degrees centigrade per mole

- $K$  = distribution coefficient  
 $f_s$  = fraction solid  
 $f_s^M$  = fraction solid when the freezing rate is a maximum  
 $f_l$  = fraction liquid  
 $\theta$  = time in minutes  
 $\theta_M$  = time at which the freezing rate is a maximum  
 $\left(\frac{df_s}{d\theta}\right)_y$  = freezing rate at a given distance from the chill, minutes<sup>-1</sup>  
 $\left(\frac{df_s}{d\theta}\right)_y^M$  = maximum freezing rate at a given distance from the chill  
 $\left(\frac{df_s}{d\theta}\right)^I$  = freezing rate in Zone I  
 $\xi$  = distance of  $T = T_s$  isotherm from the chill surface  
 $\beta$  = growth constant of  $T = T_s$  isotherm in Zone I =  $\frac{\xi}{2\sqrt{\alpha_I\theta}}$   
 $\gamma$  = growth constant of  $T = T_s$  isotherm in Zone II =  $\frac{\xi}{2\sqrt{\alpha_{II}\theta}}$   
 $D$  = diffusion coefficient centimeter<sup>2</sup> per minute  
 $D_{mm}$  = direct diffusion coefficients  
 $D_{mn}$  = cross diffusion coefficients  
 $J_m$  = flux of solute  $m$   
 $\vec{F}$  = force on a charged particle  
 $q$  = electric charge on a particle in coulombs  
 $\vec{E}$  = electric field intensity  
 $\vec{V}$  = velocity of the charged particle  
 $\vec{B}$  = magnetic induction  
 $A, B, C_1, C_2, C_3$  and  $E$  are different constants

## VIII. APPENDIX II

Calculation of Solidification Pattern when 1.0 N Potassium ChlorideSolution is Presented to a Chilled Surface at  $-70^{\circ}\text{C}$ :

The actual temperature distribution when a solution is presented to a cold chill, can be approximated by a combination of two distributions of the error function, Equations (17) and (18). The procedure for evaluating the constants of these equations is illustrated here for the particular case of 1.0 N potassium chloride solution freezing against a surface at  $-70^{\circ}\text{C}$ . In addition numerical computation of complex functions Equations (21) and (22), giving the freezing rates, has been done to illustrate the general character of solidification pattern.

Evaluation of  $T_s$  and  $C_p^{\text{II}}$  - For 1.0 N potassium chloride solution:

We determine, first of all, the temperature  $T_s$  dividing the two zones and the effective specific heats of the zones. The pertinent data for this particular solution obtained from the phase diagram (Figure 7) are following:

$$\bar{C} = 1 \text{ mole per litre} \quad T_L = -3.25^{\circ}\text{C} \quad T_E = -10.7^{\circ}\text{C}$$

$$T_M = 0^{\circ}\text{C} \quad m = 3.25^{\circ}\text{C Litres per mole}$$

The approximation line (Figure 8) in Zone II is tangent to the actual curve describing the variation in heat content at the liquidus temperature. A differentiation of equilibrium relationship (Equation 13) gives the rate of transformation at the liquidus temperature in the following form:

$$\left(\frac{df_s}{dT}\right)_{T=T_L} = - \frac{m\bar{C}}{(T_M - T_L)^2} = - \frac{1}{T_M - T_L} \quad (30)$$



Since the specific heat of zone I is taken as that of the solid ice-brine aggregate, the temperature at the zone boundary  $T_s$  effectively corresponds to the temperature at which the transformation would have ended if it had continued at the rapid rate at which it started. It is therefore estimated by an integration of Equation (30) in the following way:

$$\int_{T_s}^{T_L} dT = - (T_M - T_L) \int_{1.0}^0 df_s$$

$$\text{OR } T_s = 2T_L - T_M = -6.50^\circ\text{C} \quad (31)$$

The heat content of the solution below its liquidus temperature (Figure 9) can be described by the following equation:

$$H_T - H_0 = C_p^I (T - T_0) + (1 - f_s) \Delta H_f \quad (32)$$

where  $\Delta H_f$  is the latent heat of fusion of ice in equilibrium with the solution. It changes with temperature in the following fashion:

$$\frac{d\Delta H_f}{dT} = C_p^L - C_p^I \quad (33)$$

where  $C_p^L$  is the specific heat of the solution. A differentiation of equation (32) gives the rate of change of heat content with temperature as follows:

$$\frac{dH_T}{dT} = \frac{\Delta H_f}{(T_M - T)^2} + C_p^I \cdot f_s + C_p^L \cdot (1 - f_s) \quad (34)$$

The specific heat of Zone II is the effective specific heat of the solution at its liquidus temperature:

$$C_p^{II} = \left( \frac{\partial H}{\partial T} \right)_{T_L} = \frac{\Delta H_f}{T_M - T_L} + C_p^L \quad (35)$$

Since the thermal constants of the solution will not be very different from that of water, a substitution of  $\Delta H_f$  as 1436 calories per mole and of  $C_p^L$  as 18 calories per mole gives the following result:

$$C_p^{II} = 460 \text{ calories per mole} \quad (36)$$

#### Evaluation of Temperature Distributions:

The temperature distributions in the two zones are given by the equations:

$$T - T_i = A \operatorname{erf} \frac{y}{2\sqrt{\alpha_I \theta}} \quad (17)$$

$$T - T_L = B \operatorname{erfc} \frac{y}{2\sqrt{\alpha_{II} \theta}} \quad (18)$$

The following boundary conditions can be used to evaluate A and B: (1) The chill surface remains at the same temperature during freezing:  $T = T_i$  at  $y = 0$  (Appendix III). (2) The  $T = T_s$  isotherm is common to both zones and moves away from the chill at a parabolic rate with growth constants  $\beta$  and  $\gamma$  where:

$$\beta = \frac{\epsilon}{2\sqrt{\alpha_I \theta}} \quad (37)$$

$$\gamma = \frac{\epsilon}{2\sqrt{\alpha_{II} \theta}} \quad (38)$$

Substituting the above boundary conditions, the temperature profiles can be written in the following form:

$$\frac{T - T_i}{T_s - T_i} = \frac{\operatorname{erf} \frac{y}{2\sqrt{\alpha_I \theta}}}{\operatorname{erf} \beta} \quad (39)$$

$$\frac{T_L - T}{T_L - T_s} = \frac{\operatorname{erfc} \frac{y}{2\sqrt{\alpha_{II} \theta}}}{\operatorname{erfc} \gamma} \quad (40)$$

In order to make possible the evaluation of constants in the above equations, we assume that the densities and the thermal conductivities of the two zones are equal:

$$\rho_I = \rho_{II} \quad \text{and} \quad K_I = K_{II} \quad (41)$$

Making use of the relation between thermal conductivity and thermal diffusivity, the relation between the two growth constants can be written as:

$$\frac{\beta}{\gamma} = \sqrt{\frac{\alpha_{II}}{\alpha_I}} = \sqrt{\frac{C_p^I}{C_p^{II}}} = \frac{1}{7 \cdot 15} \quad (42)$$

Since the boundary between the two zones cannot store any heat:

$$K_I \left( \frac{\partial T}{\partial y} \right)_\xi^I = K_{II} \left( \frac{\partial T}{\partial y} \right)_\xi^{II} \quad (43)$$

Evaluating the gradients from Equations (39) and (40), and substituting them into Equation (43) one gets:

$$\frac{T_s - T_i}{\text{erf } \beta} \cdot \frac{e^{-\beta^2}}{\sqrt{\pi \alpha_I \theta}} = \frac{T_L - T_s}{\text{erfc } \gamma} \cdot \frac{e^{-\gamma^2}}{\sqrt{\pi \alpha_{II} \theta}}$$

or

$$\frac{T_s - T_i}{T_L - T_s} = \sqrt{\frac{\alpha_I}{\alpha_{II}}} \cdot \frac{e^{\beta^2} \text{erf } \beta}{e^{\gamma^2} \text{erfc } \gamma} \quad (44)$$

Substitution of Equation (42) and the values of temperature in Equation (44) gives another relation between the growth constants:

$$\frac{e^{\beta^2} \text{erf } \beta}{e^{\gamma^2} \text{erfc } \gamma} = 2 \cdot 732 \quad (45)$$

Solving Equations (42) and (45) by trial and error gives the values of growth constants:

$$\beta = 0.404 \quad (46)$$

$$\gamma = 2.888 \quad (47)$$

Equations (39) and (40) giving the temperature distribution may then be written as:

$$T = -70 + 146 \cdot 91 \text{ erf } \frac{y}{2\sqrt{\alpha_I \theta}} \quad \text{Zone I} \quad (48)$$

$$T = -3.25 - 0.7364 \cdot 10^5 \cdot \text{erfc } \frac{y}{2\sqrt{\alpha_{II} \theta}} \quad \text{Zone II} \quad (49)$$

The value of  $\alpha_I$  is evaluated from the experimental data on the movement of the isotherm  $T = T_E$  which is measured as the limit of the all-solid region (Figure 13). The fact that the value of the diffusivity of an ice-brine aggregate (Zone I) comes out as  $0.64 \text{ cm}^2$

per minute, close to that of pure ice, is an evidence of the validity of our assumptions. Substitution of diffusivity values in Equations (48) and (49) gives the temperature distribution as a function of distance from the chill and the time elapsed since the beginning of solidification:

$$T = -70 + 146.91 \operatorname{erf} \frac{0.624y}{\sqrt{\theta}} \quad \text{Zone I} \quad (50)$$

$$T = -3.25 - 0.7364 \cdot 10^5 \operatorname{erfc} \frac{4.464y}{\sqrt{\theta}} \quad \text{Zone II} \quad (51)$$

These equations are used to calculate the cooling curves at different distances from chill, which are presented in Figure 10. In addition, they lead to a description of the freezing patterns in the system, as follows:

$$T = \frac{3.25}{fs-1} = -70 + 146.91 \operatorname{erf} \frac{0.624y}{\sqrt{\theta}} \quad \text{Zone I} \quad (52)$$

$$T = \frac{3.25}{fs-1} = -3.25 - 0.7364 \cdot 10^5 \operatorname{erfc} \frac{4.464y}{\sqrt{\theta}} \quad \text{Zone II} \quad (53)$$

$$\left(\frac{dfs}{d\theta}\right)_y^I = \frac{14 \cdot 10 \cdot y \cdot (1-fs)^2}{\theta^{3/2}} \cdot \frac{2}{\sqrt{\pi}} e^{-\left(\frac{0.624y}{\sqrt{\theta}}\right)^2} \quad (54)$$

$$\left(\frac{dfs}{d\theta}\right)_y^{II} = \frac{5.04 \cdot 10^4 \cdot y \cdot (1-fs)^2}{\theta^{3/2}} \cdot \frac{2}{\sqrt{\pi}} e^{-\left(\frac{4.464y}{\sqrt{\theta}}\right)^2} \quad (55)$$

The results of the computation of these complex functions are presented in Figures 11 and 12. The freezing process at any given value of  $y$  starts out at a slow rate, increases to a maximum, and slows down towards the end of the solidification cycle. By setting the derivative of the freezing rate in Zone II equal to zero, one

gets the values of  $f_s^M$  and  $\theta^M$ , the fraction solid and the time at which the freezing rate is at a maximum, in the following form:

$$\left(\frac{4.464y}{\sqrt{\theta_M}}\right)^2 = 1.50 - \frac{0.7364 \cdot 10^5}{3 \cdot 25} \cdot \left(\frac{4.464y}{\sqrt{\theta_M}}\right) \cdot \frac{2}{\sqrt{\pi}} \cdot e^{-\left(\frac{4.464y}{\sqrt{\theta_M}}\right)^2} \cdot (f_s^M - 1) \quad (56)$$

By solution of Equations (56) and (52) one gets  $f_s^M$  as:

$$f_s^M = 0.395 \quad (57)$$

This means that the maxima in the freezing rate occurs when 0.395 fraction of solution at any level has already solidified. The time at which the maximum occurs at different levels is given by the following equation:

$$\frac{4.464y}{\sqrt{\theta_M}} = 2.958 \quad (58)$$

Substituting the values of  $f_s^M$  and  $\theta_M$  into Equation (54) one gets the value of the maximum freezing rate  $\left(\frac{d f_s}{d \theta}\right)_y^M$  as:

$$\left(\frac{d f_s}{d \theta}\right)_y^M = \frac{0.9633}{y^2} \quad (59)$$

This implies that the maximum freezing rate at any level is inversely proportional to the square of the distance from the chill. Tables II and III present some results of numerical computations of this analysis.

## IX. APPENDIX III

Analysis of Chill Surface Temperature:

When an aqueous solution at its liquidus temperature is brought in contact with the cold copper chill, temperature gradients are set up in both the chill and the solution (Figure 9). The temperature distribution in the solid zone next to the chill has been developed in Appendix II:

$$\frac{T - T_i}{T_s - T_i} = \frac{\operatorname{erf} \frac{y}{2 \sqrt{\alpha_I \theta}}}{\operatorname{erf} \beta} \quad (39)$$

The temperature distribution in the chill will correspond to that in a semi-infinite body in the initial period of its contact with the solution. It can be described by an equation of the following form:

$$T_c - T = D \operatorname{erfc} \frac{y}{2 \sqrt{\alpha_{Cu} \theta}} \quad (60)$$

Where  $\alpha_{Cu}$  is the thermal diffusivity of copper,  $T_c$  is the starting temperature of the chill. The constant D can be evaluated by the boundary condition that at the interface\*  $T = T_i$ . The temperature distribution in the chill can be written as:

$$\frac{T_c - T}{T_c - T_i} = \operatorname{erfc} \frac{y}{2 \sqrt{\alpha_{Cu} \theta}} \quad (61)$$

\* The contact resistance at the copper-ice interface is practically zero as indicated<sup>33</sup> by Figure 13.

The interface cannot store any heat, therefore:

$$K_I \left( \frac{\partial T}{\partial y} \right)_{y=0}^I = K_{Cu} \left( \frac{\partial T}{\partial y} \right)_{y=0}^{Cu} \quad (62)$$

Evaluating the gradients from Equations (39) and (61) and substituting in Equation (62) gives:

$$\frac{T_s - T_i}{T_i - T_c} = \sqrt{\frac{K_{Cu} \rho_{Cu} C_p^{Cu}}{K_I \rho_I C_p^I}} \cdot \operatorname{erf} \beta \quad (63)$$

where  $\rho_{Cu}$  and  $C_p^{Cu}$  are the density and the specific heat of copper respectively.

For 1 N potassium chloride solution and an initial chill temperature of  $-70^\circ\text{C}$ , Equation (63) gives the chill surface temperature,  $T_i$ , as  $-62.5^\circ\text{C}$ . However, this temperature increase of  $7.5^\circ\text{C}$  in the surface temperature of the chill is only for a very short transient period. After the first few seconds of contact the temperature distribution in the chill will no longer correspond to that in a semi-infinite body (Equation 61); and the interface temperature,  $T_i$ , will move closer to initial temperature  $T_c$ .

Actual temperature measurements near the chill surface have confirmed this; the temperature remained within one degree centigrade of the initial chill temperature at all times during solidification, except for a very short transient rise of four degrees centigrade at the start.



## X. APPENDIX IV

Calculation of Constitutional Supercooling in the Interdendritic Liquid:

Dendrite spacing is related to constitutional supercooling by the following equation:

$$L^2 = \frac{8D\Delta T}{m \bar{c} \left( \frac{df_s}{d\theta} \right)} \quad (12)$$

For 1 N potassium chloride

$$D = 1.892 \cdot 10^{-5} \text{ cm}^2 \text{ per second} = 113.5 \cdot 10^{-5} \text{ cm}^2 \text{ per minute}$$

(Table VI)

$$m = 3.25^\circ\text{C} \cdot \text{Litre per mole}$$

$$\bar{c} = 1 \text{ mole per litre}$$

The dendrite spacing  $L = 125 \cdot 10^{-4}$  centimeters at a maximum freezing rate of  $0.25 \text{ minutes}^{-1}$  (Figure 31).

$$\Delta T = \frac{(125)^2 \cdot 10^{-8} \cdot 3.25 \cdot 0.25}{8 \cdot 113.5 \cdot 10^{-5}} \quad ^\circ\text{C}$$

or

$$\Delta T = 0.14^\circ\text{C} \quad (64)$$

The constitutional supercooling in the interdendritic liquid is therefore of a very small order of magnitude.

TABLE I

Observations on Phase Boundary Movements During Unidirectional Freezing of 1 N Potassium Chloride Solution from a Chill at  $-70^{\circ}\text{C}$ .

| <u>Time, <math>\theta</math>,<br/>in minutes</u> | <u>Thickness of All-<br/>Solid Zone in centimeters</u> | <u>Square Root of<br/>Time (<math>\sqrt{\theta}</math>)<br/>in minutes <math>^{1/2}</math></u> |
|--|--|--|
| 0.36   | 0.40   | 0.60   |
| 1.00   | 0.50   | 1.00   |
| 1.33   | 0.70   | 1.15   |
| 1.66   | 0.80   | 1.30   |
| 2.25   | 0.90   | 1.50   |
| 2.90   | 1.00   | 1.70   |
| 3.25   | 1.10   | 1.80   |
| 4.00   | 1.20   | 2.00   |
| 4.85   | 1.30   | 2.20   |
| 5.75   | 1.40   | 2.40   |
| 6.25   | 1.50   | 2.50   |
| 7.00   | 1.60   | 2.65   |
| 7.75   | 1.70   | 2.80   |
| 9.00   | 1.80   | 3.00   |
| 10.25  | 1.90   | 3.20   |
| 11.25  | 2.00   | 3.35   |
| 12.50  | 2.10   | 3.55   |

TABLE II

Calculated Temperature and Freezing Rate Distributions at  
 2 Centimeters\* from  $-70^{\circ}\text{C}$  Chilled Surface During Unidirectional  
 Freezing of 1 N Potassium Chloride Solution.

| Time, $\theta$ ,<br>in minutes | Temperature in<br>$^{\circ}$ Centigrade | Fraction<br>Solidified ( $f_s$ ) | Freezing<br>Rate $\left(\frac{df_s}{d\theta}\right)_{y=2\text{ cm.}}$<br>in minutes <sup>-1</sup> |
|--------------------------------|---|----------------------------------|---|
| 5.00                           | -3.251                                  | 0.00037                          | 0.00119   |
| 6.00                           | -3.268                                  | 0.00551                          | 0.01304   |
| 6.50                           | -3.313                                  | 0.01908                          | 0.03127   |
| 7.00                           | -3.384                                  | 0.03978                          | 0.06454   |
| 7.50                           | -3.546                                  | 0.08348                          | 0.11306   |
| 8.00                           | -3.840                                  | 0.15376                          | 0.16961   |
| 8.25                           | -4.063                                  | 0.20027                          | 0.19656   |
| 8.50                           | -4.346                                  | 0.25230                          | 0.21828   |
| 8.75                           | -4.701                                  | 0.30878                          | 0.23317   |
| 9.00                           | -5.140                                  | 0.36771                          | 0.24340   |
| 9.05                           | -5.370                                  | 0.39500                          | 0.24080   |
| 9.25                           | -5.675                                  | 0.42739                          | 0.24000   |
| 9.50                           | -6.324                                  | 0.48609                          | 0.23329   |
| 9.75                           | -7.065                                  | 0.54000                          | 0.18862   |
| 10.00                          | -7.801                                  | 0.58339                          | 0.14949   |
| 10.25                          | -8.497                                  | 0.61752                          | 0.12193   |
| 10.50                          | -9.167                                  | 0.64550                          | 0.10138   |
| 10.75                          | -9.783                                  | 0.66800                          | 0.08626   |
| 11.00                          | -10.429                                 | 0.68837                          | 0.07325   |

\* Similar calculations were made for several distances the results are plotted in Figures 10,11 and 12.

TABLE III

Measured Dendrite Spacings and Calculated (Equation 59) Maximum Freezing Rates at Different Distances from the  $-70^{\circ}\text{C}$  Chill for 1 N Potassium Chloride Solution.

| Distance from Chill (y), Centimeters | Dendrite Spacing (L), Microns | Maximum Freezing Rate (minutes <sup>-1</sup> )<br>$\left(\frac{df_s}{d\theta}\right)_y^M = \frac{0.9633}{y^2}$ | $\sqrt{\left(\frac{d\theta}{df_s}\right)_y^M}$ |
|--------------------------------------|-------------------------------|--|--|
| 0.10                                 | 52.00                         | 96.33  | 0.102  |
| 0.20                                 | 57.00                         | 24.05  | 0.204  |
| 0.40                                 | 67.00                         | 6.02   | 0.407  |
| 0.80                                 | 80.00                         | 1.50   | 0.815  |
| 1.00                                 | 87.00                         | 0.96   | 1.02   |
| 1.20                                 | 98.00                         | 0.66   | 1.22   |
| 1.40                                 | 102.00                        | 0.37   | 1.63   |
| 1.80                                 | 115.00                        | 0.29   | 1.84   |
| 2.00                                 | 125.00                        | 0.24   | 2.04   |
| 2.20                                 | 133.00                        | 0.19   | 2.24   |
| 2.40                                 | 143.00                        | 0.16   | 2.44   |
| 2.50                                 | 144.00                        | 0.14   | 2.65   |
| 2.80                                 | 155.00                        | 0.12   | 2.85   |
| 3.00                                 | 160.00                        | 0.10   | 3.06   |
| 3.20                                 | 172.00                        | 0.08   | 3.42   |

TABLE IV

Dendrite Spacing Measurements on Droplets of Sodium Chloride  
Solutions at Different Concentrations in the Absence and in the  
Presence of External Magnetic Field.

Droplet Diameter = 0.25 inches      Freezing Rate = 0.36 minutes<sup>-1</sup>

| Sodium Chloride<br>Concentration in<br>Moles/Litre | No Field                                      |                                       | Stationary Field 4 Kg   |
|--|---|---------------------------------------|---|
|  | Thickness of Salt<br>Pocket (P) in<br>Microns | Dendrite<br>Spacing (L) in<br>Microns | Dendrite<br>Spacing (L) in the<br>presence of the<br>magnetic field |
| 0.20   | 10.00   | 84.00                                 | --  |
| 0.50   | --  | 100.00                                | 120.00  |
| 0.60   | --  | --                                    | 140.00  |
| 1.00   | 18.00   | 116.50                                | 160.00  |
| 1.50   | --  | 125.00                                | --  |
| 2.00   | 35.00   | 154.00                                | 170.00  |
| 3.00   | 46.00   | 165.00                                | 198.00  |

TABLE V

Dendrite Spacing Measurements on Ingots at Different Distances from  
a  $-70^{\circ}\text{C}$  Chilled Surface from Different Solutions:

SINGLE SOLUTES:

| Distance from<br>Chill ( $-70^{\circ}\text{C}$ ),<br>Centimeters | Dendrite Spacing (MICRONS) |              |              |             |              |               |              |              |
|--|----------------------------|--------------|--------------|-------------|--------------|---------------|--------------|--------------|
|  | 0.1N<br>KCl                | 0.1N<br>NaCl | 0.1N<br>LiCl | 0.2N<br>KCl | 0.2N<br>NaCl | 0.25N<br>NaCl | 2.5N<br>NaCl | 0.2N<br>LiCl |
| 0.50   | --                         | --           | --           | --          | --           | --            | 46.00        | --           |
| 1.0  | 26.00                      | 24.00        | --           | 29.00       | --           | 40.00         | 72.00        | --           |
| 1.50   | --                         | --           | 21.00        | --          | 45.00        | --            | --           | 32.50        |
| 2.00   | 62.00                      | 56.00        | 40.00        | 72.00       | 65.00        | 68.00         | 122.00       | 51.00        |
| 2.50   | 80.00                      | 76.00        | 61.00        | 94.00       | 85.00        | 87.00         | 148.00       | 68.00        |
| 3.00   | 97.00                      | 93.00        | 79.00        | 115.00      | 103.00       | 107.00        | 167.00       | 88.00        |

MIXED SOLUTES:

| Distance from<br>Chill ( $-70^{\circ}\text{C}$ ),<br>Centimeters | Dendrite Spacing (MICRONS) |                             |                            |                            |                              |                             |
|--|----------------------------|-----------------------------|----------------------------|----------------------------|------------------------------|-----------------------------|
|  | 0.1N KCl<br>+<br>0.1N LiCl | 0.1N NaCl<br>+<br>0.1N LiCl | 0.1N KCl<br>+<br>0.1N NaCl | 0.2N KCl<br>+<br>0.2N NaCl | 0.2N NaCl<br>+<br>0.05N LiCl | 0.2N NaCl<br>+<br>0.05N KCl |
| 0.50   | --                         | --                          | --                         | --                         | --                           | --                          |
| 1.00   | --                         | --                          | 33.00                      | 33.50                      | --                           | --                          |
| 1.50   | 41.50                      | 30.00                       | --                         | --                         | 42.00                        | 51.00                       |
| 2.00   | 60.00                      | 50.00                       | 61.50                      | 67.50                      | 62.50                        | 66.50                       |
| 2.50   | 77.50                      | 69.00                       | 79.00                      | 82.00                      | 81.00                        | 86.00                       |
| 3.00   | 92.50                      | 90.00                       | 95.00                      | 99.00                      | 101.00                       | --                          |

TABLE VI

Diffusion Coefficients for Single and Binary Solute SystemsSINGLE SOLUTES:

| Concentration<br>Moles/Litre | Diffusion Coefficient <sup>49</sup> ( $\text{cm}^2 \text{sec}^{-1} \cdot 10^{-5}$ ) at 25°C |                       |                     |                      |
|------------------------------|---|-----------------------|---------------------|----------------------|
|                              | Sodium<br>Chloride  | Potassium<br>Chloride | Lithium<br>Chloride | Hydrogen<br>Chloride |
| 0.10                         | 1.48  | 1.84                  | 1.26                | 3.05                 |
| 0.20                         | 1.47  | 1.83                  | 1.26                | 3.06                 |
| 0.50                         | 1.47  | 1.85                  | 1.27                | 3.18                 |
| 1.0                          | 1.48  | 1.89                  | 1.30                | 3.43                 |
| 1.50                         | 1.49  | 1.94                  | 1.33                | 3.74                 |
| 2.0                          | 1.51  | 1.99                  | 1.36                | 4.04                 |
| 2.50                         | 1.52  | 2.05                  | 1.39                | 4.33                 |
| 3.00                         | 1.54  | 2.11                  | 1.43                | 4.65                 |

MIXED SOLUTES:

I. For KCl - NaCl - H<sub>2</sub>O System<sup>50</sup>      1 = NaCl      2 = KCl

| C <sub>1</sub><br>Moles/Litre | C <sub>2</sub><br>Moles/Litre | Diffusivities in $\text{cm}^2 \text{sec}^{-1} \cdot 10^{-5}$ at 25°C |                 |                 |                 |
|-------------------------------|-------------------------------|--|-----------------|-----------------|-----------------|
|                               |                               | D <sub>11</sub>  | D <sub>12</sub> | D <sub>21</sub> | D <sub>22</sub> |
| 0.25                          | 0.25                          | 1.37   | -0.0053         | 0.1429          | 1.8258          |
| 0.50                          | 0.25                          | 1.41   | -0.0160         | 0.0959          | 1.8235          |
| 0.25                          | 0.50                          | 1.34   | -0.0010         | 0.2053          | 1.8381          |
| 0.50                          | 0.50                          | 1.38   | -0.0102         | 0.1536          | 1.8407          |

II. LiCl - KCl - H<sub>2</sub>O<sup>51</sup> System

1 - LiCl      2 - KCl

C<sub>1</sub> = 0.25 moles/litre      C<sub>2</sub> = 0.20 Moles/LitreD in  $\text{cm}^2 \text{sec}^{-1} \cdot 10^{-5}$  at 25°CD<sub>11</sub> = 1.145D<sub>12</sub> = 0.006D<sub>22</sub> = 1.817D<sub>21</sub> = 0.204III. LiCl - NaCl - H<sub>2</sub>O<sup>51</sup> System

1 - LiCl      2 - NaCl

C<sub>1</sub> = 0.25 Moles/Litre      C<sub>2</sub> = 0.20 Moles/LitreD in  $\text{cm}^2 \text{sec}^{-1} \cdot 10^{-5}$  at 25°CD<sub>11</sub> = 1.069D<sub>12</sub> = 0.127D<sub>22</sub> = 1.316D<sub>21</sub> = 0.250

Figure 1. Concentration Profile Ahead of a Moving Solid-Liquid Interface.

Figure 2. Actual Temperature and Liquidus Temperature Profiles Ahead of the Interface. Finite Temperature Gradient in the Liquid.

Figure 3. Same as Figure 2 Except with Negligible Temperature Gradient in Liquid.



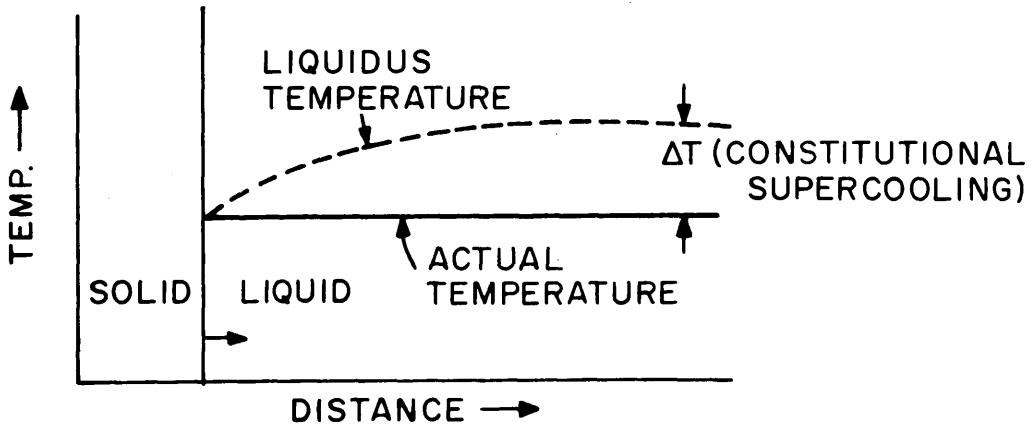
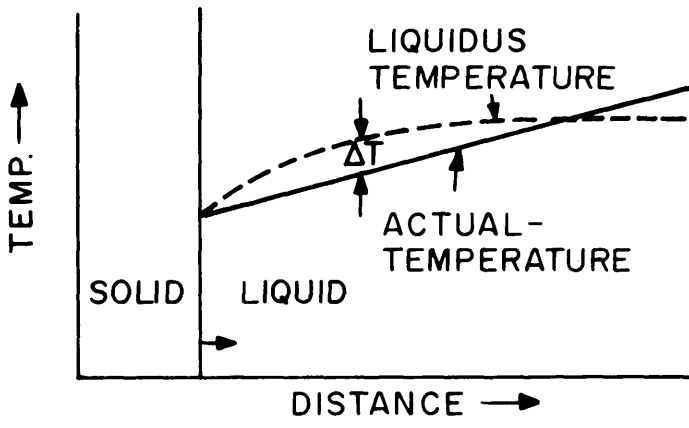
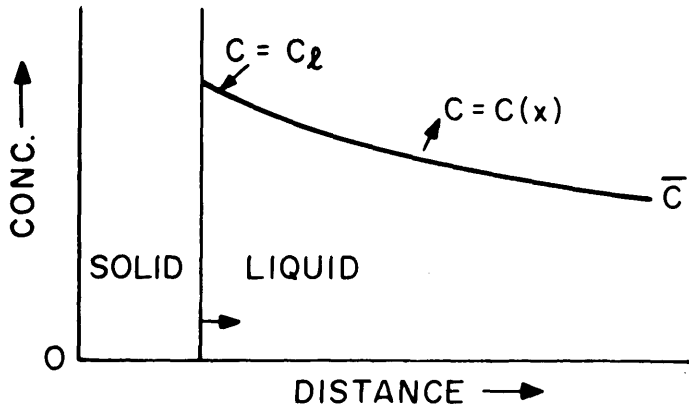


Figure 4. Schematic Representation of Concentration Distribution in the Interdendritic Liquid.

Figure 5. Actual Temperature and Liquidus Temperature Distributions in the Interdendritic Liquid.

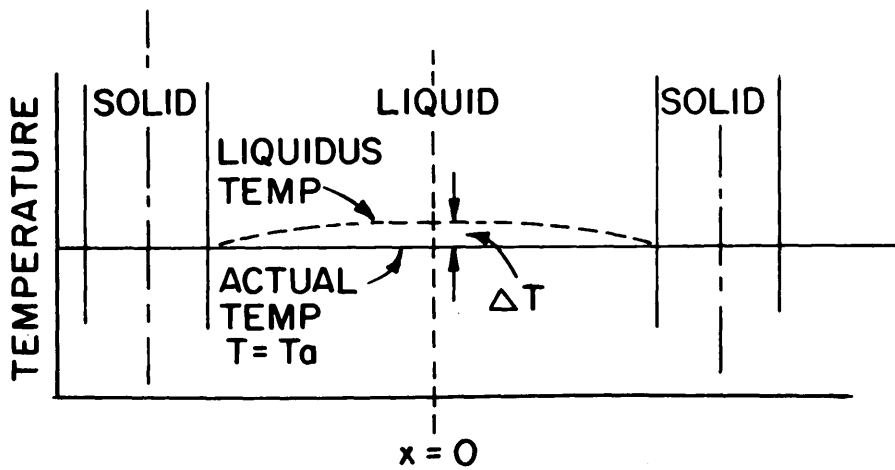
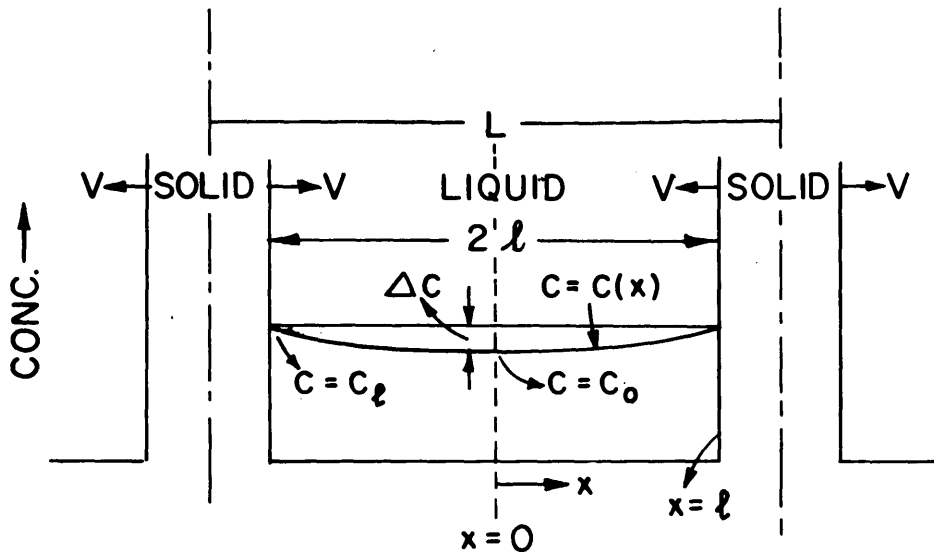


Figure 6. Concentration Profiles in the Interdendritic Liquid at Different Stages of Growth.

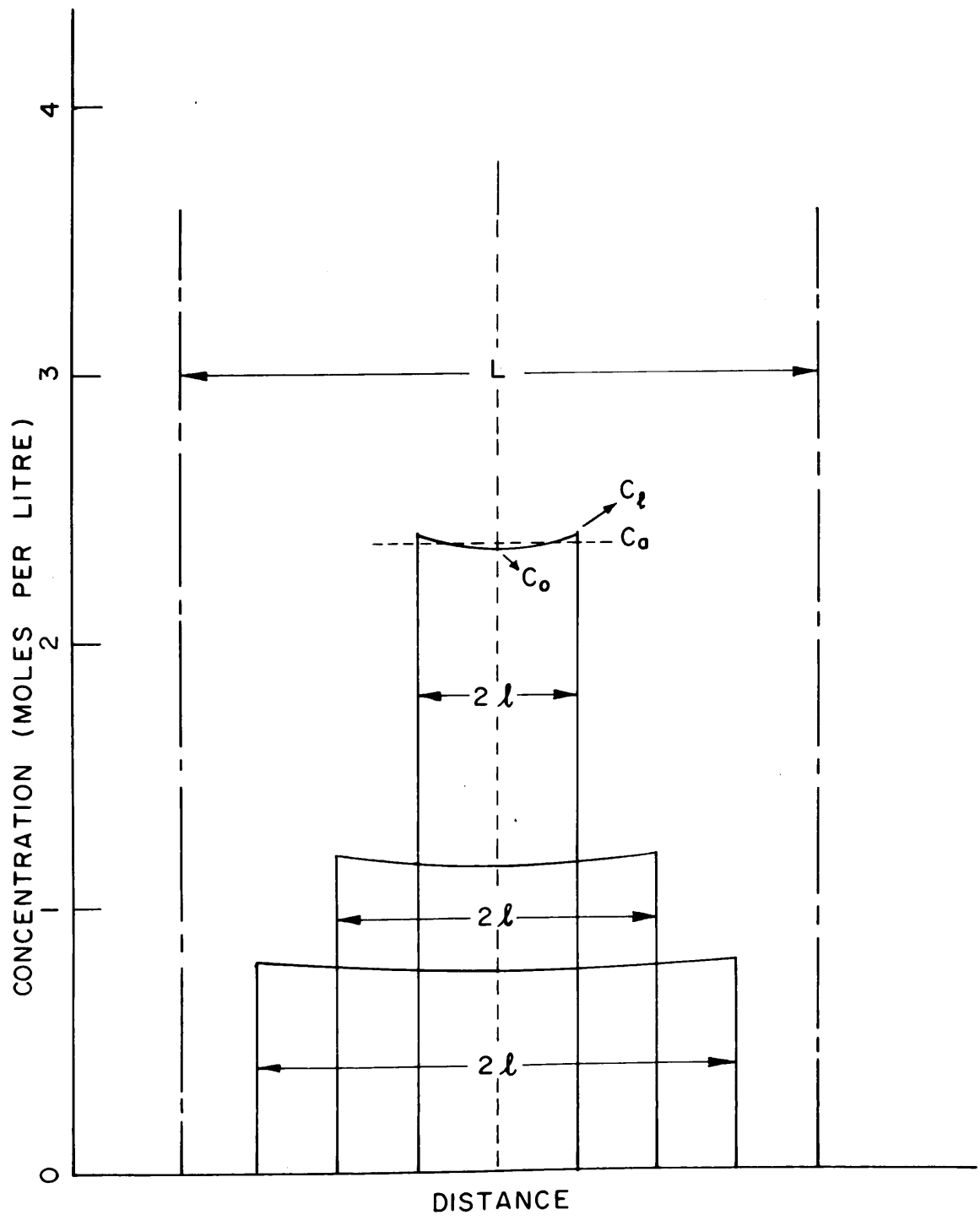


Figure 7 (a). Phase Diagram of Potassium Chloride-Water System.

Figure 7 (b). Phase Distribution Under a Temperature Gradient,  
Equilibrium Conditions.

Figure 7 (c). Phase Distribution Under a Temperature Gradient,  
Dendritic Growth.

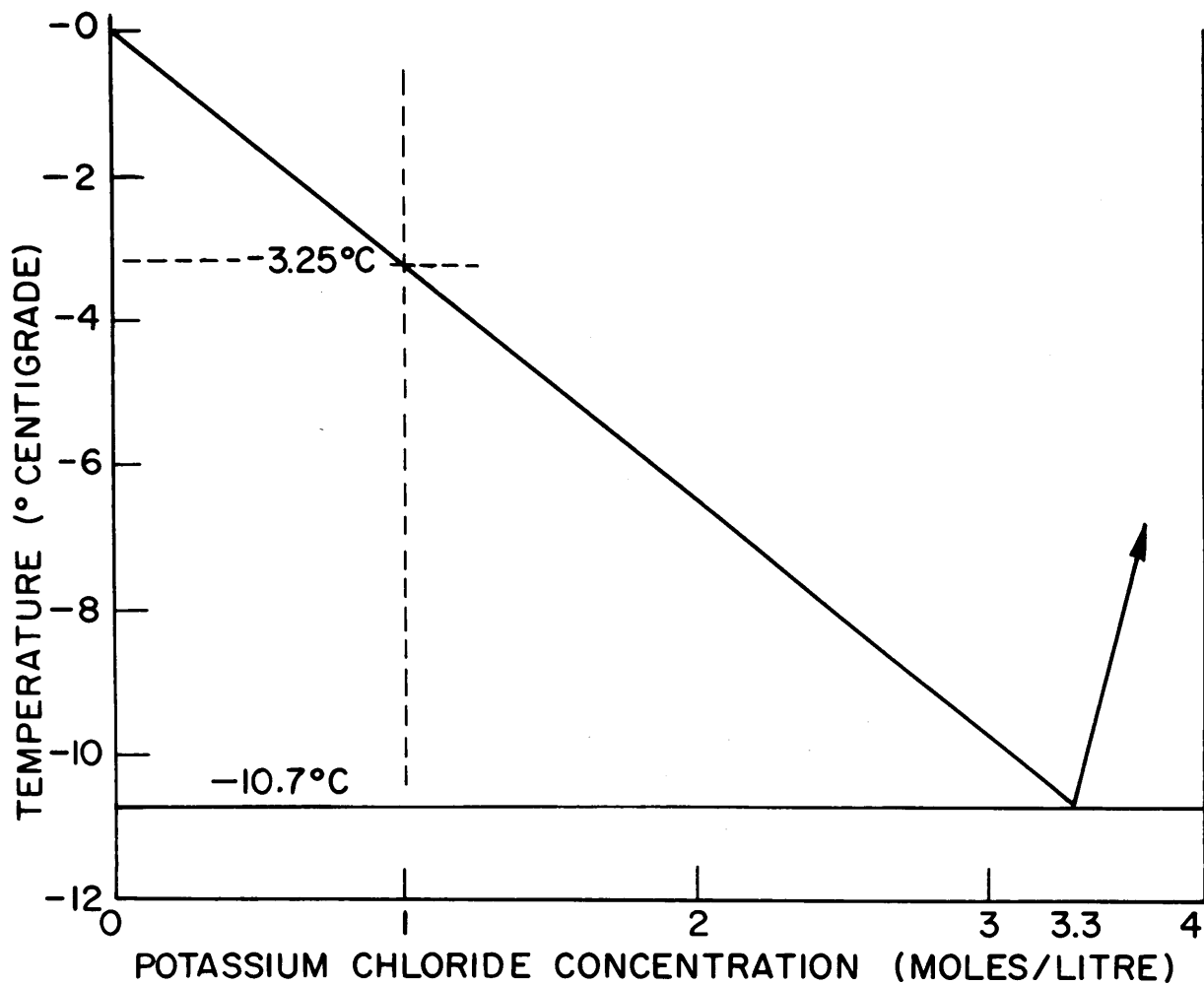
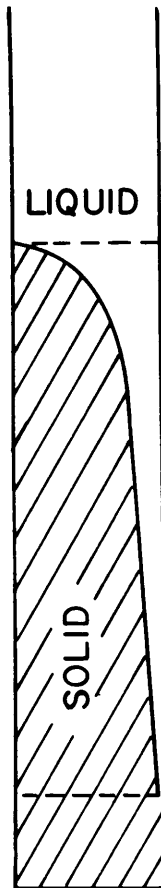
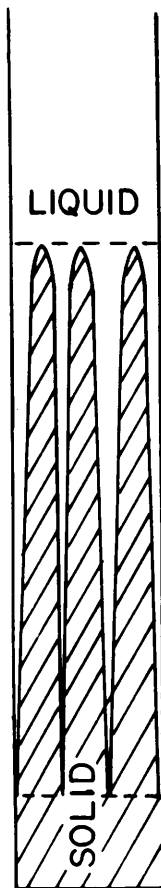


Figure 8. Schematic Representation of Variation in Heat Content of Aqueous Solutions During Solidification Cycle.



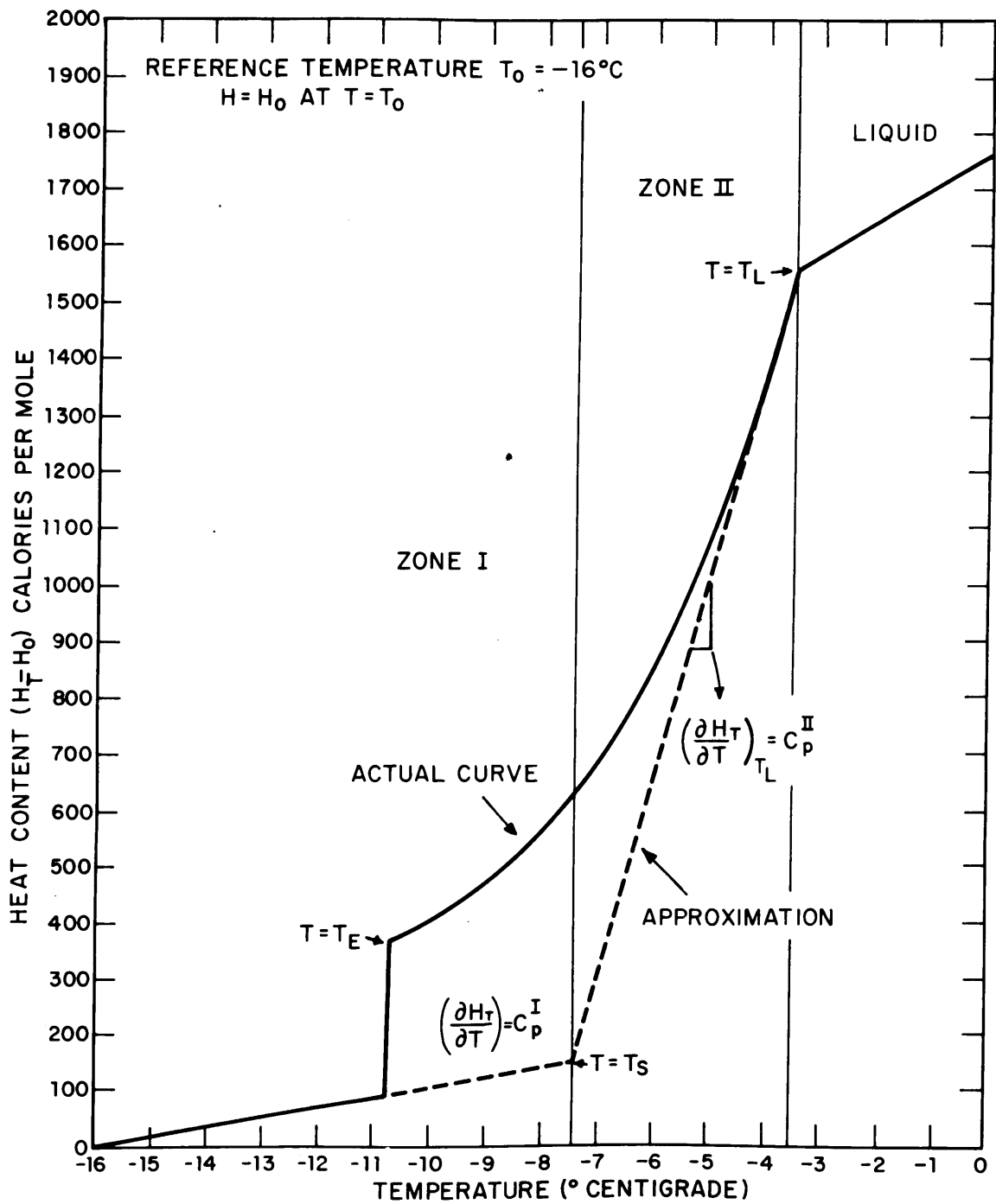


Figure 9. Schematic Representation of Temperature Profiles when an Aqueous Solution is Brought Into Contact with a Cold Chill.

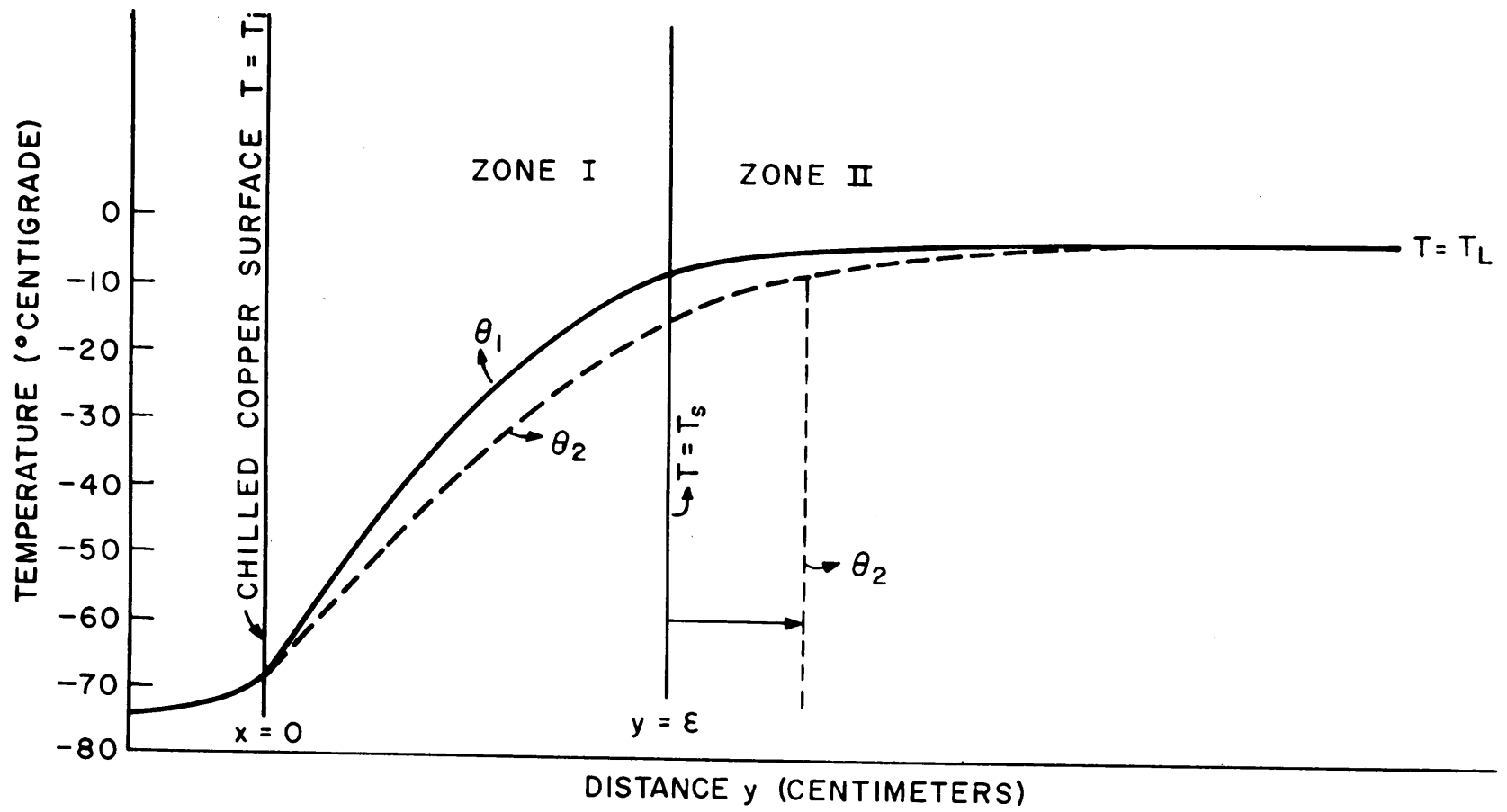


Figure 10. Calculated Cooling Curves for 1.0 N Potassium Chloride Solution at Different Distances from a Surface at  $-70^{\circ}\text{C}$ , in Contact with the Solution.

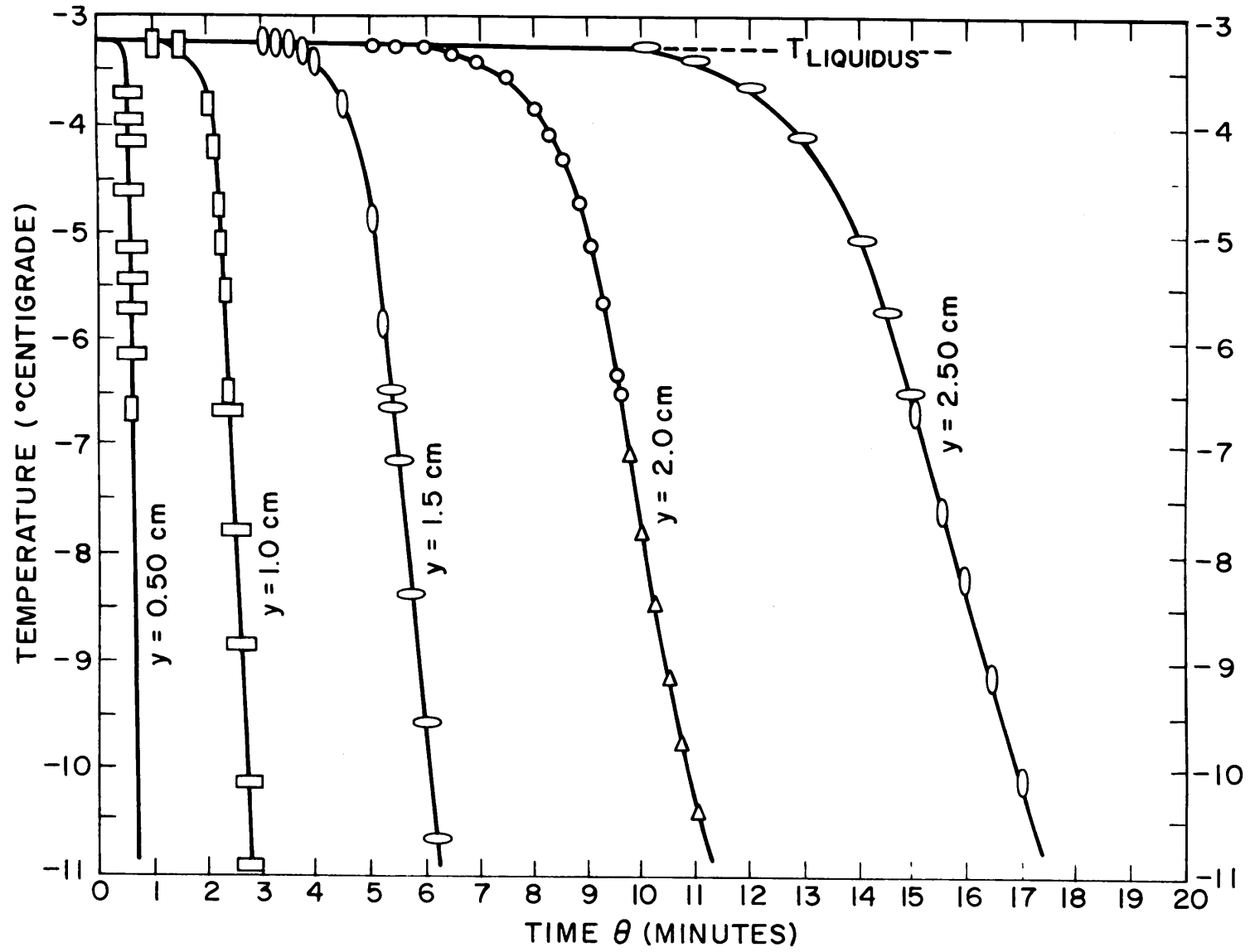
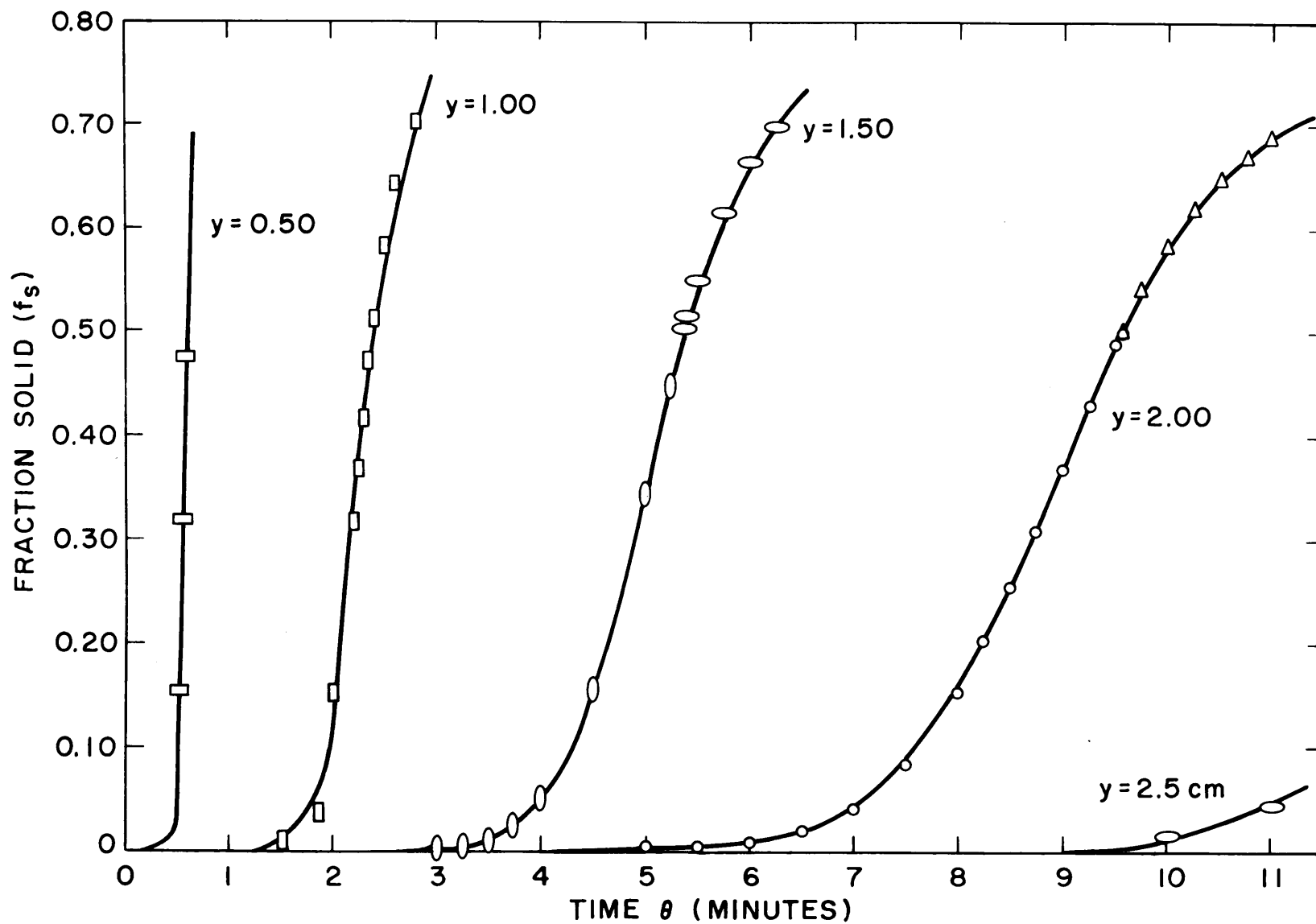


Figure 11. Fraction Solidified from 1.0 N Potassium Chloride Solution Versus Time at Different Distances from a Surface at  $-70^{\circ}\text{C}$ , in Contact with the Solution.



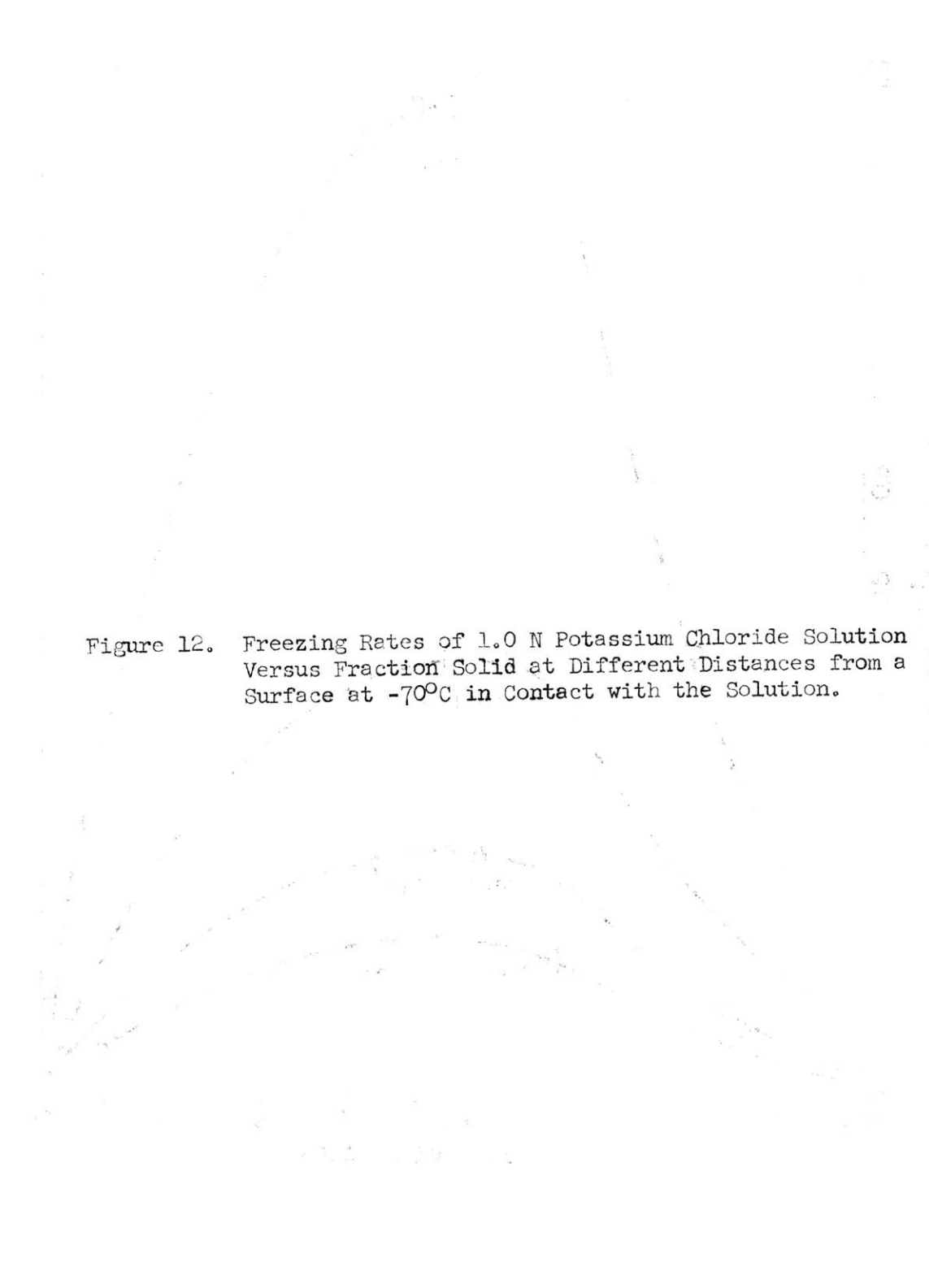


Figure 12. Freezing Rates of 1.0 N Potassium Chloride Solution Versus Fraction Solid at Different Distances from a Surface at  $-70^{\circ}\text{C}$  in Contact with the Solution.



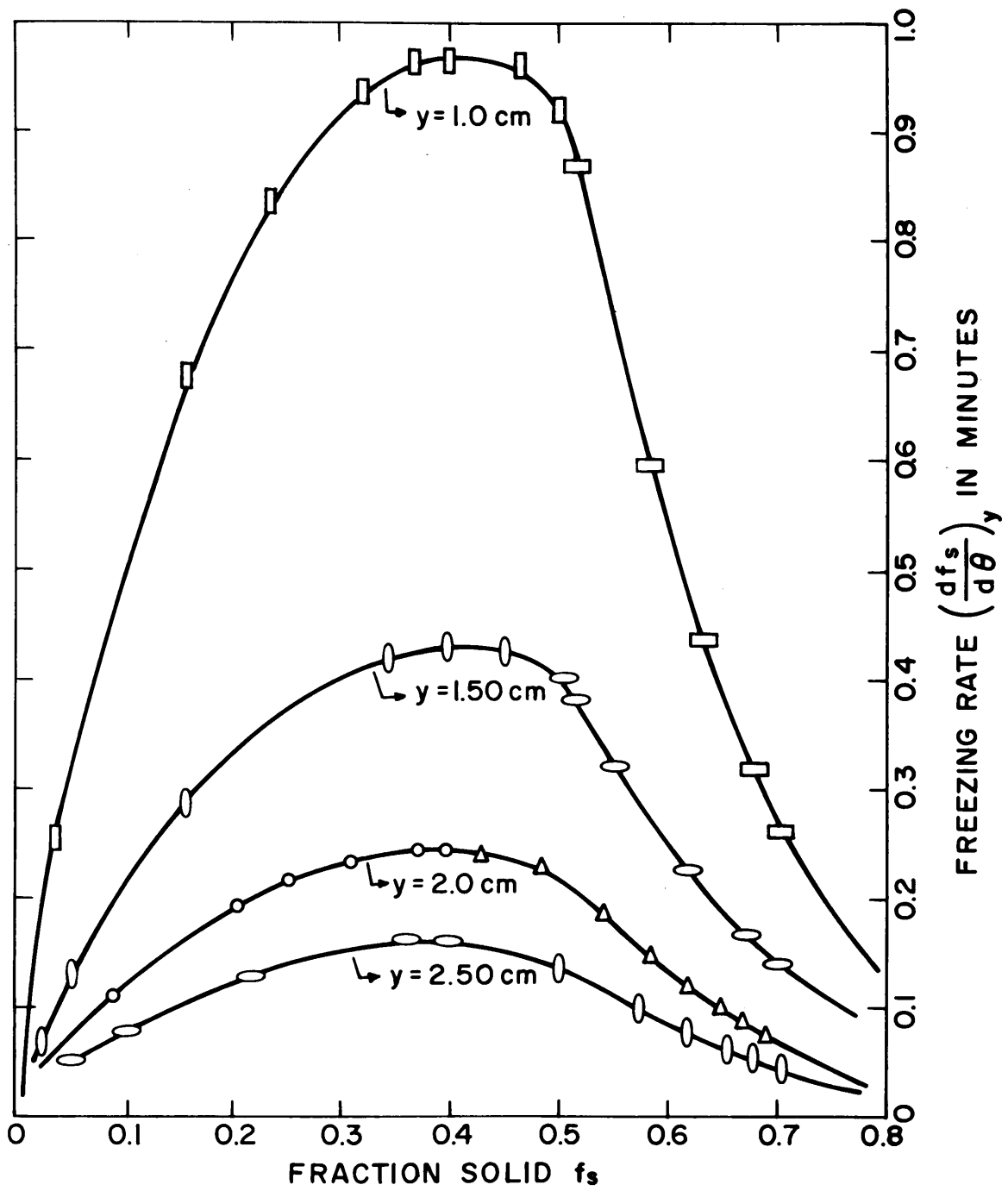


Figure 13. Distance of Eutectic Temperature  $T = T_E$  Isotherm From the Chill Surface at  $-70^\circ\text{C}$  as a Function of Time, for 1.0 N Potassium Chloride Solution. Movement of the Isotherm is Observed as the Limit of all Solid Zone in the Ingot.

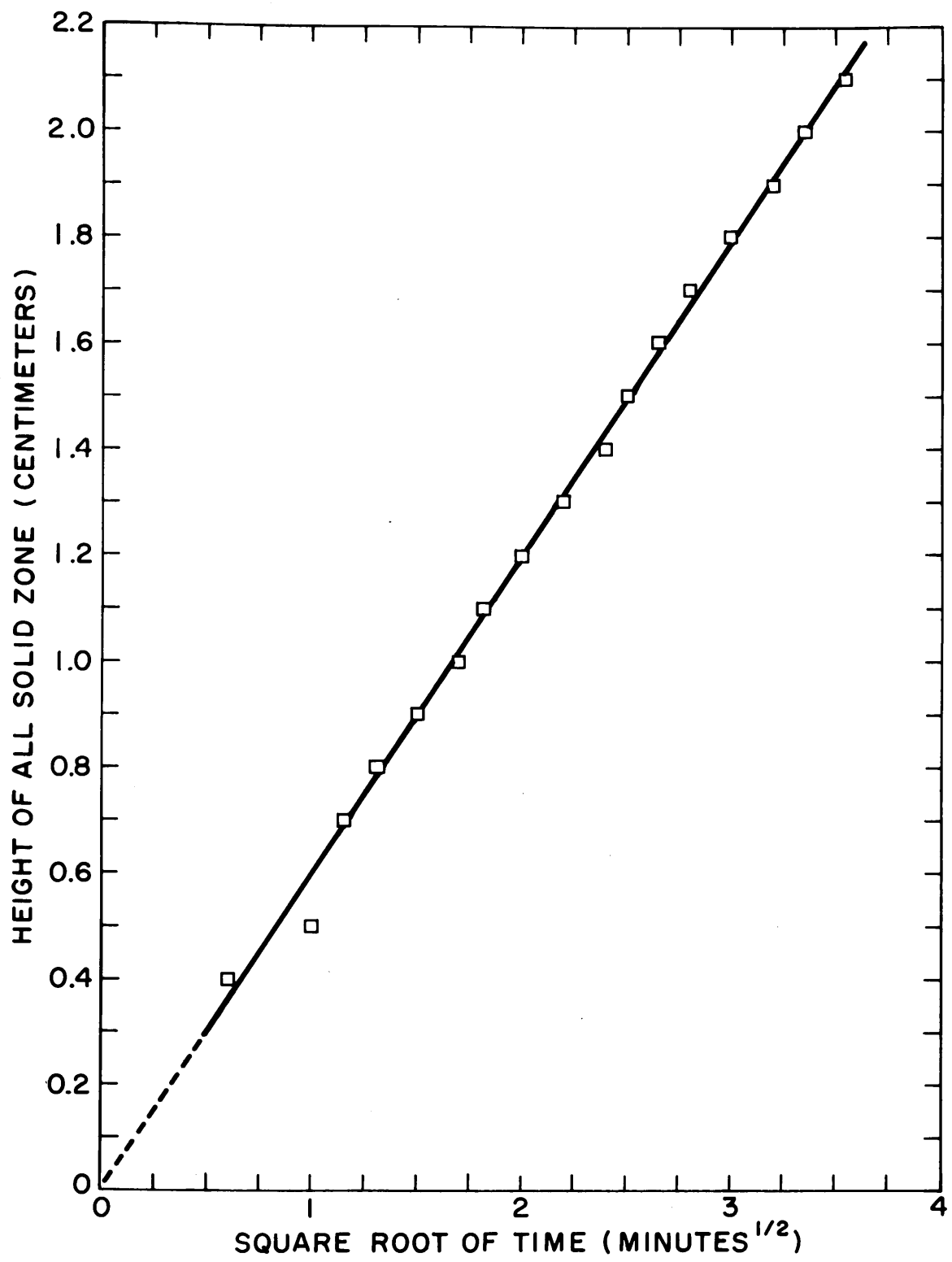


Figure 14. Schematic Representation of the Set Up for Freezing Droplets of Aqueous Solutions in Low Magnetic Fields.

Figure 15. Diagram Showing the Arrangement for Freezing Droplets of Aqueous Solutions in High Magnetic Fields.

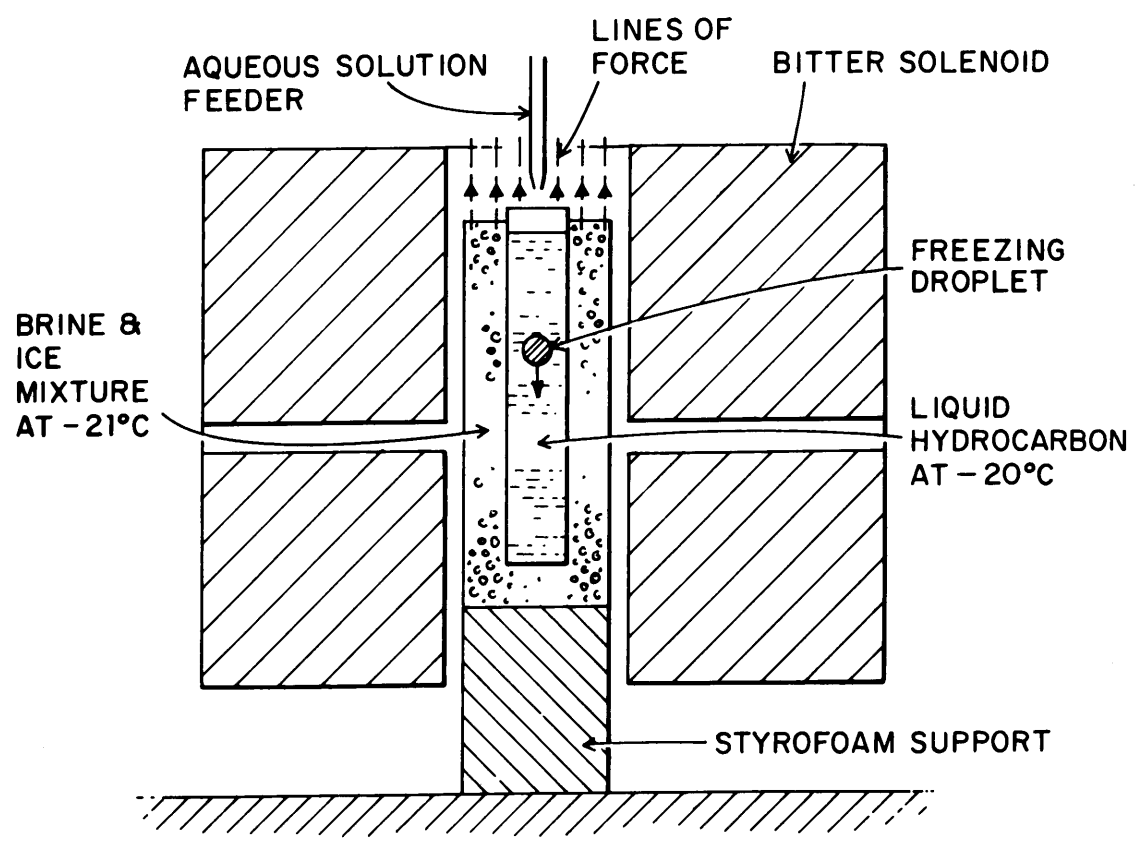
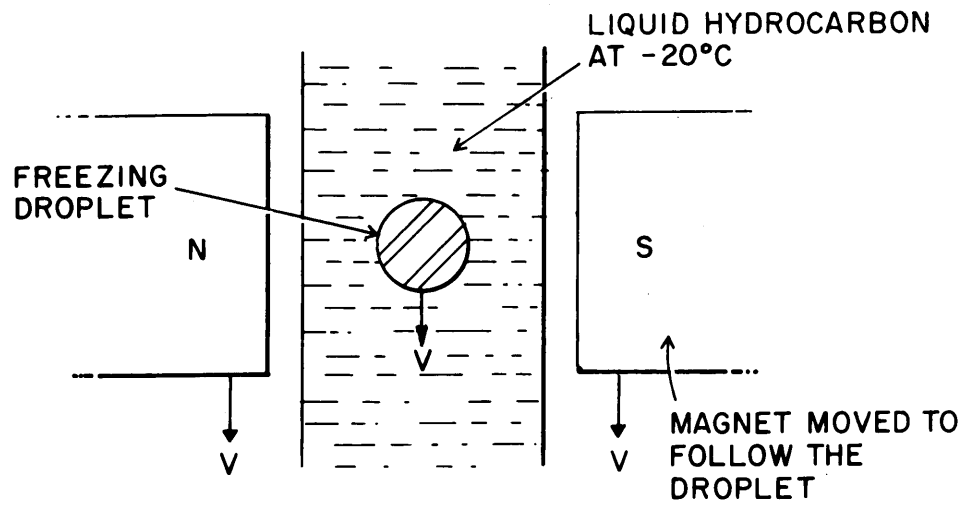


Figure 16. Diagram Showing the Assembly for Growing Unidirectional Ingots from Aqueous Solutions with High Magnetic Fields Parallel to the Growth Direction.

Figure 17. Same as Figure 16 Except for Field Being Perpendicular to the Growth Direction.

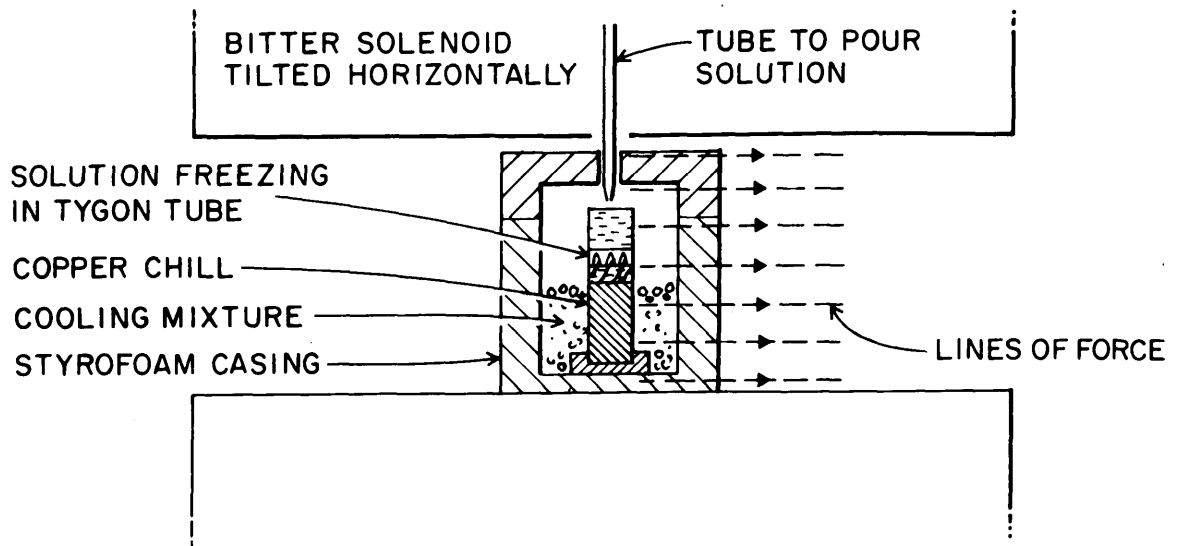
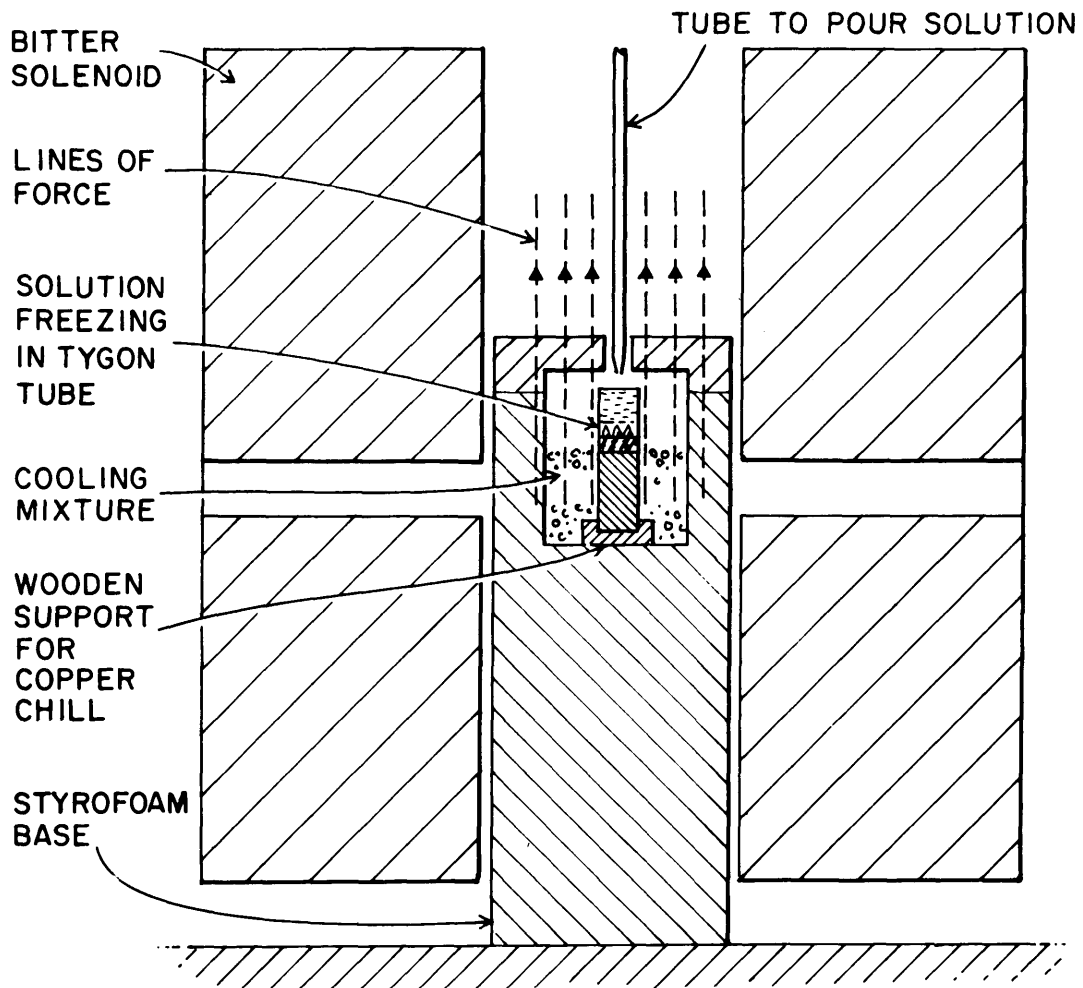


Figure 18. Unidirectional Freezing of Two Ingots One of Which Is Under the Influence of an Oscillating Magnetic Field.

Figure 19. Liquid Solid Interface During Unidirectional Freezing, Perpendicular to the Growth Direction.



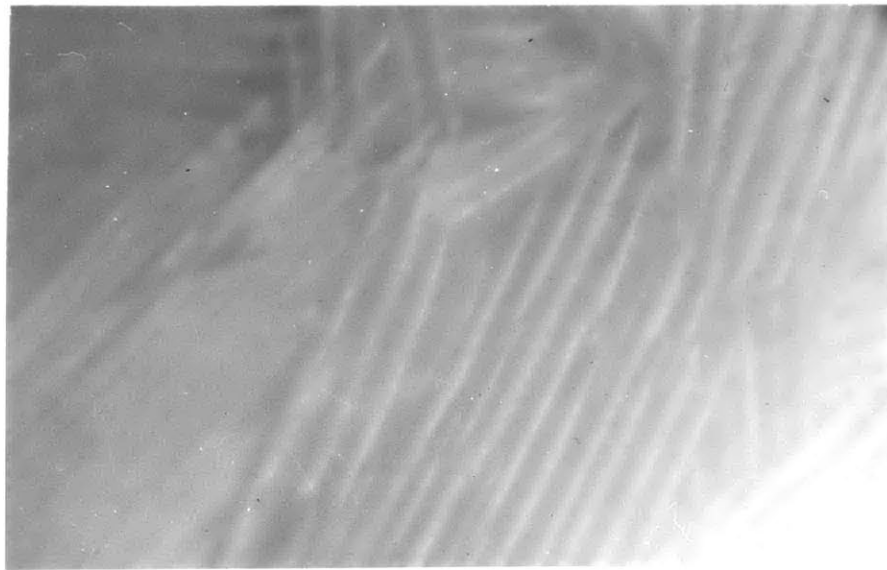
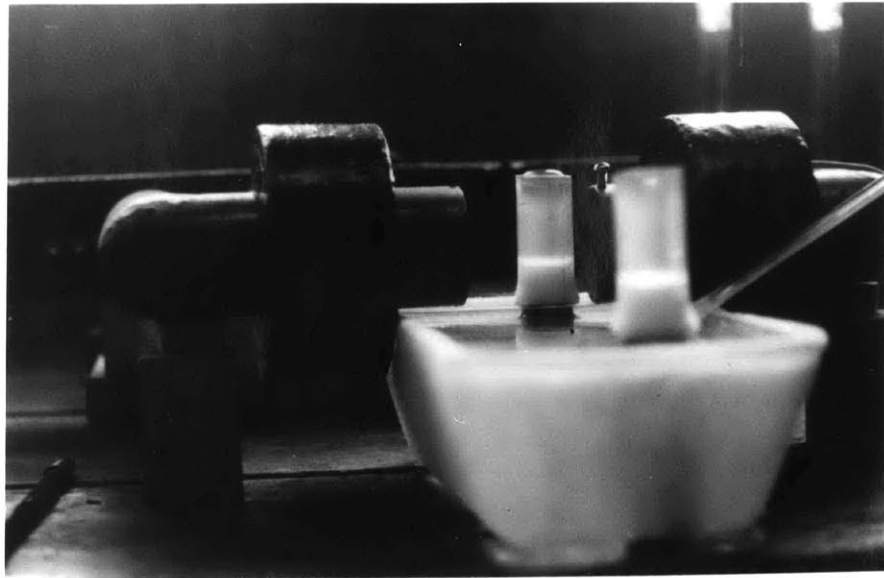


Figure 20. Typical Dendritic Aggregate of Ice and Brine Obtained on Fairly Rapid Freezing of Aqueous Solutions (Under Polarized Light).

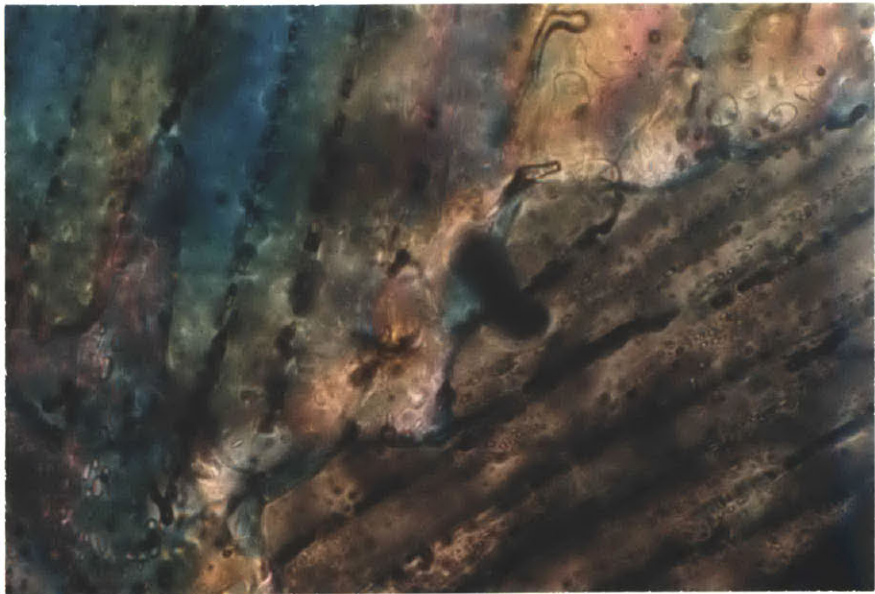
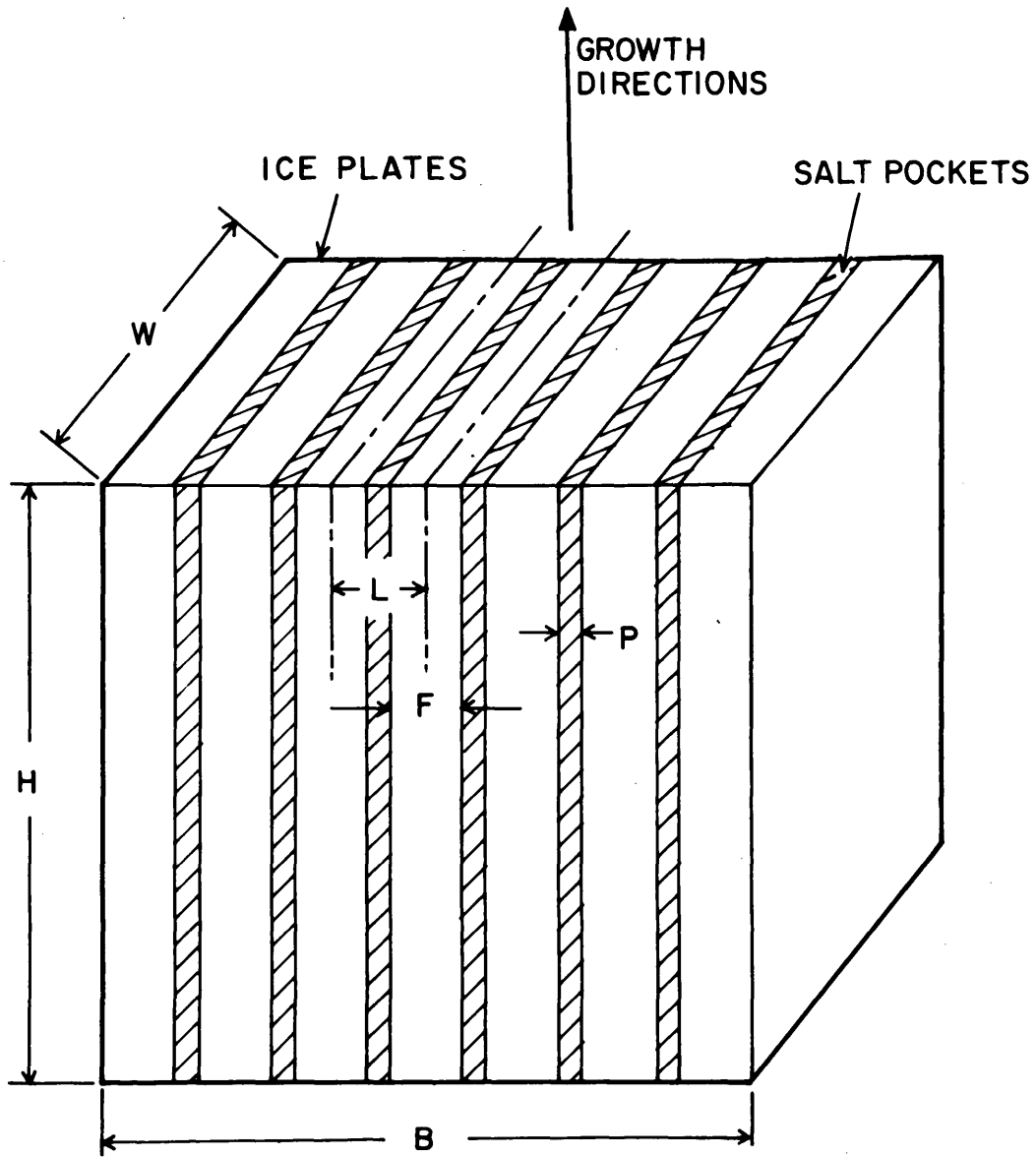


Figure 21. Characteristic Parameters of a Ice-Brine Aggregate After Dendritic Solidification.



L - DENDRITE SPACING  
 F - ICE PLATE THICKNESS  
 W - DENDRITE WIDTH

P - SALT POCKET THICKNESS  
 B - GROUP BREADTH  
 H - GROUP HEIGHT

Figure 22. Randomly Arranged Ice Crystals Produced Under Very Slow Growth Rates. Ingot from 1.0 N Potassium Chloride Solution 1.0 cm from the Chill Surface at  $-20^{\circ}\text{C}$ .

Figure 23. A Large Segregate of Salt Between Neighboring Groups of Dendrites.

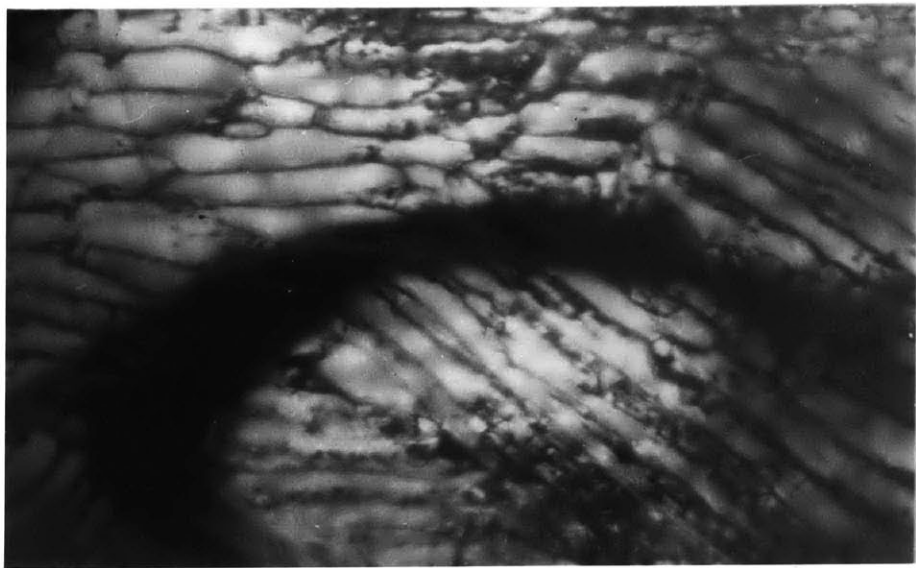
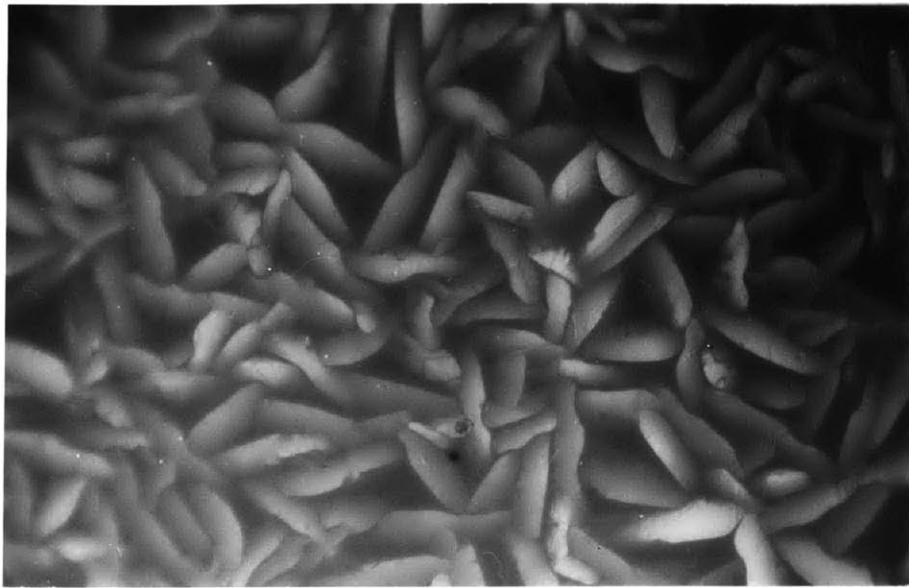


Figure 24. Transverse Section of Unidirectional Ingot from 1.0 N Potassium Chloride Solution 0.90 cm from the Chill Surface at  $-70^{\circ}\text{C}$  X26.

Figure 25. Same Ingot as in Figure 24, 1.3 cm from the Chilled Surface, X26.



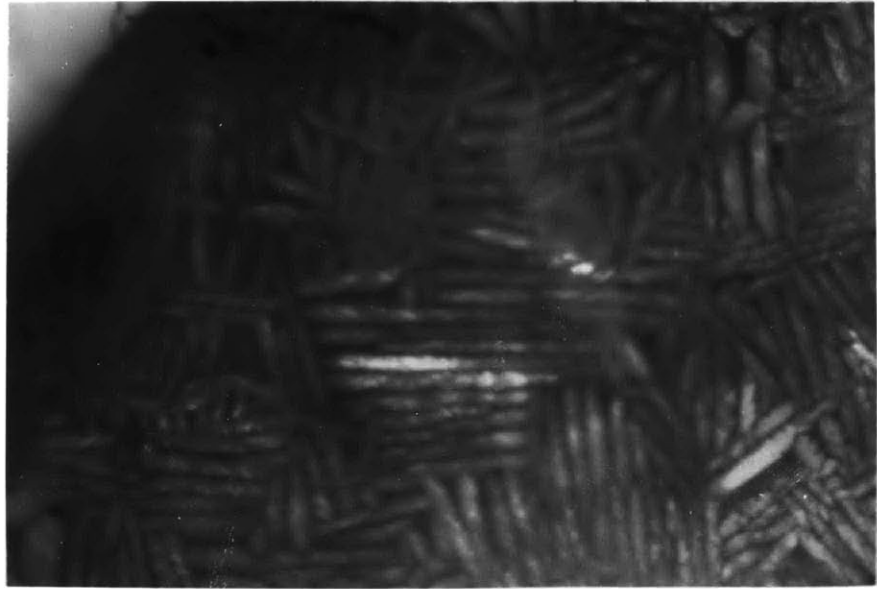


Figure 26. Same Ingot as in Figure 24, 3.0 cm from the Chilled Surface. X26.

Figure 27. Same Ingot as in Figure 24, 3.2 cm from the Chilled Surface. X26.

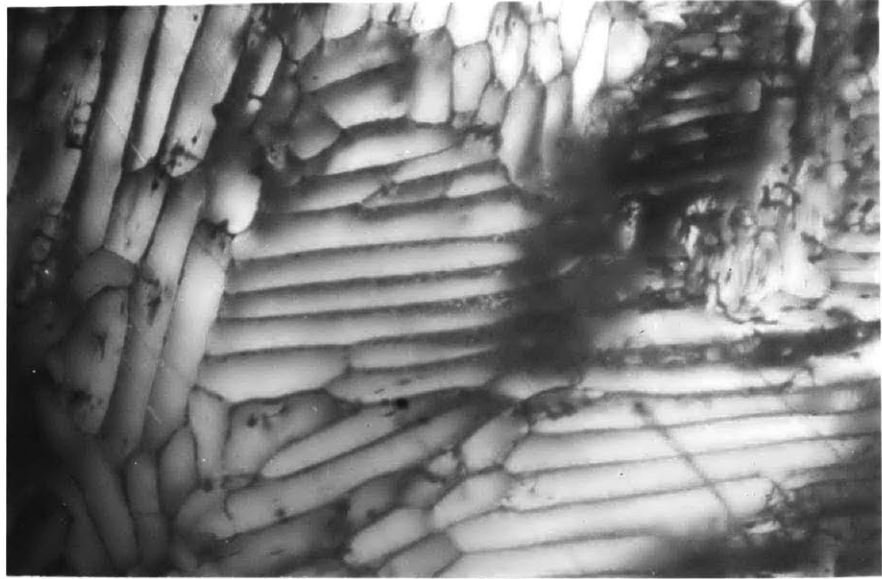


Figure 28. Transverse Section of an Ingot from 1.0 N Potassium Chloride Solution 0.80 cm from the Chill Surface, at  $-20^{\circ}\text{C}$  X26.

Figure 29. Same Ingot as in Figure 28, 1.1 cm from the Chill, but with Chill Temperature Reduced to  $-70^{\circ}\text{C}$  During Growth, Causing Faster Freezing.

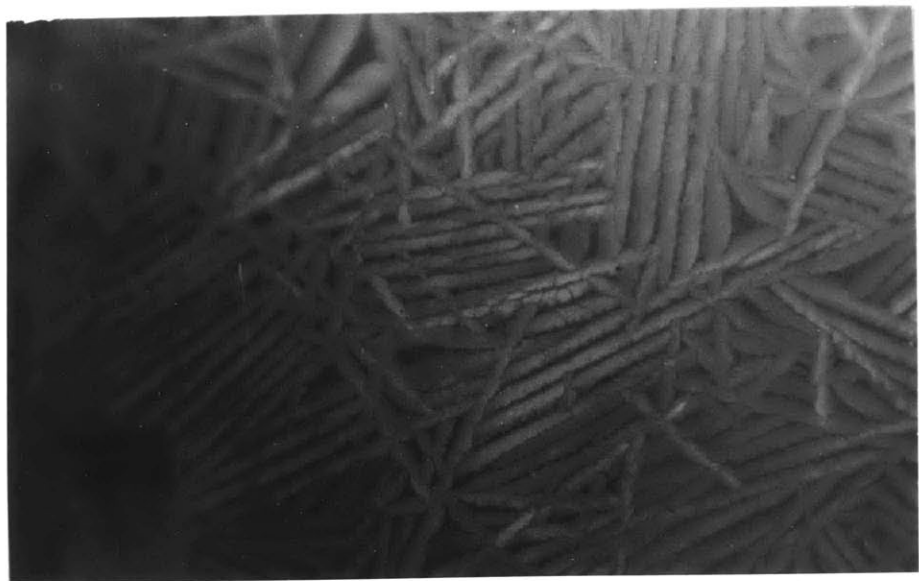
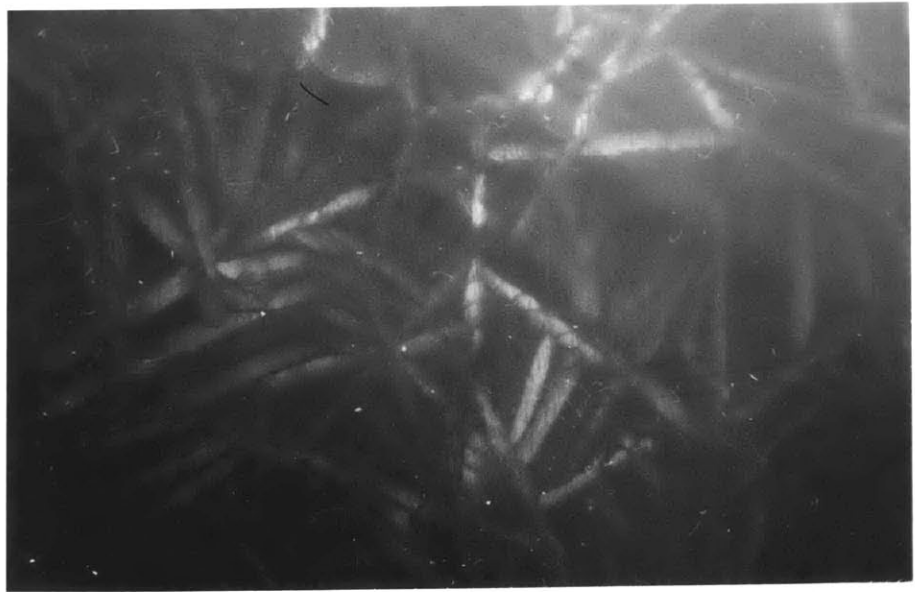


Figure 30. Variation of Dendrite Spacing with Distance from the Chill and the Effect of Concentration on Dendrite Spacing in Ingots From Potassium Chloride Solutions.

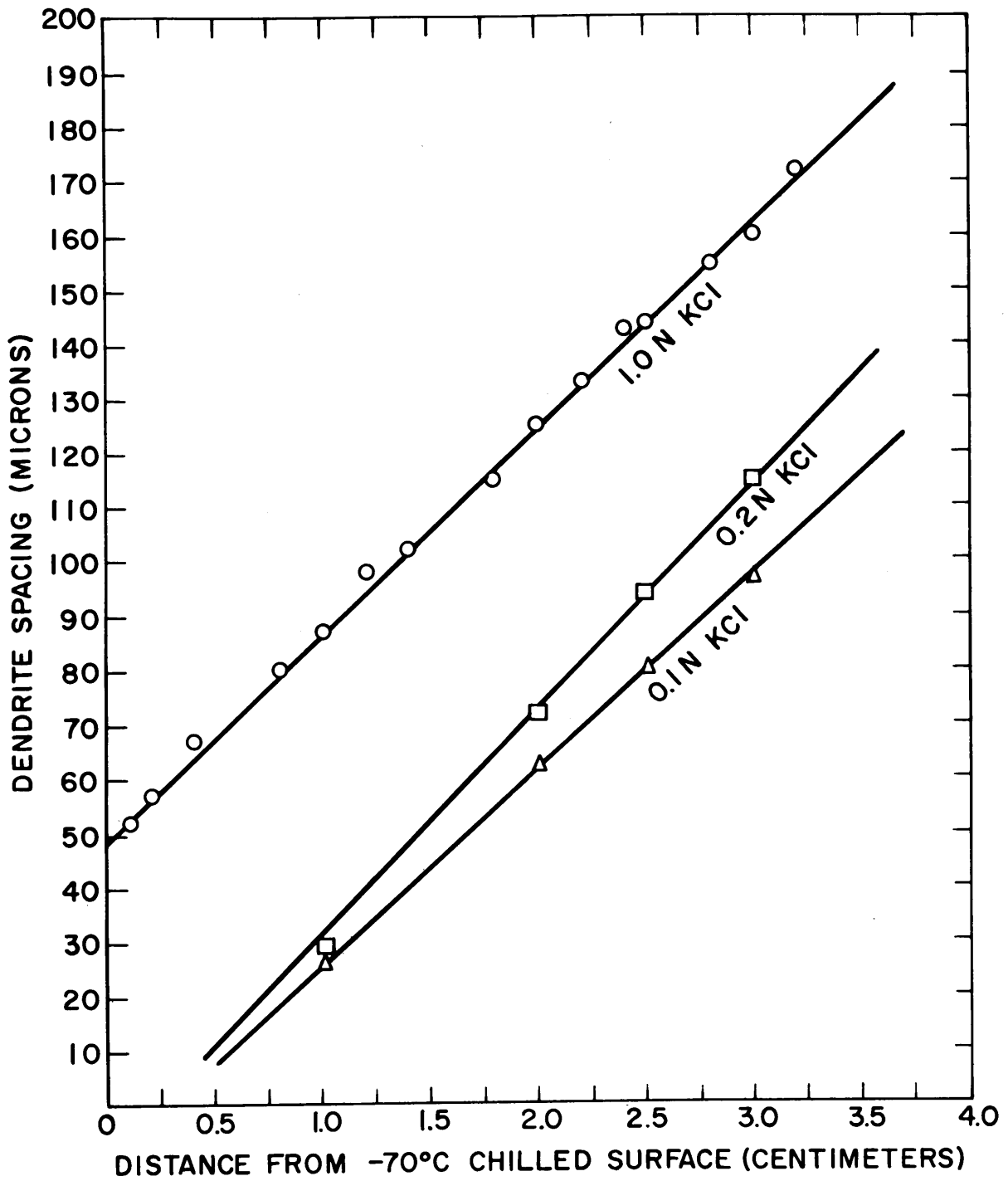


Figure 31. Plot of Dendrite Spacings in 1.0 N Potassium Chloride Ingot Versus the Reciprocal of the Square Root of the Maximum Freezing Rates at Different Distances from the Chill Surface at  $-70^{\circ}\text{C}$ .



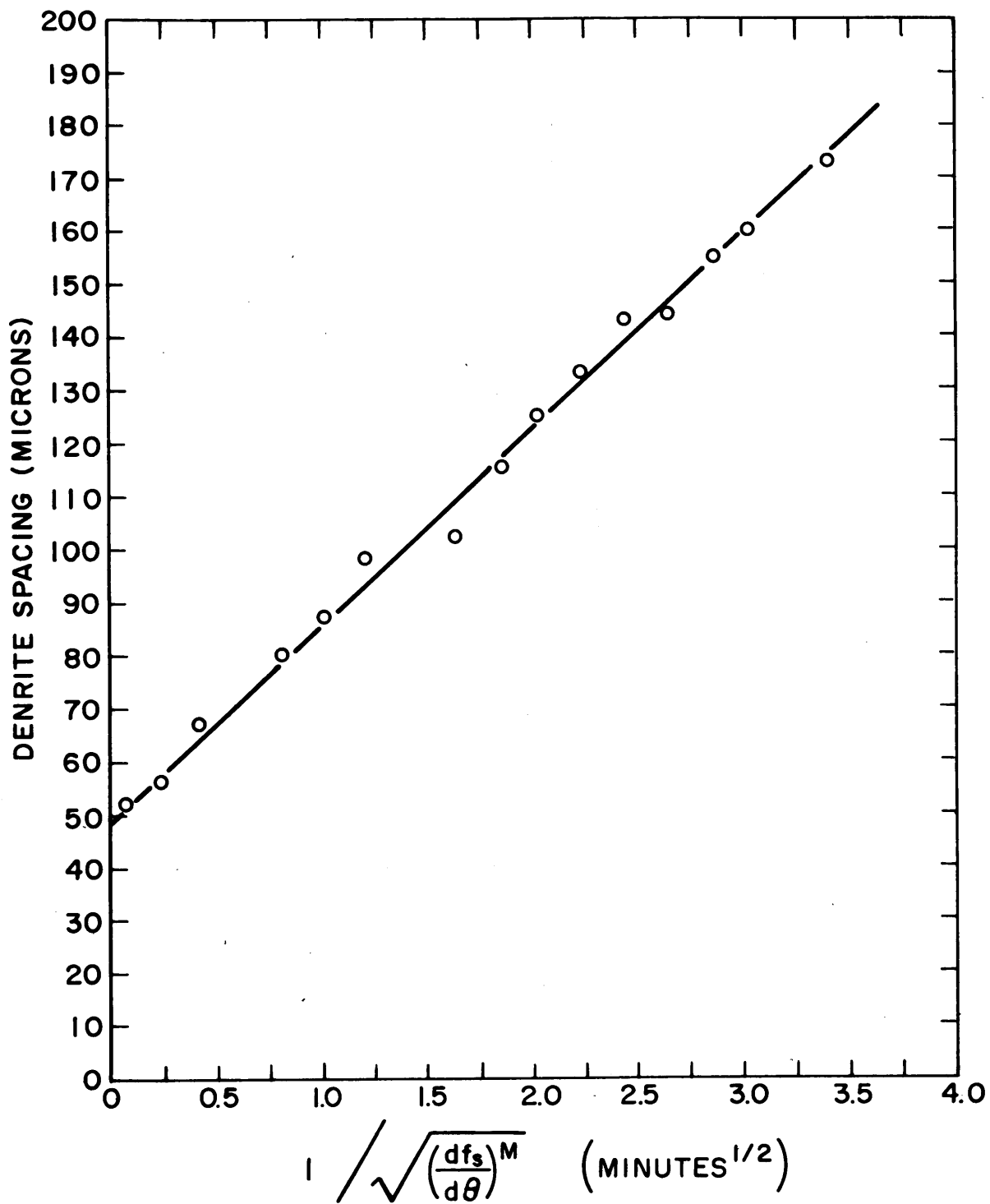


Figure 32. Dendrite Spacing and Thickness of Salt Pockets Versus Concentration in Sodium Chloride Solutions. Droplets, Freezing Rate  $0.36 \text{ minutes}^{-1}$ . Also the Effect of Superimposed Magnetic Field on Spacing.

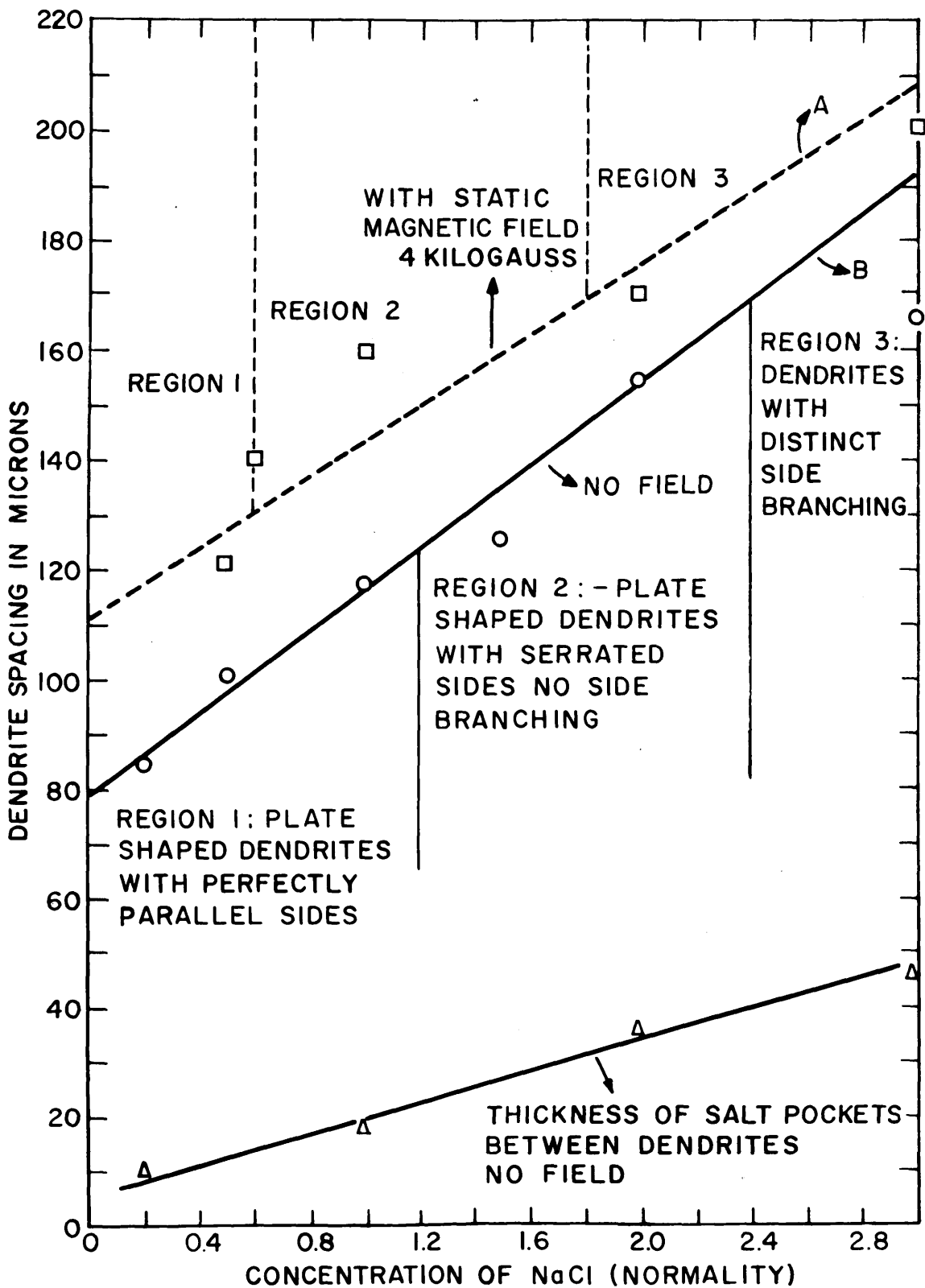


Figure 33. Effect of Concentration on Dendrite Spacing in Ingots from Sodium Chloride Solutions.

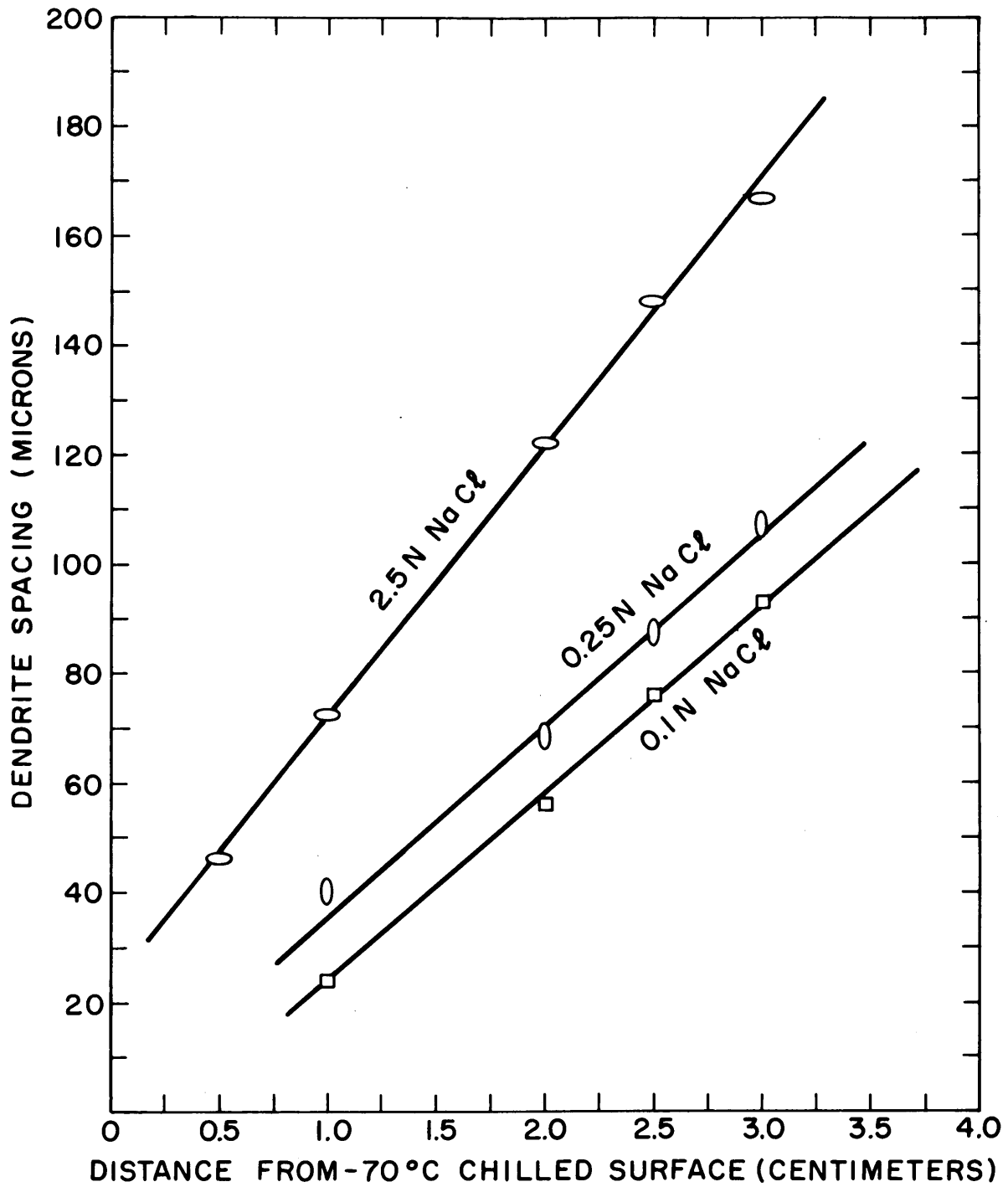


Figure 34. Effect of Concentration on Dendrite Spacing in  
Ingots from Lithium Chloride Solutions.

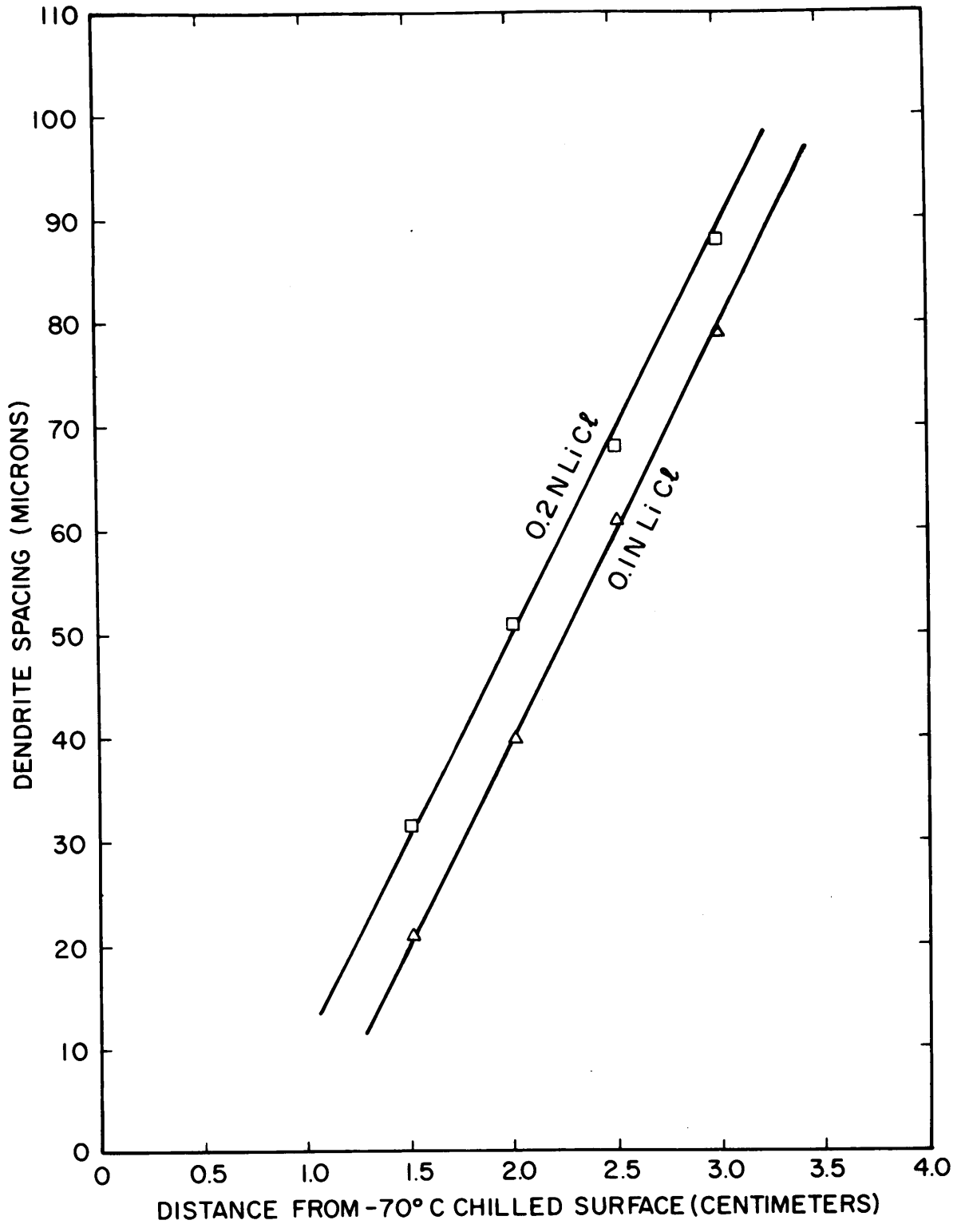


Figure 35. 0.2 N Sodium Chloride Solution Droplet, Freezing Rate  
0.36 minutes<sup>-1</sup>, X26.

Figure 36. 1.5 N Sodium Chloride Solution Droplet, Freezing Rate  
0.36 minutes<sup>-1</sup>, X26.





Figure 37. 3.0 N Sodium Chloride Solution Droplet, Freezing Rate  
 $0.36 \text{ minutes}^{-1}$ , X26.

Figure 38. 3.0 N Sodium Chloride Solution Droplet, Freezing Rate  
 $0.72 \text{ minutes}^{-1}$ , X26.

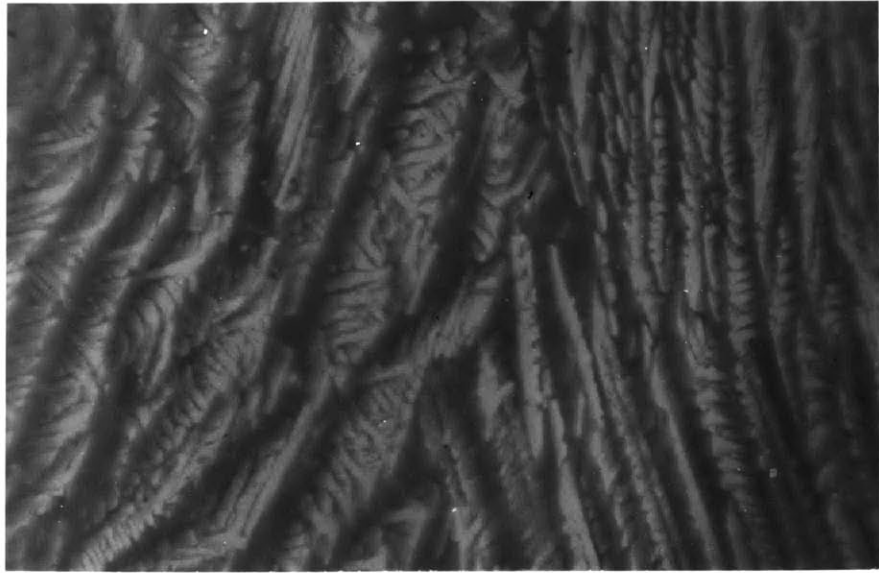


Figure 39. Liquidus Curves of Water with Sodium Chloride, Potassium Chloride, Hydrogen Chloride and Lithium Chloride as Solutes.

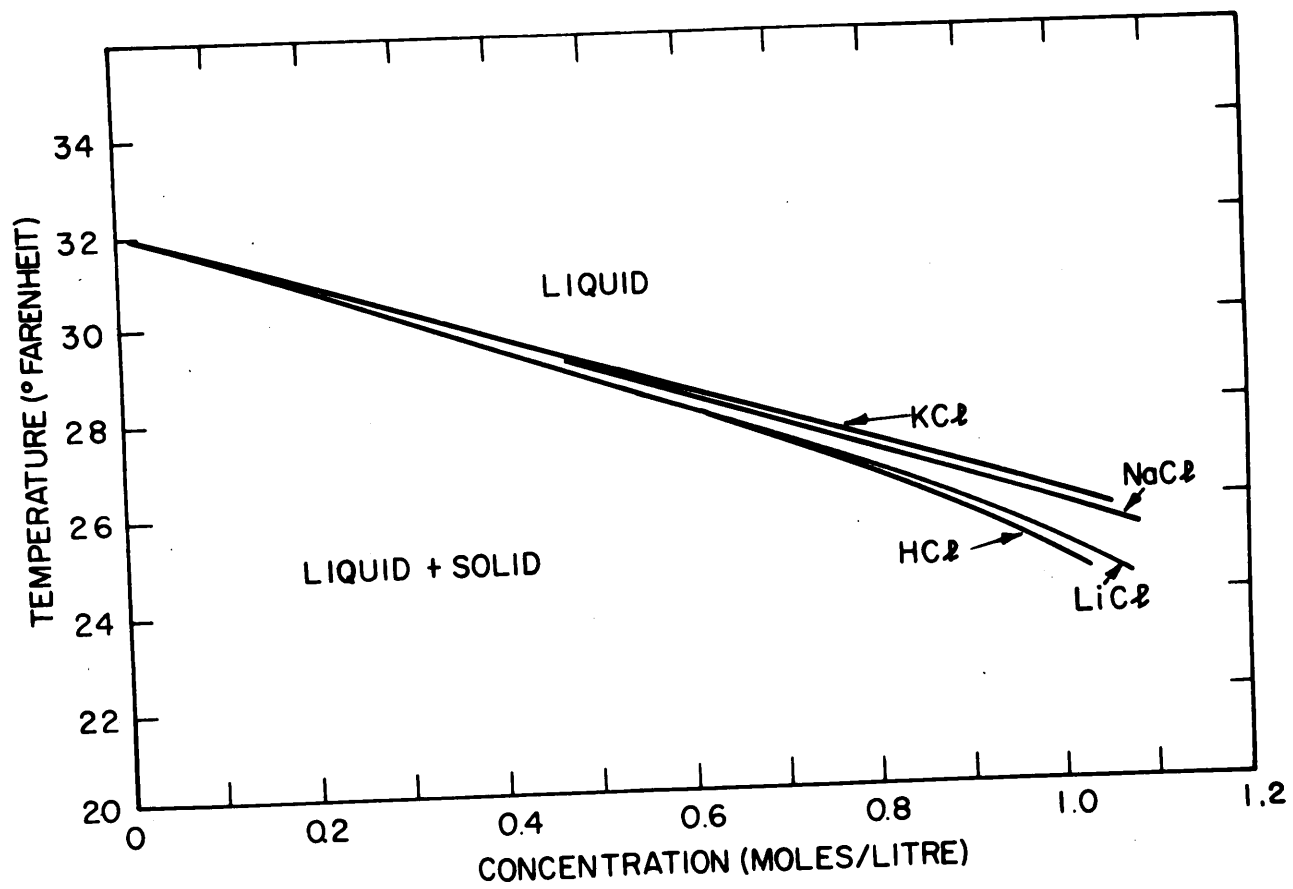


Figure 40. Effect of Solute Diffusivity on Dendrite Spacing.

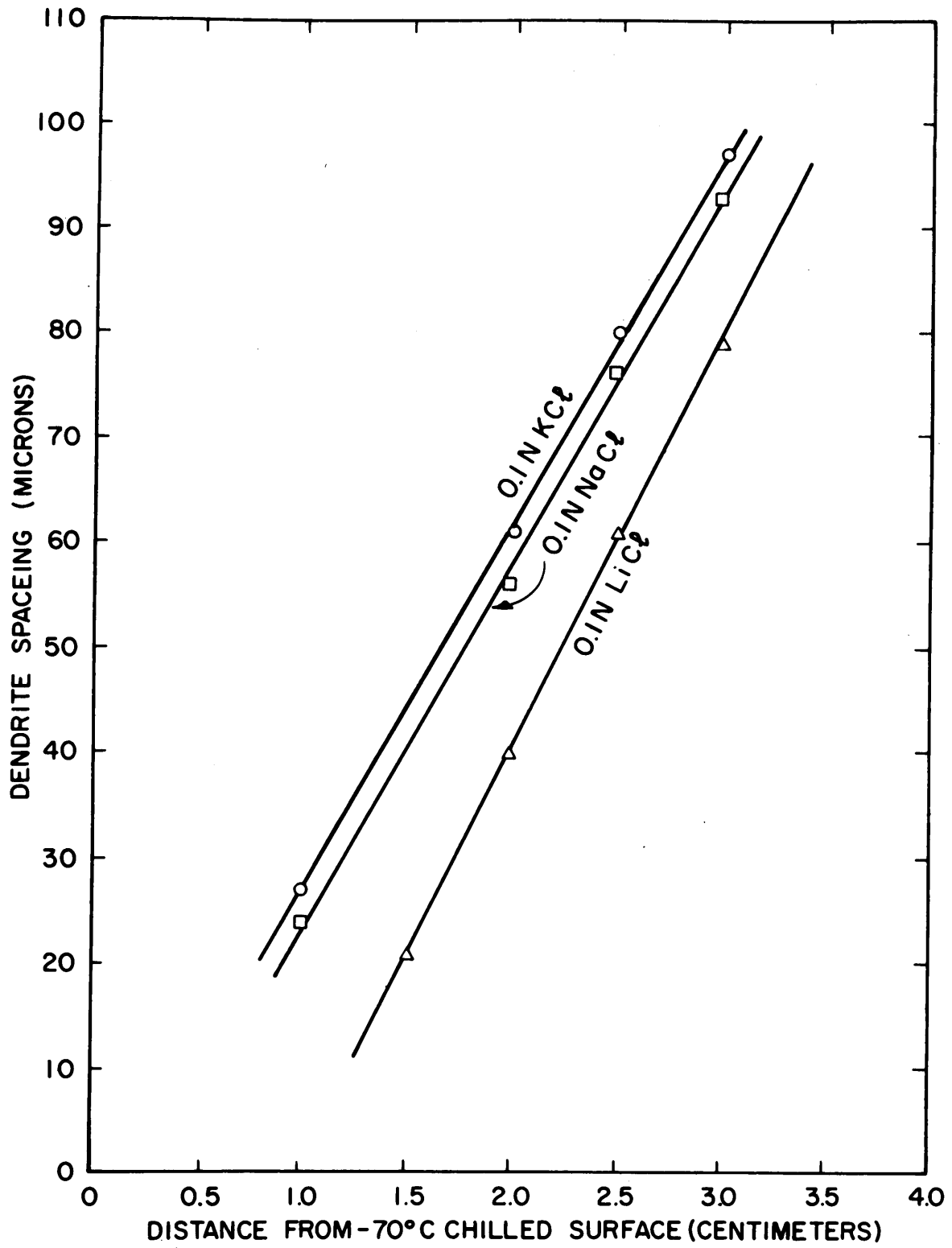


Figure 41. Effects of Small Solute Additions on Dendrite Spacings  
Obtained with 0.2 N Sodium Chloride Solution.



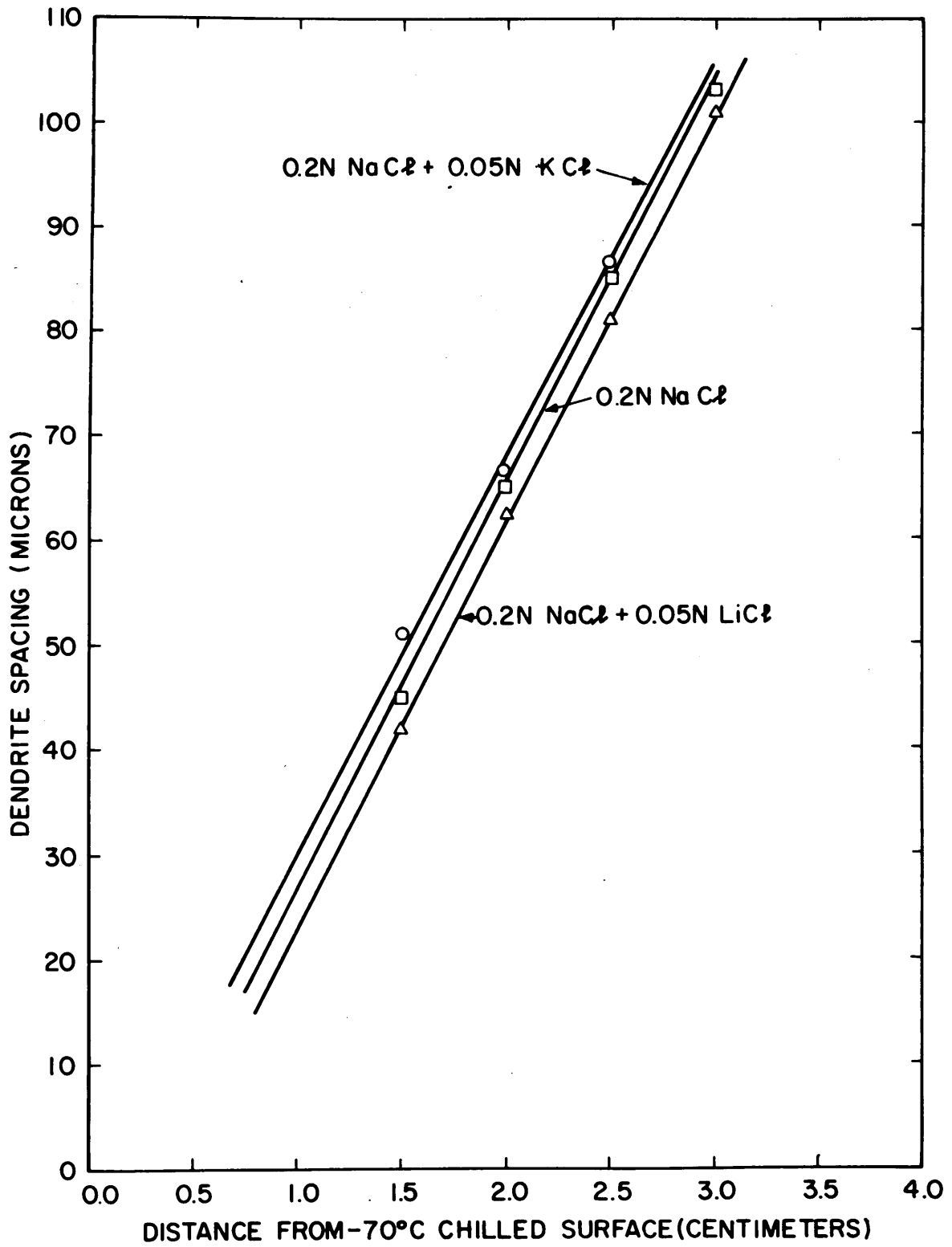


Figure 42. Effects of Large Solute Additions on Dendrite Spacings Obtained with 0.1 N Sodium Chloride and 0.1 N Lithium Chloride Solutions.

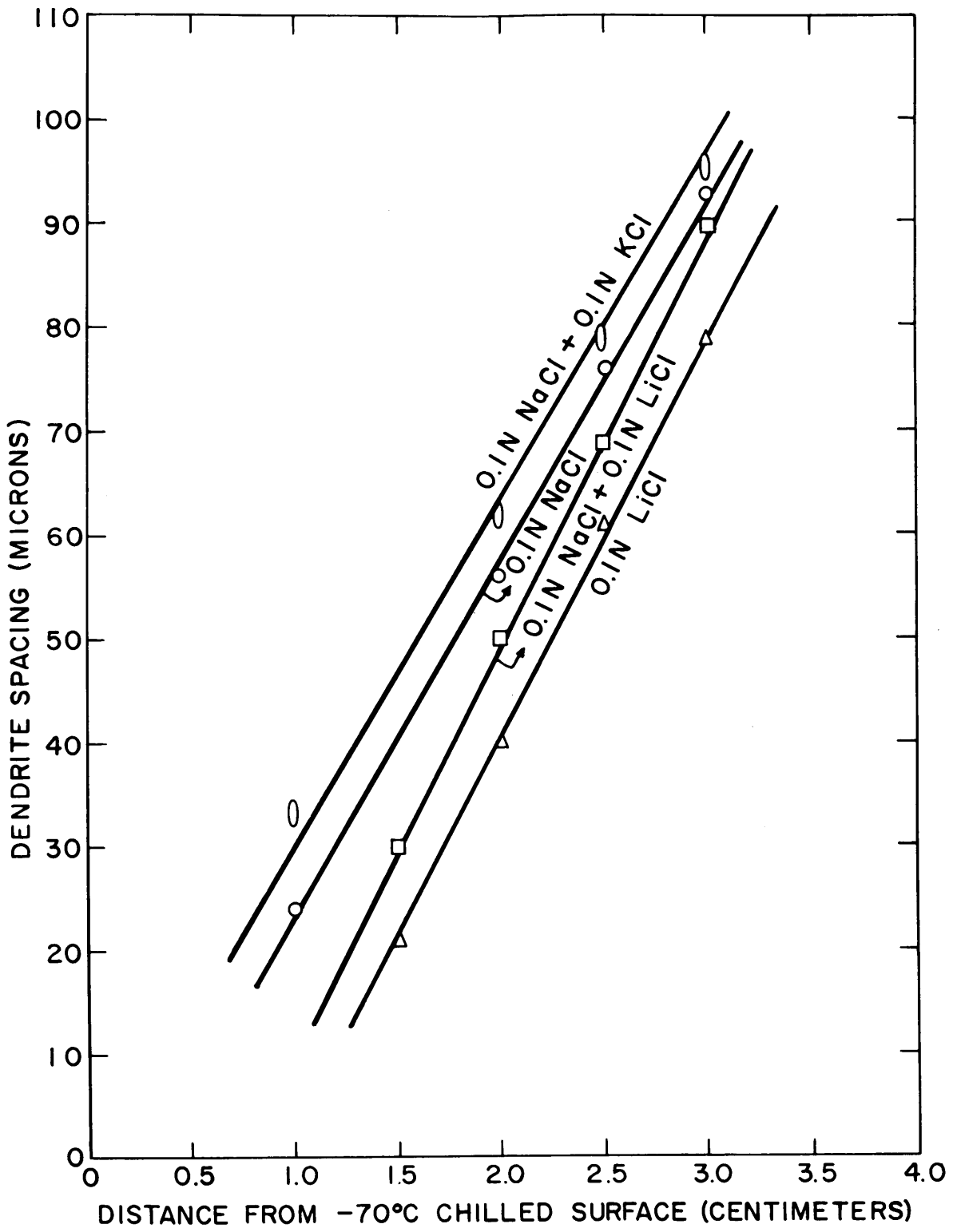


Figure 43. Effect Of Large Solute Additions on Dendrite Spacings  
Obtained with 0.1 N Lithium Chloride and 0.1 N Potassium  
Chloride Solutions.

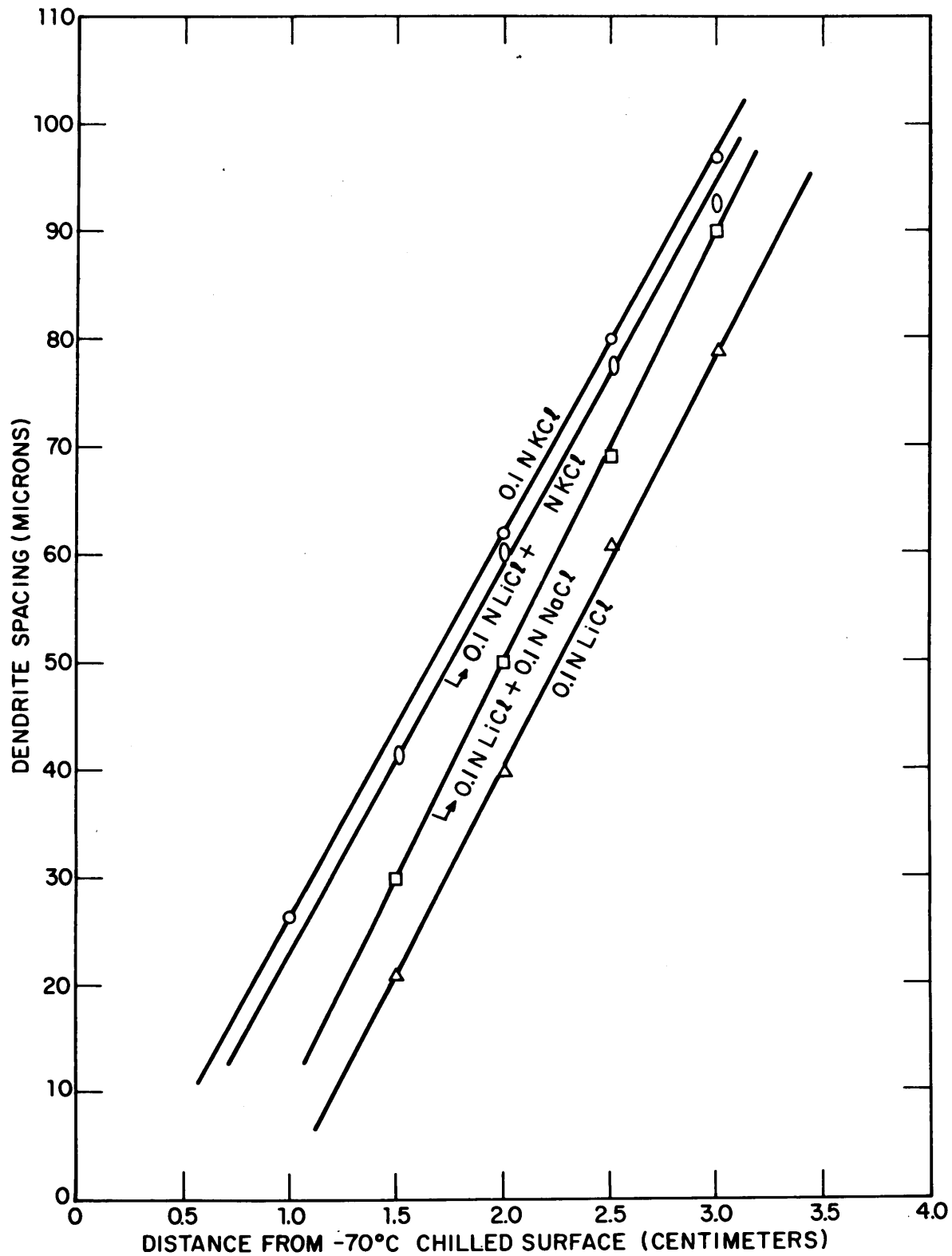


Figure 44. Ingot from 0.1 N Sodium Chloride Solution, 2.5 cm from the Chill Surface at  $-70^{\circ}\text{C}$ , X25.

Figure 45. Ingot from 0.1 N Sodium Chloride + 0.10 N Lithium Chloride Solution, 2.5 cm from the Chill Surface at  $-70^{\circ}\text{C}$ , X25.

Figure 46. Ingot from 0.1 N Lithium Chloride Solution, 2.5 cm from the Chill Surface at  $-70^{\circ}\text{C}$ , X25.

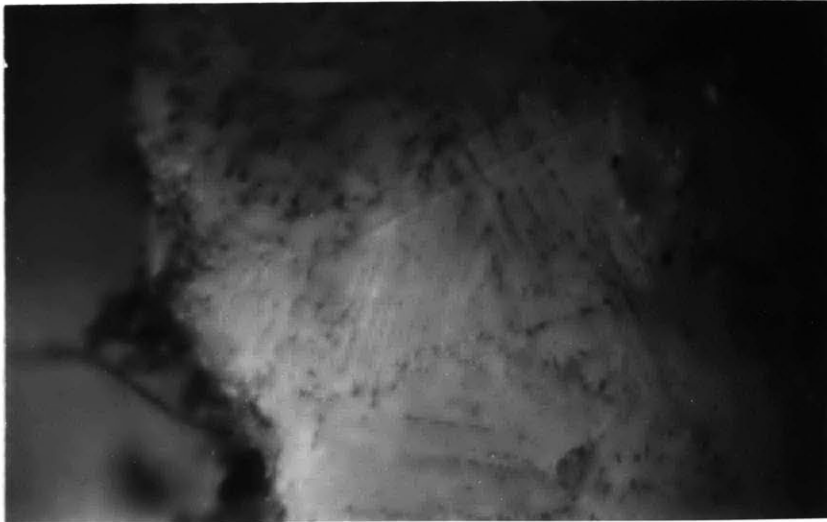
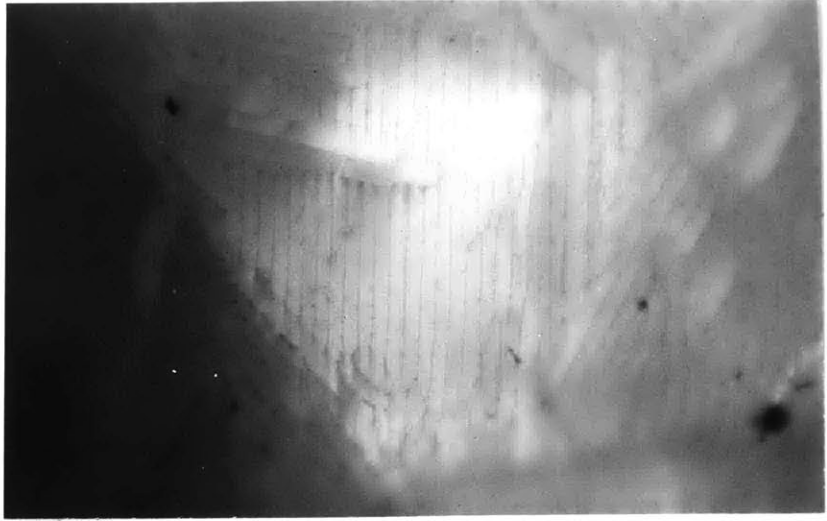


Figure 47. Effect of Total Solute Concentration on Dendrite Spacings with Solutions Containing Equal Proportions of Sodium Chloride and Potassium Chloride.



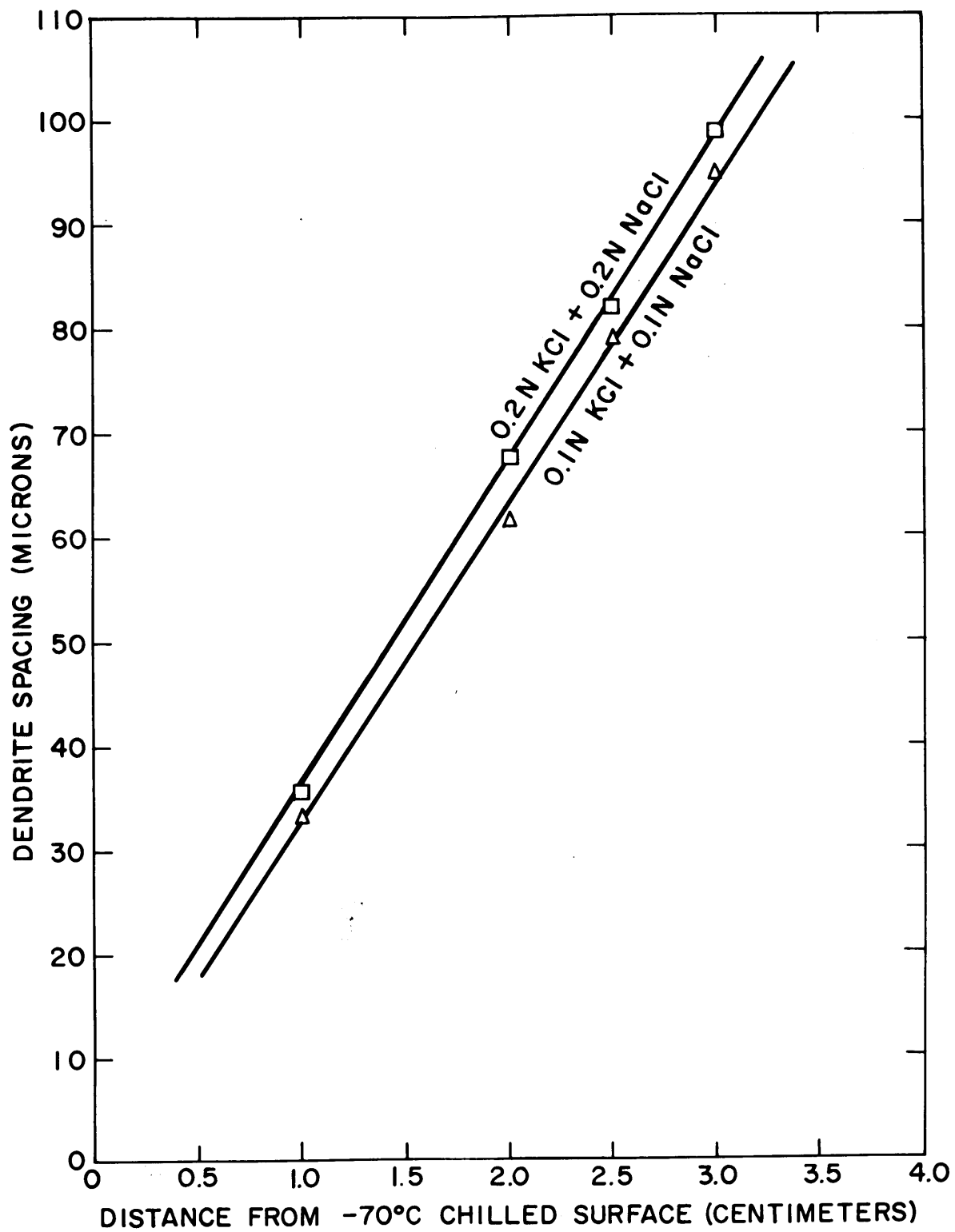


Figure 48. 0.5 N Sodium Chloride Solution Droplet, Freezing Rate  $0.36 \text{ minutes}^{-1}$ , X75, No Field.

Figure 49. 0.5 N Sodium Chloride Solution Droplet, Freezing Rate  $0.36 \text{ minutes}^{-1}$ , X75, Frozen Under the Influence of a 2 kilogauss Static Magnetic Field.

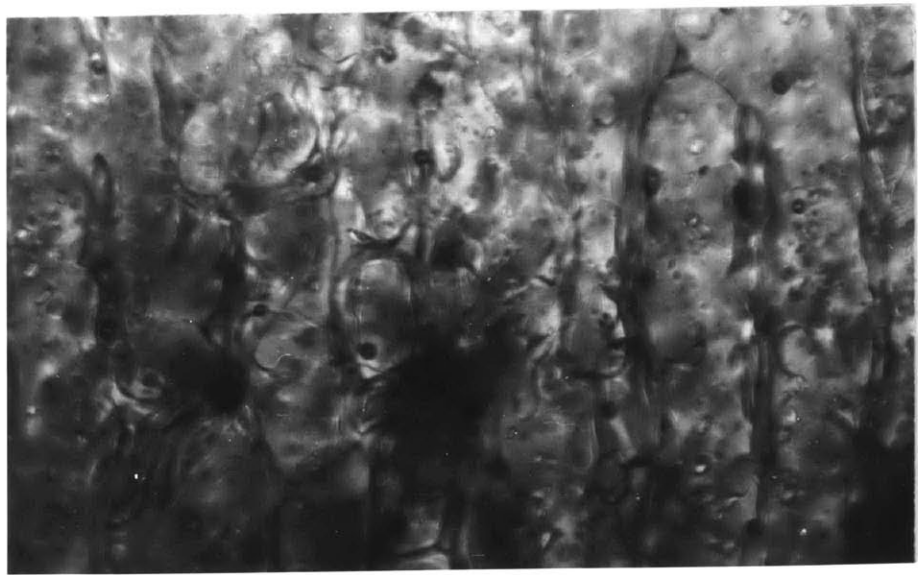
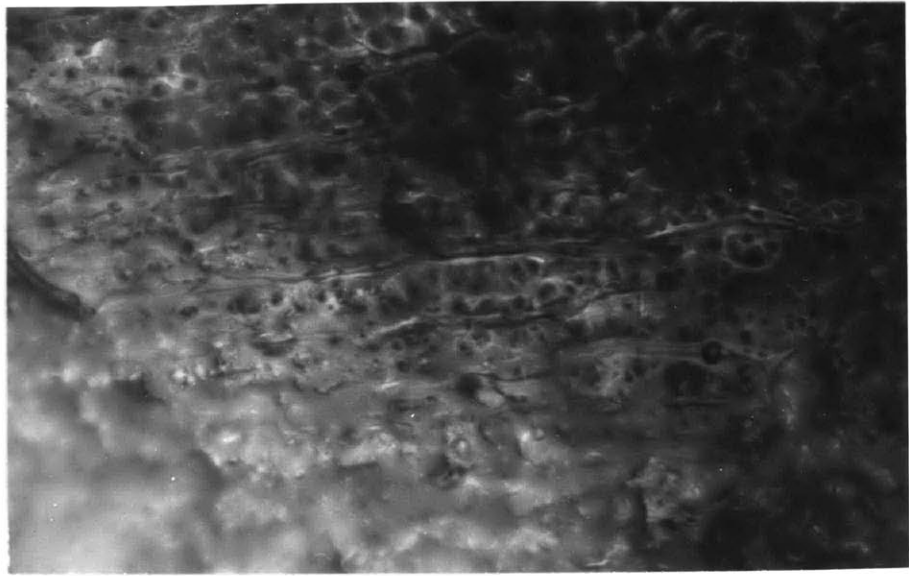
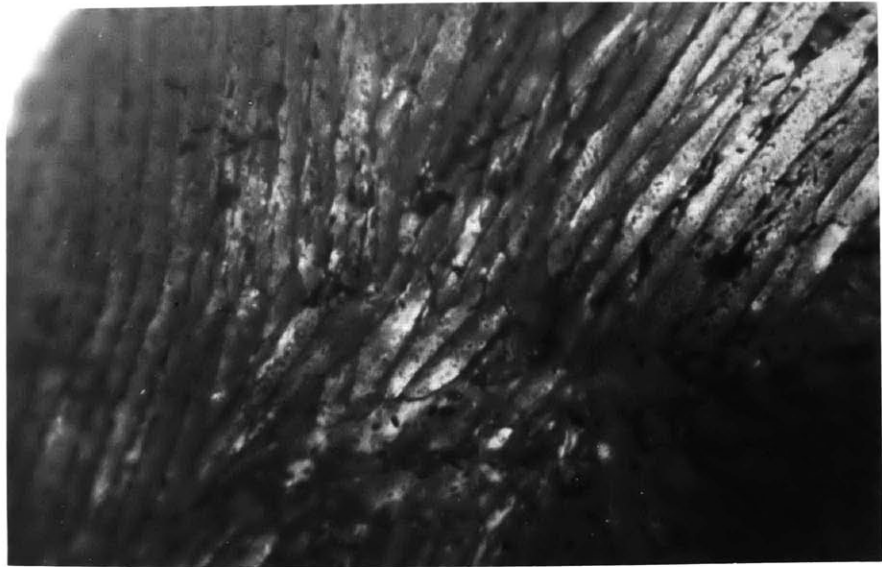


Figure 50. 1.0 N Sodium Chloride Solution Droplet, Freezing Rate  $0.36 \text{ minutes}^{-1}$ , X25, No Field.

Figure 51. 1.0 N Sodium Chloride Solution Droplet, Freezing Rate  $0.36 \text{ minutes}^{-1}$ , X25, Frozen Under the Influence of a 4.0 kilogauss Static Magnetic Field.



## XIII. BIBLIOGRAPHY

1. J. D. Bernal and R. H. Fowler, "Theory of Water and Ionic Solutions" *Journal of Chemical Physics*, Vol. 1, 1933, 515.
2. J. Morgan and B. E. Warren, "X-ray Analysis of the Structure of Water" *Journal of Chemical Physics*, Vol. 6, 1938, 666.
3. S. Katzoff, "X-ray Studies of the Molecular Arrangement in Liquids," *Journal of Chemical Physics*, Vol. 2, 1934, 841.
4. L. Pauling, "Nature of Chemical Bond", Cornell University Press, New York 1960, Chapter 12, 472.
5. R. A. Robinson and R. H. Stokes, "Electrolyte Solutions", Academic Press Inc. New York 1955, Chapters 1 and 11.
6. R. Smith-Johannsen, "Some Experiments in the Freezing of Water", "Science", Vol. 108, 1948, 652.
7. E. Miksch, "Growth of Ice in Supercooled Water", Ph.D. Thesis in Applied Physics, Harvard University, September 1963.
8. B. Chalmers, "Melting and Freezing," *Trans. A.I.M.E.*, Vol. 200, 1954, 519.
9. J. W. Rutter and B. Chalmers, "A Prismatic Substructure Formed During Solidification of Metals", *Canadian Journal of Physics*, Vol. 31, 1953, 15.
10. F. Weinberg and B. Chalmers, "Further Observations on Dendritic Growth in Metals," *Canadian Journal of Physics*, Vol. 30, 1952, 488.
11. W. C. Winegard, "Fundamentals of the Solidification of Metals," *Metallurgical Reviews*, Vol. 6, No. 21, 1961, 57.
12. P. E. Brown and C. M. Adams, "Rapidly Solidified Alloys Structures," *Trans. American Foundrymen Society*, 1962, 879.
13. D. N. French, "Solidification of Aqueous Solutions," Sc.D. Thesis, Department of Metallurgy, M.I.T., May 1962.
14. P. Rohatgi, "Solidification of Eutectic and Near Eutectic Aluminum Copper Alloys," S. M. Thesis, Department of Metallurgy, M.I.T., Jan., 1963.

15. T. S. Plaskett and W. C. Winegard, "Cell to Dendrite Transition in Tin Base Alloys," *Canadian Journal of Physics*, Vol. 38, 1960, 1077.
16. E. N. Dorsey, "The Freezing of Supercooled Water," *Trans. American Philosophical Society*, Volume 38, Part III, November, 1948.
17. J. D. Harrison and W. A. Tiller, "Controlled Freezing of Water," "Ice and Snow", M.I.T. Press, Cambridge, Mass., 1963, 215.
18. W. A. Tiller and J. D. Harrison, "Ice Interface Morphology and Texture Developed During Freezing," *Scientific Paper 63-944-116-P4*, Westinghouse Research Laboratories, Churchillborough, Pennsylvania.
19. C. A. Knight, "Curved Growth of Ice on Surfaces," *Journal of Applied Physics*, Vol. 33, No. 5, 1962, 1808.
20. R. C. Himes, S. E. Miller, W. H. Mink and H. L. Goering, "Zone Freezing in Dimineralizing Saline Waters," *Industrial and Engineering Chemistry*, Vol. 51, No. 11, 1959, 1345.
21. Jean Blandin, "The Orientation of Crystallites in Magnetic Field," *Academie Des Sciences Comptes Rendus*, Vol. 228, 1949, 1718.
22. G. Mayr, "Einfluss eines magnetischen Feldes auf die Kristallization und auf die Zusammensetzung von Mischkristallen," *Z. Naturforschg* 6a, 1951, 467.
23. F. K. Gorskii and M. E. Mikhlin, "Effect of Magnetic Fields on Solidification of Supersaturated Solutions," *Kristallizatsiya i Fazovye Perekhody*, Akad. Nauk Belorussk, 1962, 400.
24. M. I. Kozlovskii, "The Question of the Influence of an Electric Field on the Nucleation of Crystallization Centers," *Kristallografia*, Vol. 7, No. 1, 157-159.
25. F. K. Gorskii and L. T. Prishpa, "Influence of Alternating Current on the Formation of Crystal Nuclei in Undercooled Melts," *Kristallizatsiya i Fazovye Perekhody*, Akad Nauk Belorussk S.S.R. 1962, 386.
26. Y. N. Vershinin, "Effect of Variable Electric Fields on Structure Formed During Crystallization in Supersaturated Aqueous Solutions," *Kristallizatsiya i Fazovye Perekhody*, Akad Nauk Belorussk S.S.R., 1962, 391.

27. A. V. Shubinkov and V. F. Parvov, "Appearance of Crystallization Centers in a Drop of  $\text{NH}_4\text{Cl}$  Solution on Application of Electric Field," *Kristallografiya*, 6, 1961, 443.
28. W. A. Tiller, K. A. Jackson, J. W. Rutter and B. Chalmers, "The Redistribution of Solute Atoms During the Solidification of Metals," *Acta Metallurgica* Vol. 1, 1953, 428.
29. C. Wagner, "Theoretical Analysis of Diffusion of Solutes During Solidification of Alloys," *Trans. A.I.M.E.*, February 1954, 154.
30. W. G. Pfann, "Redistribution of Solute During Freezing," "Liquid Metals and Solidification," *A.S.M.*, 1958, 218.
31. K. F. Hulme, "On the Distribution of Impurity in Crystals Grown from Impure Unstirred Melts," *Proceedings of Physical Society*, Vol. 68, 7-B, 393.
32. V. G. Smith, W. A. Tiller and J. W. Rutter, "A Mathematical Analysis of Solute Redistribution During Solidification," *Canadian Journal of Physics*, Vol. 33, 1955, 723.
33. C. M. Adams, Jr., "Thermal Considerations in Freezing," "Liquid Metals and Solidification," *A.S.M.* 1958, 187.
34. Ian J. O'Donnell and Louis J. Gosting, "The Concentration Dependence of The Four Diffusion Coefficients of the System  $\text{NaCl-KCl-H}_2\text{O}$  at  $25^\circ\text{C}$ ," "The Structure of Electrolyte Solutions," John Wiley, 1959, 160.
35. Peter J. Dunlop and Louis J. Gosting, "Interacting Flows in Liquid Diffusion" *Journal of American Chemical Society*, Vol. 69, 1947, 2510.
36. Jerome R. Vinograd and James W. McBain, "Diffusion of Electrolytes and of the Ions in their Mixtures," *Journal of American Chemical Society*, Vol. 63, 1941, 2008.
37. T. K. Sherwood and J. C. Wei, "Ion Diffusion in Mass Transfer Between Phases," *Journal of American Institute of Chemical Engineers*, Vol. 1, No. 4, 1955, 525.
38. E. J. Workman and S. E. Reynolds, "Electrical Phenomenon Occuring During the Freezing of Dilute Aqueous Solutions and their Possible Relationship to Thunderstorm Electricity," *Physical Review*, Vol. 78, No. 3, 1950, 254.
39. E. R. Gilliland, Head, Department of Chemical Engineering, M. I. T., Personal Discussion, June 1963.



40. V. A. Kibardin and Ya. Ya. Guerevich, "Influence of Magnetic Field on the Motion of Particles in Electrolyte Solutions," *Doklady Akad. Nauk U.S.S.R.*, Vol. 137, 1961, 1405.
41. W. G. Pfann and R. S. Wagner, "Principles of Field Freezing", *Trans. A.I.M.E.*, Vol. 224, 1962, 1139.
42. L. Gold, "The Electric Field Contribution to Impurity Distribution in Crystal Growth Process," *Japan Journal of Applied Physics*, Vol. 2, 1963, 131.
43. W. G. Pfann, Bell Telephone Laboratories, Murray Hill, New Jersey, Personal Communication, October, 1963.
44. Ole Lamm, "The Diffusion of an Electrolyte Solution in a Superimposed Electric Field," *Acta Chem. Scandnavia*, Vol. 10, 1956, 1132.
45. M. G. B. Rao, "Movement of Electrolytes by the Combined Action of Electric and Magnetic Fields," *Journal of Scientific and Industrial Research (India)*, 20B, 1961, 606.
46. G. Piccardi, "The Structures of Water and Influence of Low Frequency Magnetic Fields," *Ricerca Science*, Vol. 29, 1959, 1252.
47. V. I. Mineko and S. M. Petrov, "Physico Chemical Principles of Magnetic Treatment of Water," *Teploenergetica*, Vol. 9, 1962, 63.
48. K. Grjotheim and J. K. Moe, "On the Correlation Between the Structure and Properties of Water," *Acta.Chem. Scandnavia*, Vol. 18, 1954, 1193.
49. "Handbook of Chemistry and Physics" Chemical Rubber Publishing Co., Cleveland, Ohio, 44th Edition.
50. G. N. Lewis and M. Randall, "Systems Involving Electric and Magnetic Fields," "Thermodynamics", McGraw Hill, 1961, 497.
51. K. Lonsdale, "Diamagnetic Susceptibility and Anisotropy of Ice," *"Nature"*, Vol. 164, 1949, 101.
52. F. Humbel, F. Jona and P. Scherrer, *Helvetica Phys. Acta*, Vol. 26, 1953, 17.
53. B. H. Alexander and F. N. Rhines, "Dendritic Crystallization of Alloys," *Trans. A.I.M.E.*, Vol. 188, 1950, 1267.
54. J. A. Howrath and L. F. Mondolfo, "Dendritic Growth" *Acta Metallurgica*, Vol. 10, 1962, 1037.

55. W. Patterson and S. Engler, "Über den Erstarrungsablauf und die Grosse und Aufteilung des Volumendefizits beim Gusslegierungen," Geisserei, Techn. Wiss-Beihefte, Vol. 13, 1961, 123.
56. W. A. Tiller, "Effect of Grain Boundaries on Solute Partitioning During Progressive Solidification," Journal of Applied Physics, Vol. 33, No. 10, 1962, 3106.

## XIV. BIOGRAPHICAL NOTE

The author was born in Kanpur, India, on February 18, 1943. He completed his high school examination in 1955 and intermediate in science in 1957 from the local schools. In the same year he entered the College of Mining and Metallurgy at the Banaras Hindu University where he received his Bachelor of Science Degree in Metallurgical Engineering in 1961. He then joined the Department of Metallurgy, M. I. T. as a graduate student and was awarded the Master of Science Degree in January, 1963. Since September 1961 he has been a Research Assistant in the Department of Metallurgy. His major area of interest has been solidification structures in metallic and aqueous solutions.

He is a recipient of the Banaras University Gold Medal and the Hadfield Medal from the Mining and Metallurgical Society of India. He is a member of the American Society for Metals and the American Institute of Mining and Metallurgical Engineers.